2086

PRODUCTION OF $\Sigma(1660)$ IN 4.2 GeV/c K^-p COLLISIONS

J.J.M. TIMMERMANS

PRODUCTION OF $\Sigma(1660)$ IN 4.2 GeV/c K^-p COLLISIONS

PROMOTOR:

PROF. DR. R.T. VAN DE WALLE

CO-REFERENT:

DR. W.J. METZGER

PRODUCTION OF $\Sigma(1660)$ IN 4.2 GeV/c K^-p COLLISIONS

P R O E F S C H R I F T

TER VERKRIJGING VAN DE GRAAD VAN DOCTOR IN DE
WISKUNDE EN NATUURWETENSCHAPPEN
AAN DE KATHOLIEKE UNIVERSITEIT TE NIJMEGEN, OP GEZAG VAN
DE RECTOR MAGNIFICUS, PROF. DR. A.J.H. VENDRIK,
VOLGENS BESLUIT VAN HET COLLEGE VAN DECANEN
IN HET OPENBAAR TE VERDEDIGEN
OP VRIJDAG 1 OKTOBER 1976
DES NAMIDDAGS TE 2 UUR PRECIES

door

JOHANNES JOSEPHUS MATHIAS TIMMERMANS
geboren te Meerssen

Druk: Offsetdrukkerij Faculteit der Wiskunde en Natuurwetenschappen
Nijmegen

Gaarne maak ik van de gelegenheid gebruik om allen te bedanken die op enigerlei wijze hebben bijgedragen tot het totstandkomen van dit proefschrift. In het bijzonder geldt deze dank

- de scansters en technici van de werkgroep Hoge Energie Fysika voor het vele scan- en meetwerk dat verricht is
- de wetenschappelijke medewerkers van deze werkgroep voor de leerzame discussies
- de staf en medewerkers van het Universitair Rekencentrum
- de afdelingen Illustratie en Fotografie
- de typekamer en de Offsetdrukkerij.

I wish to thank the staff of the C.E.R.N.-PS and the operating crews of the C.E.R.N. 2 metre bubble chamber, the scanning, measuring and computing staffs in Amsterdam and C.E.R.N.. I also like to thank all colleagues for their cooperation and for the many enlightening discussions during our collaboration meetings.

Het onderzoek beschreven in dit proefschrift vormt een onderdeel van het onderzoeksprogramma van de Stichting voor Fundamenteel Onderzoek der Materie (F.O.M.), welke financieel gesteund wordt door de Nederlandse Organisatie voor Zuiver Wetenschappelijk Onderzoek (Z.W.O.).

Aan mijn ouders

TABLE OF CONTENTS

INTRODUCTION

The 4.2 GeV/c K^-p experiment started in 1967 as a collaboration between the bubble chamber groups from the University of Amsterdam and the University of Nijmegen. The goal was to make a series of exposures of the C.E.R.N. 2 metre bubble chamber totalling an amount of 700,000 pictures. In 1971 the C.E.R.N. Track Chamber Division joined the collaboration and it was decided to extend the experiment to a statistical level of 3 million pictures. The primary aim of this extension was to make a detailed study of rare reactions, especially reactions involving the production of Ξ^* resonances. A bubble chamber group from the University of Oxford joined the collaboration in 1973. The final pictures were taken in October 1974. The measuring of the events was completed in the middle of 1976.

The study of resonances plays an important role in the understanding of strong interactions. Production experiments are particularly important for the study of resonances which are either inaccessible to formation experiments (such as Ξ^* resonances) or have a small coupling to the initial state particles available in formation experiments (such as Y^* resonances with a small coupling to the proton and K-meson).

One of the early aims of the 4.2 GeV/c experiment was the study of the production of Y^* resonances. The study of one of the most important of these resonances, the so-called $\Sigma(1660)$, forms the subject of this thesis. This resonance has been observed before, both in formation and in production experiments. However, there has always been a discrepancy between the results of these two types of experiments, especially in terms of branching ratios. While in the formation experiments a

dominant decay into $\Sigma\pi$ was found, in production experiments one observed not only a large decay fraction for $\Sigma\pi$ but also for $\Lambda(1405)\pi$. In later production experiments a variation in the $\Lambda(1405)/\Sigma\pi$ branching ratio as a function of the production angle was found, indicative of the existence of at least two $\Sigma(1660)$ resonances.

In this thesis we study the reaction $K^-p \to \Sigma^+(1660)\pi^-$ in the following channels:

$$K^-p \to \Sigma^+\pi^-\pi^+\pi^-$$
$$K^-p \to \Sigma^-\pi^+\pi^+\pi^-$$
$$K^-p \to \Sigma^o\pi^+\pi^-$$
$$K^-p \to \Sigma^+\pi^o\pi^-$$
$$K^-p \to \Lambda\ \pi^+\pi^-$$
$$K^-p \to p\ \bar{K}^o\pi^-$$
$$K^-p \to \Lambda\ \pi^+\pi^o\pi^-$$

Chapters I and II describe in detail the collection of the events and the calculations for the cross sections of the above channels. Chapter III gives a short historical review of the discovery of the $\Sigma(1660)$. In chapter IV we give a description of the production characteristics of the $\Sigma(1660)$ as it is observed in the above channels. Chapter V contains spin-parity analyses. Results from general moments analyses, an Adair analysis and Byers-Fenster analyses (using three-step decay distributions) are presented. For the decay $\Sigma^+(1660) \to \Lambda(1405)\pi^+ \to \Sigma^-\pi^+\pi^+$ we perform a Dalitz-Miller analysis. Finally, in chapter VI we determine branching ratios of the $\Sigma(1660)$ and compare them both with results from formation experiments and with predictions from SU(3) and SU(6) model fits. The possibility of the $\Sigma(1660) \to \Lambda(1405)\pi$ being a $J^P = 3/2^-$ member of the $[70,1^-]$ multiplet of SU(6) is examined.

CHAPTER I.

E X P E R I M E N T A L D E T A I L S.

The data presented in this thesis are collected from a sample of approximately 1.5 million pictures exposed at C.E.R.N. in 6 runs during 1967, 1969, 1971 and 1973. The pictures were taken in the C.E.R.N. 2 metre bubble chamber filled with liquid hydrogen, exposed to an electrostatically separated beam of K^- mesons. The nominal value of the momentum of the beam particle varied for the various runs between 4.09 GeV/c and 4.25 GeV/c. A more detailed description of the beam and the bubble chamber is given in the thesis of H.G. Tiecke [Ti74] . In this chapter we give an outline of the data collection for this experiment. We also describe the special problem of the kinematic reconstruction of the decays of charged particles and present the event selection criteria used.

I.1. Scanning, measurement and data reduction chain.

In the scanningproces the pictures are searched for interactions of the beam particles with the protons in the liquid hydrogen. The interactions thus found are then recorded according to their topology, defined as "lmnS", where:

- l = the number of outgoing tracks at the vertex
- m = the number of kinks (a kink is the decay of a charged particle into one charged and one or more neutral particles); S indicates the charge of the decaying particle
- n = the number of V^o's (a V^o is the decay of a neutral particle into one positive charged and one negative charged particle).

In general the film was scanned once and then rescanned partly or totally in order to obtain a scanning efficiency.

The measurement of an event consists of recording the coordinates (relative to a fixed origin) of fiducial marks, vertices and some 8 to 15 points on each track in each of the three stereoscopic views. In Amsterdam and Nijmegen this was partly done on conventional film plane digitisers (ENETRA type) and the rest was measured on the H.P.D. (Hough Powell Device [Bo70]) in Amsterdam and on P.E.P.R. (Precision Encoding and Pattern Recognition [Cr74]) in Nijmegen. In C.E.R.N. all the events were measured on the Spiral Reader, also called L.S.D. (Lecteur à Spirale Digitisée [LS72]). The latter three devices are automatic measuring devices, although operator intervention is explicitly built into the measuring system and required in order to keep a reasonable measuring efficiency. The least count of the measurements is of the order of 2.5 micron in the film plane for both the automatic and the non-automatic machines.

The measurements of points and tracks in the three views are then used by a computer programme (THRESH or MDT [Cp1]) to perform a spatial reconstruction of the event. The results of these calculations are the x, y and z coordinates of the interaction point(s) and the curvature, the dip angle and the azimuthal angle of the tracks, all with respect to a reference frame fixed in the bubble chamber.

Next the programme GRIND [Cp1] is called to find the correct kinematical hypotheses for each event. This programme assigns all possible masses to each track in turn. The measured value of the momentum of the particles is determined (in MeV/c) from:

$$p = \frac{0.3\ \rho\ H}{\cos\ \lambda} \qquad \text{(I.1)}$$

where: ρ is the radius of the track in cm,

λ is the dip angle,

H is the magnitude of the magnetic field (in kGauss) at a point in the middle of the track.

For each mass hypothesis a least squares fit is done using Lagrangian multipliers to determine the best estimates of the momentum, the dip angle and the azimuthal angle satisfying the momentum and energy conservation laws.

For a hypothesis with no neutral particle produced at the vertex, the conservation laws impose 4 constraint equations. These fits are therefore called 4-C fits. If the production of one neutral particle of known mass is hypothesized, three unknown variables enter the problem and only one constraint is left (1-C fits). If there is more than one neutral particle produced, one can only calculate the sum of the four-vectors of the missing neutrals.

The square of the invariant mass of the missing neutrals (the magnitude of the missing four-vector) is given by:

$$\begin{aligned} MM^2 &= (\text{missing energy})^2 - (\text{missing momentum})^2 \\ &= (E - \sum_i E_i)^2 - (\vec{P} - \sum_i \vec{P}_i)^2 \end{aligned} \qquad \text{(I.2)}$$

where E, $\vec{P}$ are the total energy and momentum of the initial state, E_i, $\vec{P}_i$ the energy and momentum of the particle i and the summation runs over all visible particles in the final state.

A 4-C fit is tried whenever MM^2 is within 3 standard deviations of zero and the missing energy within 3 standard deviations of being positive. GRIND tries a 1-C fit if MM^2

is within 3 standard deviations from the square of the mass of the neutral particle involved and again the missing energy positive within 3 standard deviations. The situation is called a multi-neutral (or 0-C) fit if $MM^2 + 3(\Delta MM^2)$ is greater than the lowest neutral mass squared; the missing energy condition must also here be satisfied.

Knowing the momentum and the mass of a charged particle one can calculate the bubble density of the particle track, because it is a (known) function of the velocity of the particle. Comparison of these calculated bubble densities with the visible bubble densities of the tracks on the photograph, gives the possibility of deciding between different hypotheses. However, for momenta above $\sim$ 0.8 GeV/c one cannot distinguish by eye a π-meson from a K-meson and above $\sim$ 1.5 GeV/c the bubble densities of a π-meson and a proton become comparable. With an automatic measuring device it is possible to measure the bubble density of the tracks and then do the comparison by computer programme. The limits for the distinction of the π, K and p are approximately the same as in the case of comparison by eye [Ma74] .

Finally, the correct hypotheses are selected from the GRIND output tape by the programme SLICE [Cp1] , which then calculates the necessary quantities for the further analysis and writes them onto the Data Summary Tape.

I.2. Kinematic reconstruction of the decay of a charged particle.

A special case of kinematic fitting with very specific problems is the 2-body decay of a charged particle. In the reactions we are considering in this thesis, the following

2-body decays occur:

$$\Sigma^- \rightarrow \pi^- n$$

$$\Sigma^+ \rightarrow \pi^+ n$$

$$\Sigma^+ \rightarrow p \pi^o$$

Other decay modes of these hyperons will not be considered since they are very rare (decay fraction $\sim 2\ ^o/oo$).

If both charged tracks are completely and well measured, one has a genuine 1-C fit, because there are only 3 unknown variables. As starting values for the fit, the 3 unknows are simply calculated from the difference in momentum of the two charged particles.

In most cases however, the track formed by the decaying particle is too short to allow an accurate measurement of its curvature and thus of its momentum. The fit is then unconstrained (0-C fit) and the three unknown variables of the neutral particle and the unknown momentum of the decaying particle are calculated using the four equations for energy and momentum conservation. Since these equations are non-linear in the 4 unknowns, the result is a quadratic equation for the momentum of the decaying Σ-particle:

$$A\, p_\Sigma^2 + B\, p_\Sigma + C = 0 \qquad \text{(I.3)}$$

with: $A = p_c^2\ (\cos^2\Theta - 1) - m_c^2$

$$B = p_c \cos\Theta\ \ (m_\Sigma^2 + m_c^2 - m_n^2)$$

$$C = \tfrac{1}{4}\ [\ (m_\Sigma^2 + m_c^2 - m_n^2)^2 - m_\Sigma^2\ \ (p_c^2 + m_c^2)\ ]$$

and where (see figure I.1):

p_c is the momentum of the charged decay particle, Θ the angle between the Σ and the charged decay particle,

m_Σ , m_c, m_n the masses of the Σ, the charged decay particle and the neutral decay particle respectively.

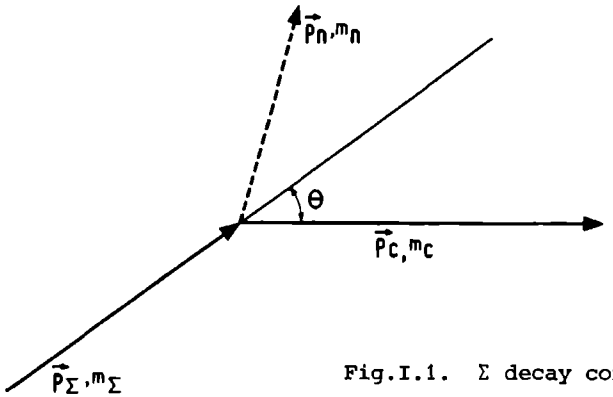

Fig.I.1. Σ decay configuration in the lab system.

This equation has in general 2 physical (i.e. $p_\Sigma > 0$) solutions. These solutions are then 'improved' by applying a correction for the curvature of the kink-track, thus far considered to be straight. The correction on the azimuthal angle of the kink-track is given by:

$$\Delta\varphi = \arcsin\left(\frac{0.3\ H\ L}{2\ p_\Sigma}\right) \qquad \text{(I.4)}$$

where H is the magnetic field strength and L is the length of the kink-track (see figure I.2).
With this correction on φ and thus on Θ (figure I.1), one then calculates a new value for p_Σ using (I.3) and then again a new $\Delta\varphi$. After a few steps p_Σ changes by less than 1 MeV/c and the iteration is stopped.

Due to measurement errors (especially on the decay point) it may happen, that the discriminant of (I.3) is negative and hence no real solution exists. This is because the measured

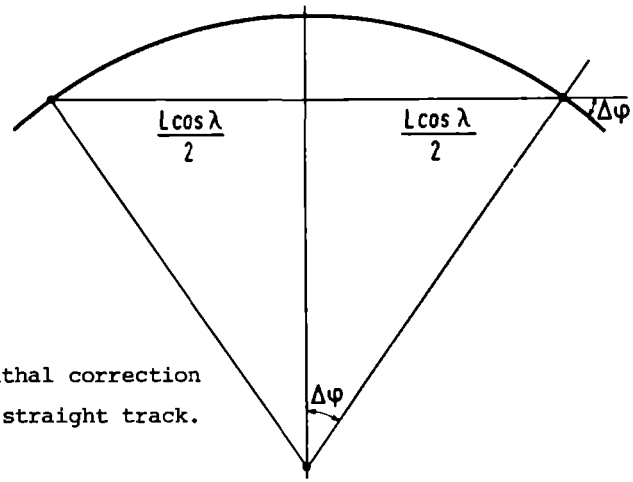

Fig.I.2. Azimuthal correction on a straight track.

transverse momentum p^T of the decay particle is larger than the centre-of-mass momentum p^* for that particular hypothesis. It is clear that this is mostly the case when the CMS decay angle θ^* with respect to the line of flight of the Σ (figure I.3) is near 90 degrees. A recovery procedure in GRIND then changes, within certain limits, the values of the measured quantities such that p^T becomes smaller then p^* (see for example the thesis of A.J. de Groot [Gr75]).

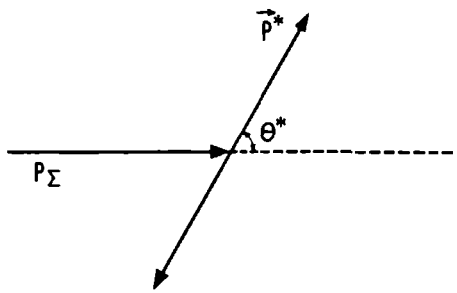

Fig.I.3. Centre-of-mass decay configuration of the Σ.

In figure I.4 we show distributions of the CMS decay cosine $\cos \theta^*$ of Σ-decays: (a) for a sample of decays where a physical solution was possible without going into the recovery procedure, (b) for the decays where a recovery was needed to find a solution, and (c) for the total sample. It is clearly seen, that the recovery is a necessary procedure to prevent a loss of events around $\cos \theta^* = 0$.

I.3. Event selection; solution of ambiguities.

In the outputscan stage the results of the fitting programme are compared with the picture of the event [Os74]. First the quality of the measurement is checked. If it is below certain pre-set standards, the event is remeasured. If the momentum of a secondary track is unmeasurable because of an interaction of that particle close to the production vertex, the event is rejected from the sample. The final results are corrected for such rejected events (see chapter II).

In many cases there is more than one hypothesis kinematically possible in GRIND. Then the following criteria are applied to reduce the number of ambiguities:

1) The calculated bubble density of the tracks has to be in agreement with the observed bubble density.

2) 4-C fits are preferred over fits with lesser constraints, since studies with Monte Carlo generated events have shown that it is very unlikely that a 1-C event simulates a fit with 4 constraints.

3) The χ^2 probability of the production vertex fit has to be greater than 0.01 in case of a 4-C fit and greater than 0.05 for a 1-C fit.

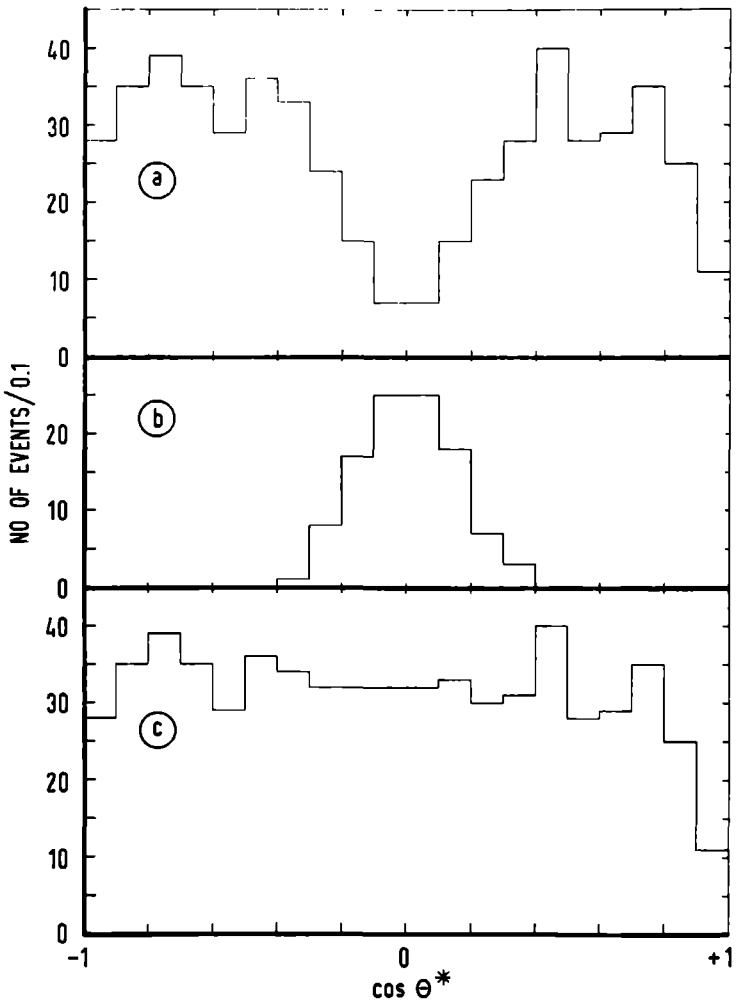

Fig. I.4. Centre-of-mass decay angular distributions of Σ: (a) for decays having a physical solution, (b) for decays where a recovery procedure was needed, (c) for the total sample.

4) For hypotheses in the same constraint class, one discards all fits having a confidence level 5 times smaller than the most probable one.

5) To choose between a 1-C fit and its corresponding 0-C solution, various criteria have been applied. In Amsterdam and Nijmegen the 1-C fit was preferred if:

$$MM^2 - n.\ (\Delta MM^2) \leq m_o^2$$

where MM^2 is the square of the missing mass, ΔMM^2 is the error on MM^2, m_o is the mass of the neutral particle in the 1-C fit and n a constant (equals 2 for Amsterdam events; equals 1 for Nijmegen events (*)). In C.E.R.N. one has always chosen the 1-C solution, if present.

If, after applying the above criteria, 3 or more acceptable solutions remain or no hypothesis is left, the event is rejected. A correction for the rejected events is applied to the cross section (cf. chapter II).

For the channels being used in this analysis of $\Sigma(1660)$ (cf. introduction), we present in tables I.1-3 and I.5 the ambiguities, remaining after the application of the above criteria. The 'internal' ambiguities in the channels $\Sigma^+\pi^+\pi^-\pi^-$, $\Sigma^-\pi^-\pi^+\pi^+$ and $\Sigma^+\pi^-\pi^o$ are the results of the possible proton and π-meson decay mode of Σ^+ and of the two possible solutions for the momentum of the $\Sigma^\pm$ when the curvature of the track cannot be measured.

(*) For the Nijmegen choice of n, we find that approximately 50% of the 1-C events with a χ^2 probability below 0.3 are selected as 0-C events. In the analysis we have therefore required the χ^2 probability for the Nijmegen 1-C events to be greater than 0.3.

From an inspection of tables I.1 and I.2 one sees that for the 4-C channels $\Sigma^{\pm}\pi^{\mp}\pi^{+}\pi^{-}$ the ambiguity level is low ($\lesssim$ 2%). One does not introduce a large bias by using both hypotheses from ambiguous events, but each with a weight ½.

Table I.3 however shows that there is a large ambiguity level in the $\Sigma^{+}\pi^{-}\pi^{o}$ channel. In the ambiguous reactions (4) - (10) one has either three strange particles in the final state or a final state with K^{+} and Ξ^{o}. The cross sections for these reactions are small compared to that for $\Sigma^{+}\pi^{-}\pi^{o}$. They are typically of the order of 10 - 20 μb or less [Br72] (*), while that for $\Sigma^{+}\pi^{-}\pi^{o}$ is of the order of 200 μb. In table I.4 we give rough upper limits for the number of events expected in the topology 210+ for each of these final states. These limits are obtained from the numbers of events in these final states with visible K^{o} or Λ decay and taking into account the probability of K^{+}-decay inside the chamber volume. From these numbers it seems justified to ignore the 'external' ambiguities with the reactions (4)-(10) (**). To resolve the remaining ambiguities $\Sigma^{+}\pi^{-}\pi^{o}/\Sigma^{+}\pi^{-}\pi^{o}$ and $\Sigma^{+}\pi^{-}\pi^{o}/\Sigma^{+}\pi^{-}$ (mm), we proceeded as follows [Ga74]: The 'internal' ambiguity $\Sigma^{+} \to \pi^{+}$ and $\Sigma^{+} \to p$ was resolved in favour of the hypothesis with the higher χ^{2} probability (mostly in favour of $\Sigma^{+} \to p$). In the case of a $\Sigma^{+} \to \pi^{+}/\Sigma^{+} \to \pi^{+}$ ambiguity, the solution having the smallest

---

(*) The cross section for $K^{-}p \to K^{+}K^{-}\Lambda$ is somewhat larger (64 ± 3 μb [Ga76]).

(**) Possible systematic errors are taken into account in the error quoted for the $\Sigma^{+}\pi^{-}\pi^{o}$ channel cross section (cf. chapter II).

Table I.1. Ambiguities for Events with Hypothesis $\Sigma^+\pi^+\pi^-\pi^-$.

$\Sigma^+\pi^+\pi^-\pi^-$	no. of hypotheses
uniques	7359
$\Sigma^+\pi^+\pi^-\pi^-$	128
$\Sigma^+K^+K^-\pi^-$	2
$K^+p\ K^-K^-$	2
Total	7491

Table I.2. Ambiguities for Events with Hypothesis $\Sigma^-\pi^-\pi^+\pi^+$.

$\Sigma^-\pi^-\pi^+\pi^+$	no. of hypotheses
uniques	6698
$\Sigma^-\pi^-\pi^+\pi^+$	40
$\Sigma^-K^-\pi^+K^+$	2
$K^-\pi^-p\ \pi^+$	21
$K^-K^-p\ K^+$	1
Total	6762

Table I.3. Ambiguities for Events with Hypothesis $\Sigma^+\pi^-\pi^o$.

$\Sigma^+\pi^-\pi^o$	no. of hypotheses
(1) uniques	4977
(2) $\Sigma^+\pi^-\pi^o$	3032
(3) $\Sigma^+\pi^-$ (mm)	569
(4) $\Sigma^+K^-K^o$	1536
(5) Σ^+K^- (mm)	5
(6) $K^+\pi^-\Xi^o$	1662
(7) $K^+\pi^-$ (mm)	1614
(8) $K^+K^-\Lambda$	859
(9) $K^+K^-\Sigma^o$	464
(10) K^+K^- (mm)	71
Total	14789

Table I.4. Expected number of events in the 210+ topology for final states being ambiguous with $\Sigma^+\pi^-\pi^o$.

final state	expected number of events	actual number of ambiguities
$\Sigma^+K^-K^o$	< 260	1536
$K^+\pi^-\Xi^o$	< 130	1662
$K^+\pi^-$ (mm)	∿ 75	1614
$K^+K^-\Lambda$	∿ 50	859
$K^+K^-\Sigma^o$	∿ 35	464
K^+K^- (mm)	< 150	71

Table I.5. Ambiguities for Events with Hypothesis $\Lambda\pi^+\pi^-$, $\Sigma^o\pi^+\pi^-$, $\Lambda\pi^+\pi^-\pi^o$ or $p\pi^-\bar{K}^o$.

	$\Lambda\pi^+\pi^-$	$\Sigma^o\pi^+\pi^-$	$\Lambda\pi^+\pi^-\pi^o$	$p\pi^-\bar{K}^o$
uniques	5921	2878	25941	15298
$p\ \pi^-\bar{K}^o$	11	13		
$p\ \pi^-\bar{K}^o\pi^o$		11	81	
$p\ \pi^-\bar{K}^o$ (mm)		1	29	
$\pi^+\pi^-\bar{K}^o n$			178	
$\pi^+\pi^-\bar{K}^o$ (mm)			77	
$\pi^+\pi^-\Lambda$		5493		11
$\pi^+\pi^-\Sigma^o$	5493		1463	13
$\pi^+\pi^-\Lambda\ \pi^o$		1463		
$\pi^+\pi^-\Lambda$ (mm)		3		
$\pi^+\pi^-\Lambda\ \gamma$		393	6643	
$K^+K^-\Lambda$		120		
$K^+K^-\Sigma^o$		4	359	
$K^+K^-\Lambda\ \pi^o$		1	210	
$K^+K^-\Lambda\ \gamma$			12	
$K^+\pi^-\Lambda\ \bar{K}^o$			51	
$K^+\pi^-\Xi^o$		2	324	
$\pi^+K^-\Lambda\ \bar{K}^o$			77	
$K^+\pi^-\bar{K}^o\Lambda$			1	
$\pi^+K^-\bar{K}^o\Lambda$			4	
$K^+K^-\bar{K}^o n$			1	
$\pi^+\pi^-K^o\Xi^o$			7	
Total	11425	10382	35458	15322

momentum for the Σ^+ was preferred; this preference was based on the fact that this choice makes the Σ^+ decay angular distribution more isotropic. We were not able to find a comparable criterion in the case of the ambiguity $\Sigma^+ \to p/\Sigma^+ \to p$. The main problem here is the loss of Σ's having a small projected decay angle, which is more severe than in the case of $\Sigma^+ \to \pi^+ n$ decays. In view of this problem we have ignored in the further analysis all $\Sigma^+\pi^-\pi^o$ events where the Σ^+ decays into $p\pi^o$. Finally, the ambiguity between the $\Sigma^+\pi^-\pi^o$ and $\Sigma^+\pi^-$ (mm) was resolved by accepting the $\Sigma^+\pi^-\pi^o$ fit. The adequacy of this choice was checked by inspection of the missing mass distribution for these events.

From table I.5 one can see that the $p\pi^-\bar{K}^o$ final state does not present any special problem in terms of ambiguity solution. Here too, the ambiguity level is so low, that there is little or no bias in using all hypotheses and giving the ambiguous events a weight ½.

However the problems in the final states $\Lambda\pi^+\pi^-$, $\Sigma^o\pi^+\pi^-$ and $\Lambda\pi^+\pi^-\pi^o$ are more serious. The solution of this type of ambiguity has been described in detail by W.J. Metzger [Me75]. The method is based on the fact that the electromagnetic decay of Σ^o into Λ and γ is a parity conserving $J = ½$ decay and therefore that all Σ^o decay angular distributions are isotropic. In order to assign an event to the $\Sigma^o\pi^+\pi^-$ final state one defines a probability ratio:

$$W_{\Sigma^o} = \frac{P(\Sigma^o)}{P(\Sigma^o) + P(\text{amb.})}$$

where $P(\Sigma^o)$ is the χ^2 probability of the Σ^o fit and P(amb.) the χ^2 probability of the ambiguous fit. The selection criteria arrived at for $\Sigma^o\pi^+\pi^-$, are then:

a) the χ^2 probability of the $\Sigma^o\pi^+\pi^-$ fit has to be greater than 0.05.

b) a unique Σ^o fit is always taken.

c) if there is an ambiguity with $\Lambda\pi^+\pi^-$, $\Sigma^o\pi^+\pi^-$ is selected only if $W_{\Sigma o} > 0.99$.

d) if $\Sigma^o\pi^+\pi^-$ is ambiguous with $\Lambda\pi^+\pi^-\pi^o$, the $\Sigma^o\pi^+\pi^-$ assignment is accepted only if $W_{\Sigma o} > 0.1667$.

e) if the number of constraints of any other ambiguous fit is greater than 2, the event is never accepted as $\Sigma^o\pi^+\pi^-$.

f) the $\Sigma^o\pi^+\pi^-$ fit is always selected if the number of constraints of the ambiguous fit is $\leq$ 2.

These selection criteria were derived empirically by varying the constants involved and choosing those constants yielding the best isotropic Σ^o decay distributions.

The selection of a $\Lambda\pi^+\pi^-\pi^o$ fit was done according to the following criteria:

a) the χ^2 probability of the $\Lambda\pi^+\pi^-\pi^o$ fit had to be greater than 0.05.

b) if the $\Lambda\pi^+\pi^-\pi^o$ fit is ambiguous with a 4-C fit, it is never selected.

c) if the $\Lambda\pi^+\pi^-\pi^o$ fit is ambiguous with a $\Sigma^o\pi^+\pi^-$ fit, it is selected only if $\frac{P(\Lambda\pi^o)}{P(\Lambda\pi^o) + P(\Sigma^o)}$ is greater than 0.83.

d) if the number of constraints of any other ambiguous fit is $\leq$ 2, the event is accepted as $\Lambda\pi^+\pi^-\pi^o$.

Application of all these selections results in the final samples of events used in the analysis. The numbers of events in each final state are shown in table I.6.

Table I.6. Number of Events Entering the Analysis.

Final State	Number of Events
$\Sigma^+\pi^+\pi^-\pi^-$	7491
$\Sigma^-\pi^-\pi^+\pi^+$	6762
$\Sigma^+\pi^-\pi^o$	7649
$\Lambda\ \pi^+\pi^-$	11923
$\Sigma^o\pi^+\pi^-$	4460
$\Lambda\ \pi^+\pi^-\pi^o$	33153
$p\ \pi^-\bar{K}^o$	15322

CHAPTER II.

MICROBARN EQUIVALENTS AND CHANNEL CROSS SECTIONS.

In this chapter we determine the cross sections for the channels in which we study the production of $\Sigma(1660)$. A channel is defined by the identities of the stable and/or semi-stable particles (i.e., particles which do not decay strongly) in the final state and thus includes all intermediate states through which the final state is produced. Generally speaking, the final state particles live long enough to travel a measurable distance in the bubble chamber (exceptions are the π^o-meson and the Σ^o-hyperon, having lifetimes of 0.83×10^{-16} and $< 1.0 \times 10^{-14}$ seconds respectively). A list of the channels studied can be found in table II.1.

If we specify the final state not by its ultimate particles, but by the particles which are directly produced, we refer to a reaction. The subject of this thesis is the reaction $\bar{K}\, p \rightarrow \Sigma^+(1660)\pi^-$. The cross section for this reaction will be given in chapter IV.

II.1. Calculation of cross sections.

Cross sections can be calculated from the (corrected) number of events belonging to the particular class of events considered, together with the microbarn equivalent of the experiment. The microbarn equivalent (μb-equiv.) is defined as the total number of events divided by the total cross section in microbarns (1 μb = 10^{-30} cm^2), i.e. the number of events corresponding to a cross section of 1 μb. The microbarn equivalent is topology dependent because the corrections to be

applied to events which either have not been measured or have not entered the final sample for other reasons is topology dependent. We therefore present microbarn equivalents for all the topologies involved in this study.

The cross section is defined as the proportionality constant between the number of interactions per second N_i/T and the product of the number of particles in the target and the incoming flux. The cross section σ_i for a particular class of events may then be written as:

$$\sigma_i = \frac{N_i}{\rho L}$$

where: N_i = the (corrected) number of events in class i;

ρ = proton density in the liquid hydrogen;

L = total incident track length (in our case of the incident kaons).

This method is based on the counting of the number of beam tracks; the counted raw number has to be corrected for pion and muon contamination [Ti74] .

However we prefer and present the results of cross section calculations based on the counting of τ decays (i.e. $K^- \rightarrow \pi^-\pi^-\pi^+$). The number of τ decays is 0.937 times the number of 3-prongs scanned(*). The cross section σ_i can also be written as [Pi67]:

$$\sigma_i = \frac{N_i/TV}{\rho_b \rho_t v_{lab}}$$

(*) The remaining 3-prong decays result from the decays $K^- \rightarrow \pi^-\pi^0$, $K^- \rightarrow \mu^-\pi^0\nu$, $K^- \rightarrow e^-\pi^0\nu$ and $K^- \rightarrow \pi^-\pi^0\pi^0$ with the π^0 decaying into $e^+e^-\gamma$.

where T and V are the time interval and the interaction volume under consideration respectively, ρ_b and ρ_t the volume densities (in the laboratory system) of the beam and target particles respectively and v_{lab} the velocity of the incoming particles in the lab system. The number of τ decays per second N_τ/T is proportional to the number of incident K^- particles. The proportionality constant is the decay rate Γ, which is the inverse of the mean lifetime of the K^-. Γ is given by [Pi67] :

$$\Gamma = \frac{N_\tau / TV}{\rho_b'}$$

where ρ_b' is the density of the beam particles in their rest system.

Combining the above expressions for σ_i and Γ yields:

$$\sigma_i = \frac{N_i}{N_\tau} \cdot \left[\frac{A\ f_\tau\ m_{K^-}}{N\ \rho\ ct_{K^-}\ P_{K^-} c}\right] = \frac{N_i}{N_\tau} \cdot \frac{1.976}{P_{K^-}\ c}\ [\text{mbarn}] \qquad \text{(II.1)}$$

where: $A = 1.007$ [amu] : atomic mass of the proton

$f_\tau = 0.0559$: branching ratio for τ decay

$m_{K^-} = 0.4937$ [GeV] : mass of the beam particle

$N = 6.0220 \times 10^{23}$ [mole^{-1}] : Avogadro's number

$\rho = 0.063$ [gr/cm^3] : density of liquid hydrogen

$ct_{K^-} = 370.9$ [cm] : mean decay length of K^-

P_{K^-} : beam momentum in GeV/c

II.2. Corrections to numbers of classified events.

In order to obtain cross sections, we have to apply the following corrections to the raw numbers of classified events:

(a) a correction factor for scanning efficiency.

(b) a correction for events rejected during processing in

the different phases of the data reduction chain, because:

- event is unmeasurable
- event is lost in bookkeeping
- event is not properly measured, even after 2 measurements
- event has more than 2 kinematical solutions, even after the application of the selection criteria mentioned in section I.3.

(c) a correction factor for the cut-off applied on the χ^2 probability (section I.3).

(d) a weight factor for events with neutral particles decaying outside the fiducial volume or decaying too close to the production vertex to be seen.

(e) a weight factor for the loss of low momentum decay particles.

(f) a weight factor for the loss of events with charged particles having a small decay angle in the lab.

For the corrections (a), (b) and (c) one calculates directly an average value; the weight factors (d), (e) and (f) are calculated on an event by event basis and averaged afterwards.

II.2.1. The length-dependent weight.

Events with a strange particle decaying close to the production vertex or close to the boundary of the illuminated region of the bubble chamber are frequently lost. We therefore require the projected decay length of these particles to have a minimum value (L'_{min}) and the decay to lie within an appropriate decay fiducial volume. For V^o's we have used L'_{min} = 0.2 cm and for charged decays L'_{min} = 0.4 cm.

The accepted events are weighted by the inverse of the probability for decaying with a projected decay length $\geq L'_{min}$ and a spatial decay length $\leq L_{pot}$; L_{pot} is the so-called potential path, i.e. the distance from the interaction point to the boundary of the decay fiducial volume in the direction of the line-of-flight of the decaying particle.
The weight W_L is thus given by:

$$W_L = \frac{1}{e^{-L'_{min}/\lambda'} - e^{-L_{pot}/\lambda}} \qquad \text{(II.2)}$$

where $\lambda = \beta\gamma c\tau$ and λ' are the mean free path and the projected mean free path respectively (β and γ are the usual Lorentz-factors and τ the mean lifetime of the decaying particle). The average values of W_L for the channels involved are given in table II.1.

Table II.1. Average Weights for Length Cuts.

Channel	W_L
$\Sigma^+ \pi^+ \pi^- \pi^-$	1.16
$\Sigma^- \pi^- \pi^+ \pi^+$	1.08
$\Sigma^+ \pi^- \pi^o$	1.20
$\Lambda \pi^+ \pi^-$	1.10
$\Sigma^o \pi^+ \pi^-$	1.10
$\Lambda \pi^+ \pi^- \pi^o$	1.10
$p \pi^- \bar{K}^o$	1.08

II.2.2. Weight for loss of small momentum Σ-decay secondaries.

If the momentum of the charged decay particle from the decay of $\Sigma^{\pm}$ is small, the track left in the bubble chamber is short and will often not be seen during the scanning of the pictures. This results in a loss of events for which the decay angle cosine of that particle in the rest system of the $\Sigma^{\pm}$ is near -1.0. A minimum momentum p_{min} imposes a limit on this cosine, given by:

$$\cos \Theta^{*} \geqslant \frac{E_{min} - \gamma E^{*}}{\gamma \beta p^{*}} \qquad \text{(II.3)}$$

with : $\beta = \frac{p_{\Sigma}}{E_{\Sigma}}$ and $\gamma = \frac{1}{\sqrt{1-\beta^{2}}}$

and where:

$E_{min} = \sqrt{p_{min}^{2} + m^{2}}$ is the minimum energy;

p^{*}, E^{*} are the momentum and energy of the decay particle in the $\Sigma^{\pm}$ rest system;

p_{Σ}, E_{Σ} are the momentum and energy of $\Sigma^{\pm}$ in the lab system.

As explained in the next section, this limit on cos Θ^{*} must be combined with limits resulting from small decay angle losses. The values used for p_{min} were 50 MeV/c for $\pi^{\pm}$ and 200 MeV/c for protons.

II.2.3. Weight for loss of small angle Σ-decays(*).

If the projected decay angle is small, it is likely that the decay of a charged particle is not recognised on the scanning table. In order to correct for these lost events, one has to determine the detection efficiency ε of the decays as a function of their projected decay angle ψ . Possible efficiency functions are shown in figure II.1. One usually assumes one of these forms and determines the parameters involved (ψ_c,ψ'_c,ε_1) from the data sample. An assumption common to all hypotheses is that events having a projected decay angle $\psi \geqslant \psi_c$ are all seen.

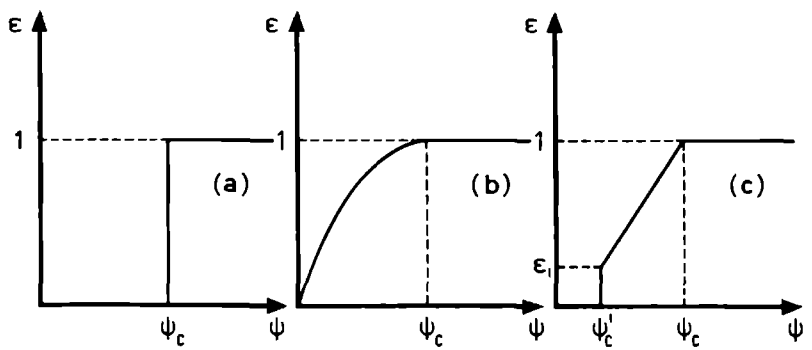

Fig. II.1. Some possible detection efficiency functions for the decay of charged particles.

(*) This subject has previously been discussed in many reports, such as [A167] , [He69] , [Ma71] , [Ma76] , [Me72] , [To74] and [Va72] .

Using an efficiency function of the type shown in figure II.1a has the disadvantage of removing all of the events which were actually seen but with a projected decay angle smaller than ψ_c. In figure II.2 we plotted the projected decay angle versus the projected Σ momentum for a sample of Monte-Carlo generated $\Sigma^+ \rightarrow p\pi^o$ decays. As can be seen, one removes most of the sample for any reasonable value of the cut-off angle. As a result we prefer an efficiency curve as in figure II.1b, where we can assume some analytic form for the efficiency function between 0 and ψ_c (e.g. an ellips or a parabola).

The angle ψ_c is determined as follows: for a given Σ momentum p_Σ, one calculates the projected decay angle distribution, based on the isotropy of the decay in the Σ rest frame and an assumed efficiency function $\epsilon(\psi; \psi_c)$. Integration over ψ then results in a weight factor for the particular Σ momentum considered. Using the experimental momentum distribution of the Σ's, weighted by these (ψ_c dependent) factors, one can now calculate the expected ψ distribution averaged over p_Σ. Comparison of the experimental ψ distribution and the distributions expected for various values of ψ_c is then used to choose the 'best value' for ψ_c. The details of these calculations were described by Toet [To74] . The forms of the efficiency functions and the cut-off angles ψ_c giving the best fits to the experimental projected decay angular distribution for each channel and Σ decay mode considered, are given in table II.2.

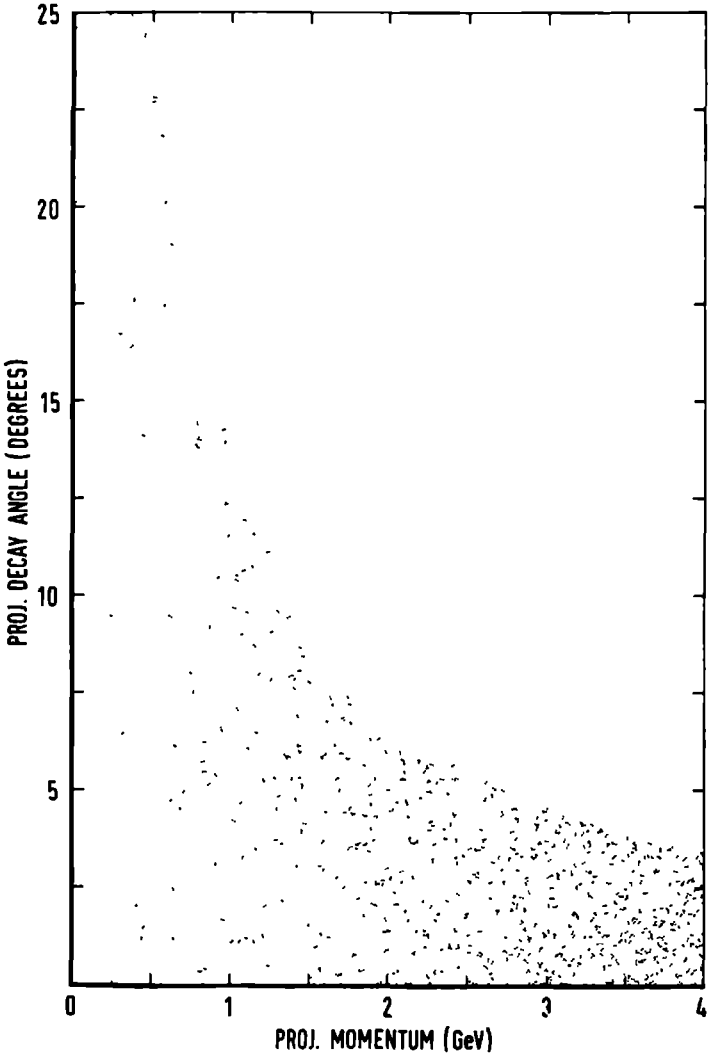

Fig.II.2. Projected decay angle versus the projected Σ momentum of Monte-Carlo generated $\Sigma^+ \rightarrow p\pi^o$ decays.

Table II.2. Results for the Projected Decay Angle Efficiency Function.

Decay mode	Channel	Functional form	Cut-off angle ψ_c (in degrees)	Average weight W_ψ
$\Sigma^+ \to \pi^+ n$	$\Sigma^+\pi^-\pi^+\pi^-$	ellipse	15 ± 2	1.12
$\Sigma^+ \to p\,\pi^o$	$\Sigma^+\pi^-\pi^+\pi^-$	parabola	11 ± 2	1.77
$\Sigma^- \to \pi^- n$	$\Sigma^-\pi^+\pi^+\pi^-$	ellipse	13 ± 2	1.07
$\Sigma^+ \to \pi^+ n$	$\Sigma^+\pi^o\pi^-$	ellipse	16 ± 2	1.13

Given the above parameterisation of the projected decay angle efficiency function $\varepsilon(\psi)$, we are now able to calculate the probability P for detecting an event with a Σ of momentum p_Σ and dip angle λ_Σ. Since the decay of the Σ is isotropic in any reference frame chosen independently of the polarisation vector of the Σ, this probability P is given by:

$$P(p_\Sigma,\lambda_\Sigma) = \frac{\int_0^{2\pi}\int_{-1}^{+1} \varepsilon \, d\cos\Theta^* \, d\phi^*}{\int_0^{2\pi}\int_{-1}^{+1} d\cos\Theta^* \, d\phi^*} = \frac{\int_0^{2\pi}\int_{-1}^{+1} \varepsilon \, d\cos\Theta^* \, d\phi^*}{4\pi} \qquad \text{(II.4)}$$

As a reference frame we choose a frame having a z-axis in the Σ-direction and an x-axis perpendicular to the plane formed by the Σ-direction and the optical axis of the bubble chamber. This reference system satisfies the condition mentioned above, because the polarisation vector is always perpendicular to the Σ production plane.

However ε, being a function of ψ, has to be expressed in terms of ϕ^* and $\cos\Theta^*$. For any given λ_Σ, ϕ^* and ψ we can calculate the corresponding lab decay angle Θ and the two centre-of-mass decay angles Θ_1^* and Θ_2^* ($\Theta_1^* > \Theta_2^*$). The latter two angles are the solutions of a quadratic equation in $\cos\Theta^*$:

$$\cos^2\Theta^*\left(1 + \frac{1}{\gamma^2 tg^2\Theta}\right) + \frac{2\beta E^*}{p^*}\cos\Theta^* + \frac{\beta^2 E^{*2}}{p^{*2}} - \frac{1}{\gamma^2 tg^2\Theta} = 0$$

where $\beta = \frac{p_\Sigma}{E_\Sigma}$ and $\gamma = \frac{1}{\sqrt{1-\beta^2}}$ are the factors used in the Lorentz transformation from the lab system to the rest system of the Σ. p_Σ (E_Σ) and p^* (E^*) are the momentum (total energy) of the Σ in the lab system and the rest system respectively.

The fraction P of decays with a lab decay angle Θ' greater than Θ, is then given by:

$$P(\Theta' \geq \Theta) = \frac{\cos\Theta_1^* - \cos\Theta_2^*}{2} \qquad \text{(II.5)}$$

These $\cos\Theta^*$ limits are now combined with the $\cos\Theta^*$ limit from the minimum momentum cut for the decay particle (eq. II.3) to give the minimum $\cos\Theta^*$ interval.

Approximating the efficiency function ε by a step function ε_i ($i = 0,1,\ldots N$; $i = 0$ at $\psi = 0$ and $i = N$ at $\psi = \psi_c$) we then obtain for the integral over $\cos\Theta^*$ in (II.4):

$$\int_{-1}^{+1} \varepsilon \, d\cos\Theta^* = 2\varepsilon_o + \sum_{i=1}^{N} (\varepsilon_i - \varepsilon_{i-1}) - (\cos\Theta_{1i}^* - \cos\Theta_{2i}^*)$$

Note that Θ_{1i}^* and Θ_{2i}^* are still functions of ϕ^*, ψ and λ_Σ. The weights thus obtained are in principle a function of the Σ momentum p_Σ and its dip angle λ_Σ. It has been pointed out however, that to a good approximation, the weight only depends

on the projected Σ momentum $p_{\Sigma\|} = p_\Sigma \cos \lambda_\Sigma$ [Al67, Va72] . This is illustrated in figure II.3, where we have plotted decay angle weights versus the projected Σ momentum for artificially generated Σ^+ decays. The Σ momentum of these events was chosen between 0.2 and 4.0 GeV/c and their dip angle varied between 0 and 80 degrees.

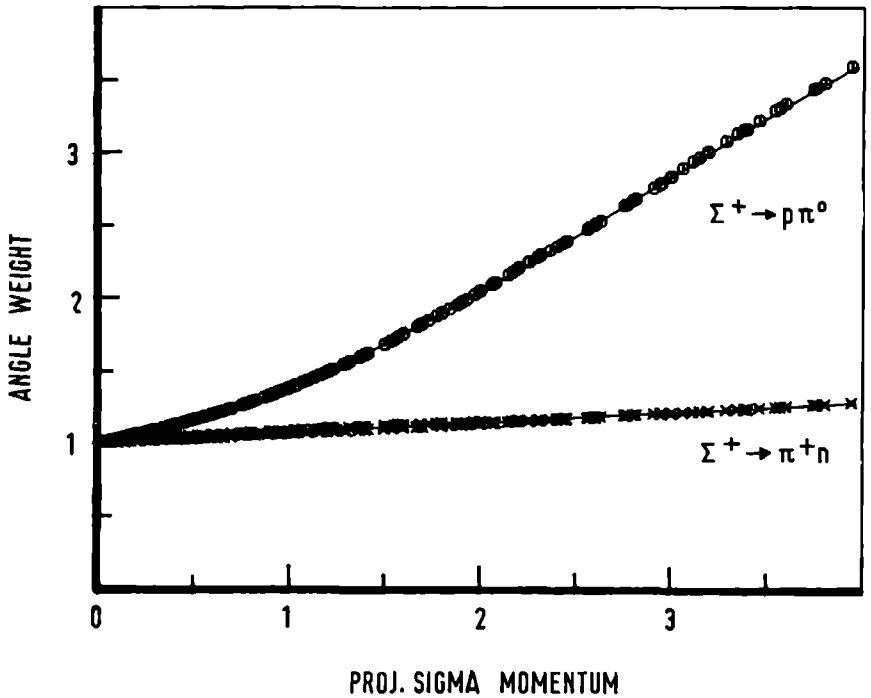

Fig.II.3. Decay angle weight vs. projected Σ momentum for generated Σ^+ decays. The Σ's have a momentum between 0.2 and 4.0 GeV/c and a dip angle running from 0 to 80 degrees.

II.3. Results.

After the discussion of the corrections, we are now able to give the microbarn equivalents for the various topologies as well as the channel cross sections.

From eq. II.1 one immediately sees that the microbarn equivalent for the events in topology i is

$$(\mu b - \text{equiv.})^i = \frac{c\, P_{K^-}}{1976} \cdot \frac{N_\tau \cdot N^i_{DST}}{N^i_{DST} + N^i_{Reject}}$$

where N^i_{DST} is the actual number of events on the DST for topology i and N^i_{Reject} the number of events from topology i that are not on the DST for reasons mentioned in section II.2. The numbers used in the calculations of the microbarn equivalents are presented in table II.3. A scanning efficiency correction of 0.98 is included in the final result for the microbarn equivalents.

The cross sections for the channels used in this study, together with the applied correction factors, are given in table II.4. The correction factor W_P is due to the minimum χ^2 probability cut (see section I.3). W_D is the decay weight, i.e. W_L for V^o's and the combined weight for minimum length, escape probability, minimum momentum of decay particle and small decay angle loss in the case of Σ decays. The column 'unseen decays' gives the correction factor for the unseen decay modes of $\bar{K}^o$ and Λ and where applicable the unused $\Sigma^+ \to p\, \pi^o$ decay mode.

The values for the cross sections (last column of table II.4) were obtained by using the numbers of events as given in the table, except for the $\Sigma^+\pi^o\pi^-$ and $\Lambda\pi^+\pi^o\pi^-$ channels. Being 1-C channels, one expects a certain amount of contamination

from the corresponding multi-neutral channels. We have estimated the cross sections for the 1-C channels by using only events for which $MM^2 \leq m_{\pi^o}^2$. Since the mass resolution is poor in the $\Sigma^+\pi^o\pi^-$ channel, we expect a non-negligible contamination even in this low MM^2 region. The estimate for the number of $\Sigma^+\pi^o\pi^-$ events was therefore derived from the MM^2 distribution of the combined $\Sigma^+\pi^o\pi^-$ and $\Sigma^+\pi^-$ (mm) samples.

The errors given on the cross sections include both statistical and systematic errors. The latter have been estimated from the spread in the cross sections for the various runs.

In figure II.4 we compare our values for the cross sections with the values obtained at various neighbouring energies [Br72] . There is good agreement between our values and the values expected from a smooth behaviour of the cross section with energy.

Table II.3. μb - Equivalents for the Topologies 201, 210+, 410+ and 410-.

number of τ decays : 34632 average beam momentum : 4.18 GeV/c				
Topology	N_{DST}	N_{Reject}	Fraction of events on DST	μb - equiv.
201	216636	25471	0.895	64.2 ± 0.4
210+	28094 (*)	4559 (*)	0.860 (*)	56.1 ± 0.5 (*)
410+	28263	6281	0.818	58.7 ± 0.5
410-	35231	6772	0.839	60.2 ± 0.5

(*) Because of a loss in the scanning of the topology 210+ for the 1971 run in Nijmegen, we have not used that part of the sample for further analysis. The corresponding number of τ decays is 31458.

Table II.4. Channel Cross Sections.

Channel	# events	W_P	W_D	Unseen decays	σ (μb)
$\Sigma^+\pi^-\pi^+\pi^-$	7300	1.01	1.58	--	200 ± 30
$\Sigma^-\pi^+\pi^+\pi^-$	6666	1.01	1.19	-	130 ± 20
$\Sigma^o\pi^+\pi^-$	4402	1.05	1.10	1.56	125 ± 15
$\Sigma^+\pi^o\pi^-$	7171	1.08	1.35	2.07	210 ± 45
$\Lambda\ \pi^+\pi^-$	11335	1.01	1.10	1.56	310 ± 30
$p\ \bar{K}^o\pi^-$	15248	1.01	1.08	2.91	750 ± 50
$\Lambda\ \pi^+\pi^o\pi^-$	32963	1.12	1.10	1.56	810 ± 80

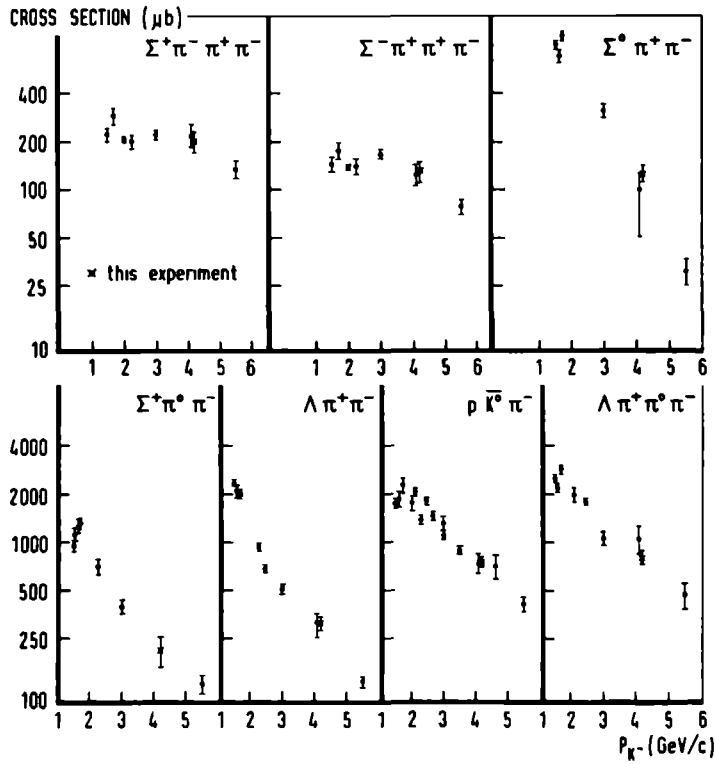

Fig.II.4. Channel cross sections at various beam momenta. Data points are taken from [Br72].

CHAPTER III.

H I S T O R Y O F T H E Σ(1660) R E S O N A N C E.

In this chapter we give a short historical review of the discovery of the Σ(1660) resonance, a baryon with a mass of approximately 1660 MeV, and discuss the major contributions establishing its existence and properties. In doing so it will be unavoidable to refer to analysis techniques and variables, the definitions of which we defer to subsequent chapters.

Two types of experiments can be performed to detect a resonance. They are called formation and production experiments respectively. In a formation experiment the resonance is formed by giving the beam particle a momentum such that the total energy of the colliding beam and target particles in their centre-of-mass system equals the mass of the resonance. The Σ(1660) can be formed in the following way:

$$\begin{array}{l} K^- + p \rightarrow \Sigma(1660) \\ \qquad\quad \big\lfloor\!\!\rightarrow \Sigma^+ + \pi^- \end{array} \qquad \text{(III.1)}$$

if the laboratory momentum of the K^- meson is about 715 MeV/c. A diagram representing this reaction is shown in figure III.1. Such a resonance may be detected by looking for enhancements in the channel cross sections as a function of the incident beam momentum. A spin-parity assignment of the resonant state can, at least in principle, be obtained from a partial wave decomposition of the scattering amplitude and the energy dependence of these partial wave amplitudes.

In a production experiment the resonance is produced together with one or more other particles. Here the condition

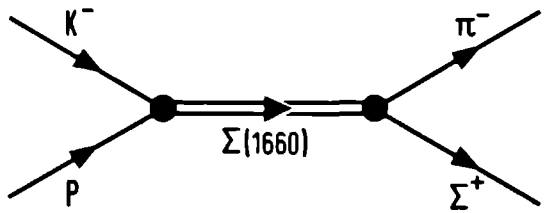

Fig. III.1. Schematic representation of the formation of a $\Sigma(1660)$, decaying into Σ^+ and π^-.

on the beam momentum is less severe; it only has to be above the threshold for the final state considered. In practice, to avoid phase space limitations, the beam momentum must be well above threshold in order for the resonance to be produced with a significant cross section. The $\Sigma(1660)$ resonance may be produced in a K^-p experiment in the following reaction:

$$K^- + p \rightarrow \Sigma^+(1660) + \pi^- \quad \text{(III.2)}$$
$$\hookrightarrow \Sigma^o + \pi^+$$

for any K^- momentum $\gtrsim$ 1.0 GeV/c. Figure III.2 shows the diagram for this reaction.
In a production experiment resonances are seen as enhancements in effective mass distributions or as bands in a Dalitz plot (details on the procedures used to extract these resonances will be presented in chapter IV).

The first indications for the existence of the $\Sigma(1660)$ resonance were found by Alexander et al. [Al62] and by Bastien et al. [Ba62] . Alexander et al. possibly observed the

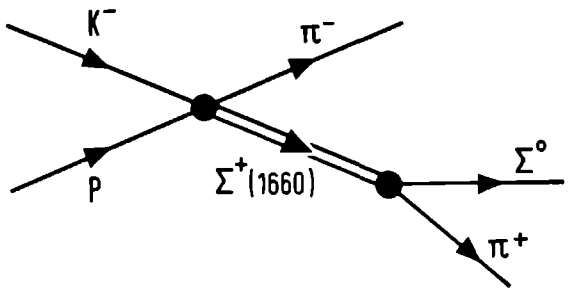

Fig.III.2. Schematic representation of the production of a $\Sigma^+(1660)$ (together with a π^-) decaying into Σ^0 and π^+.

production of $\Sigma(1660)$ in π^-p interactions between 1.89 and 2.24 GeV/c. An enhancement of events was seen in the $(\Lambda\pi)^+$ and $(\Sigma\pi)^+$ effective mass distributions at a mass of $\sim$ 1685 MeV and with a width of $\sim$ 50 MeV. Bastien et al., in a formation experiment of the type $K^-p \to \Sigma\pi$, saw an enhancement in the cross section at p_{K^-} = 760 MeV/c, corresponding to a mass for the K^-p system of 1680 MeV. In a later updated version of their results [Ba63] the authors quoted 3/2 as a plausible spin assignment. This was based on the absence of $\cos^3\theta$ terms and the presence of a large $\cos^2\theta$ term in the angular distribution of the Σ with respect to the incoming K^- meson direction.

Additional evidence came from a production experiment performed by Alvarez et al. [Al63] . They studied, at an incoming K^- momentum of 1.51 GeV/c, the same three- and four-body final states as in our experiment. The statistical signi-

ficance of their experiment was 5 events/μb. Enhancements in the effective mass spectra of $\Lambda\pi$, $\Sigma\pi$, $\Lambda\pi\pi$ and $\Sigma\pi\pi$ were seen and the relative decay rates quoted for these modes were 1.2:1.0: 0.67:0.67(*). An upper limit of 0.17 was given for the relative rate of decay into $\bar{K}N$. The errors on these numbers were of the order of 25%.

Since then many conflicting results have been published for the branching ratios and the spin-parity of the $\Sigma(1660)$. We will not list these contributions separately, because they were at a low statistical level and higher statistics data are now available. The early experimental situation (as of 1966) has been reviewed by M. Ferro-Luzzi [Fe66] .

From a sample of approximately 300 events, Eberhard et al. [Eb67] determined the spin and the parity of the $\Sigma(1660)$ produced between 2.45 and 2.7 GeV/c opposite a π^- in K^-p interactions. An Adair analysis was used to extract the information on the spin, while the parity determination was based on a Dalitz-Miller analysis [Da61] ; this analysis was done for the $\Sigma\pi\pi$ decay mode of the $\Sigma(1660)$. These authors found

---

(*) From an analysis in the momentum range 1.0 - 1.75 GeV/c, including the data of Alvarez et al., Huwe [Hu69] obtained (0.15 ± 0.07) for the $\Lambda\pi/\Sigma\pi$ branching ratio.

that the $\Sigma\pi\pi$ decay mode consisted mainly of $\Sigma(1660)\rightarrow\Lambda(1405)\pi^+$. The Adair analysis yielded 3/2 as the most likely spin; the χ^2 probability ratios for the spin 1/2 and spin 5/2 hypotheses were found to be ≤ 0.002. Assuming spin 3/2 and making dynamical assumptions about the states in which the $(\Sigma\pi\pi)^+$ system decays and about the backgrounds present in the decay, they derived a negative parity for the $\Sigma(1660)$.

Support for the above result came from J. Button-Shafer [Bu68] in a study of the $\Sigma^o\pi^\pm$ decay mode of the $\Sigma(1660)$ produced in K^-p interactions at 1.7 and 2.1 GeV/c. The spin and parity hypotheses $3/2^+$ and $3/2^-$ were tested by a maximum likelihood fit to the decay chain $\Sigma^+(1660) \rightarrow \Sigma^o\pi^+$; $\Sigma^o \rightarrow \Lambda\gamma$; $\Lambda \rightarrow p\pi^o$, using a Byers-Fenster parameterisation(*). Here too, the result found was a preference for negative parity in the sub-sample of 'backward' produced events at 1.7 GeV/c. For the 'forward' events and for the events at 2.1 GeV/c (both 'backward' and 'forward'), the results were inconclusive. No higher spin hypotheses were tried.

Results on branching ratios were also given. The ratio $\Lambda\pi^+/\Sigma^o\pi^+$ was found to be (0.22 ± 0.11), in agreement with Huwe [Hu69]. Including the data on $\Sigma\pi\pi$ of Eberhard et al. [Eb67], the ratios $\Sigma\pi/\text{total} = 0.51 \pm 0.10$ and $\Lambda(1405)\pi/\text{total} = 0.49 \pm 0.10$ were found.

The next important paper (in chronological order) is the one from the CERN-Heidelberg-Saclay collaboration [Ar69-2], studying the $\Sigma(1660)$ resonance in a formation experiment.

(*) See chapter V for details of this method.

A $\Sigma(1660)$ enhancement was found in the D13 partial wave of the K^-p system, thus directly establishing a $J^P = 3/2^-$. For the branching fractions the following results were found: (0.09 ± 0.02) into $\bar{K}N$, (0.49 ± 0.11) into $\Sigma\pi$ and $\sim$ 0.28 into $\Lambda\pi$. For the decay into $\Lambda(1405)\pi$ an upper limit of 0.06 was given. This last branching fraction was in strong disagreement with the results of the production experiments, where, as stated above, the decay into $\Lambda(1405)\pi$ was found to be one of the dominant modes [Bu68] .

Eberhard et al. [Eb69] were the first to present evidence for the production of two $\Sigma(1660)$ resonances in a 12.8 events/μb K^-p experiment at beam momenta of 2.58, 2.61 and 2.70 GeV/c. They looked at the effective mass distribution for the particle combinations $(\Sigma^{\pm}\pi^{\mp}\pi^+)$, $(\Sigma^o\pi^+)$ and $(\Sigma^+\pi^o)$ in three c.m.s. production angular regions. In the most forward angular region they observed a pronounced peak in the $(\Sigma\pi\pi)^+$ effective mass distribution and almost no signal in the $(\Sigma\pi)^+$ distribution. However in the least forward angular region, the signal in the $(\Sigma\pi\pi)^+$ mass distribution was much less evident, while a very significant peak was seen in the $(\Sigma\pi)^+$ mass distribution. Thus the $\Sigma\pi\pi/\Sigma\pi$ branching ratio varied significantly with the production angle, only the ratio in the least forward angular region being consistent with the result of the CHS collaboration. The authors explain this effect as being due to the existence of two $\Sigma(1660)$ resonances: one resonance decaying mainly into $\Sigma\pi\pi$ and very peripherally produced; the second one, decaying into $\Sigma\pi$ and less peripherally produced.

A confirmation of the hypothesis, that there indeed exist

two $\Sigma(1660)$ resonances, came from Aguilar-Benitez et al. [Ag70] . They also studied the $\Sigma^{\pm}\pi^{\mp}\pi^{+}$ and $\Sigma^{o}\pi^{+}$ decay modes of $\Sigma(1660)$, produced in $K^{-}p$ interactions, now at 3.9 and 4.6 GeV/c. A clear peak was seen at 1660 MeV both in the $\Sigma^{o}\pi^{+}$ and in the $(\Sigma\pi\pi)^{+}$ effective mass spectrum. Requiring the $(\Sigma\pi)^{o}$ mass to lie in the $\Lambda(1405)$ mass region, they observed again a very significant peak in the $(\Sigma\pi\pi)^{+}$ mass plot. From the numbers of events in the peaks of both the $(\Sigma\pi\pi)^{+}$ and $\Lambda(1405)\pi^{+}$ distributions they concluded that the decay of the $\Sigma(1660)$ into $\Sigma\pi\pi$ was consistent with 100% decay into $\Lambda(1405)\pi$. Next they studied the dependence of the effects on the c.m.s. production angle cosine $\cos\theta^{*}$. The production angle region was divided into two parts. No $\Sigma(1660)$ signal was observed in the $\Lambda(1405)\pi^{+}$ effective mass distribution for the events having $\cos\theta^{*} < 0.7$, while there was about equal production of $\Sigma(1660)$ in the two angular regions for the $\Sigma^{o}\pi^{+}$ decay mode. The two decay modes also showed a different energy dependent behaviour, the ratio of the production cross sections

$$\frac{\sigma(\Sigma(1660) \rightarrow \Sigma^{o}\pi^{+})}{\sigma(\Sigma(1660) \rightarrow \Sigma^{+}\pi^{-}\pi^{+})}$$

being 1.3 at 3.9 GeV/c and 3.6 at 4.6 GeV/c.

Supporting evidence for the two $\Sigma(1660)$ hypothesis came from an early analysis of this experiment [NA71] and subsequently from Clark and Radojicic [Cl73] , who analysed the production of $\Sigma^{+}(1660)$ by $K^{-}p$ collisions at 3.13 and 3.3 GeV/c.

Recent results for the same reactions at 2.87 GeV/c K^{-} momentum, published by the Brandeis-Maryland-Syracuse-Tufts

collaboration [Ap74] are partially in disagreement with the branching ratio results from [Eb69], [Ag70] and [C173]. The latter authors did not observe this large difference in the branching ratio $\Sigma\pi\pi/\Sigma\pi$ for the different production angular regions. However, they again concluded that two $\Sigma(1660)$ resonances were being produced, now based on the difference in the slope of the differential cross section and the difference in the ratio of 'forward' to total events for the $\Sigma\pi\pi$ and $\Sigma\pi$ decay modes.

Apsell et al. also performed a spin-parity analysis of the $\Sigma(1660)$. An Adair analysis and a Byers-Fenster analysis of the $\Lambda(1405)\pi^+$ decay could only rule out spin 1/2; it did not give any discrimination between spin 3/2 and spin 5/2. Concerning the parity, no results could be determined in a model-independent way. Only after making the following dynamical assumptions: (a) the production of $\Sigma(1660)$ proceeds mainly via K^* exchange, (b) the Stodolsky-Sakurai model of vector meson exchange [St63, St64] is valid, and (c) the spin of $\Sigma(1660)$ is 3/2, strong evidence for negative parity was obtained. However, no checks on the validity of the assumptions (a) and (b) were reported, while the data showed only a slight preference for assumption (c).

To conclude: up to now, almost all the production experiments observe the branching ratio $\Sigma\pi\pi/\Sigma\pi$ of the $\Sigma(1660)$ to vary with the production angle, the ratio in the non-forward region being compatible with results from formation experiments [Ar69-2]. These experimental facts support the existence of two $\Sigma(1660)$ resonances with different branching fractions and different production properties.

CHAPTER IV.

PRODUCTION CHARACTERISTICS OF $\Sigma(1660)$ IN THE REACTION $K^- p \to \Sigma^+(1660)\, \pi^-$

We investigate the production of $\Sigma(1660)$ in the following channels:

$$K^- p \to \Sigma^+ \pi^- \pi^+ \pi^- \qquad \text{(IV.1)}$$

$$K^- p \to \Sigma^- \pi^+ \pi^+ \pi^- \qquad \text{(IV.2)}$$

$$K^- p \to \Sigma^0 \pi^+ \pi^- \qquad \text{(IV.3)}$$

$$K^- p \to \Sigma^+ \pi^0 \pi^- \qquad \text{(IV.4)}$$

$$K^- p \to \Lambda\, \pi^+ \pi^- \qquad \text{(IV.5)}$$

$$K^- p \to p\, \bar{K}^0 \pi^- \qquad \text{(IV.6)}$$

$$K^- p \to \Lambda\, \pi^+ \pi^0 \pi^- \qquad \text{(IV.7)}$$

The numbers of events in each of these final states have been given in table II.4.

In this chapter we first describe the fit-procedures used for the estimation of the amount of resonance production. Next we present the results of these fits. We then study the dependence of the resonance production on the production angle. Finally we calculate the cross sections for $\Sigma(1660)$ production in the different channels.

IV.1. Methods used for the estimation of resonance production.

The production of a resonance can be observed through enhancements in effective mass distributions. The effective mass squared of a system of N particles is defined as:

$$M^2(m_1, \ldots, m_N) = \Big(\sum_{i=1}^{N} E_i\Big)^2 - \Big(\sum_{i=1}^{N} \vec{p}_i\Big)^2 \qquad \text{(IV.8)}$$

where m_i, E_i and $\vec{p}_i$ are the mass, total energy and momentum, respectively, of particle i.

Because of the short lifetime of the resonance, the distribution of the effective mass of the particles into which the resonance decays will show a spread around the central mass M_o of the resonance. In practice a resonance will be observed as a peak or bump around the central mass of the resonance on top of a more or less smoothly varying background. This background can be due either to pure phase or to the 'reflection' of resonances produced in the other particle combination.

In the study of resonance production in a three-body final state a + b → 1 + 2 + 3, it is very useful to examine the Dalitz plot [Da53] . The Dalitz plot is a two-dimensional plot in which each event is represented by a point, the coordinates of that point being the value of the square of the effective mass of the particles 1,2 vs. the value of the square of the effective mass of the particles 2,3 (or 1,3). Conservation of momentum and energy restricts the points to lie within a closed boundary. If no resonances are produced and no other correlations in the final state are present, i.e. if the events are produced purely following phase space, the distribution of the points in the Dalitz plot should be uniform. If however resonances are produced, one will see bands in the Dalitz plot which are more populated than the rest of the diagram. These bands will be centred around the mass of the resonance. As an example we show the Dalitz plot for the channel $K^-p \rightarrow \Lambda\pi^+\pi^-$ in figure IV.1. Clear resonance production is seen in the $\Lambda\pi^+$ combination around 1.9 GeV^2 and in the $\Lambda\pi^-$ combination at about the same value. More details on this

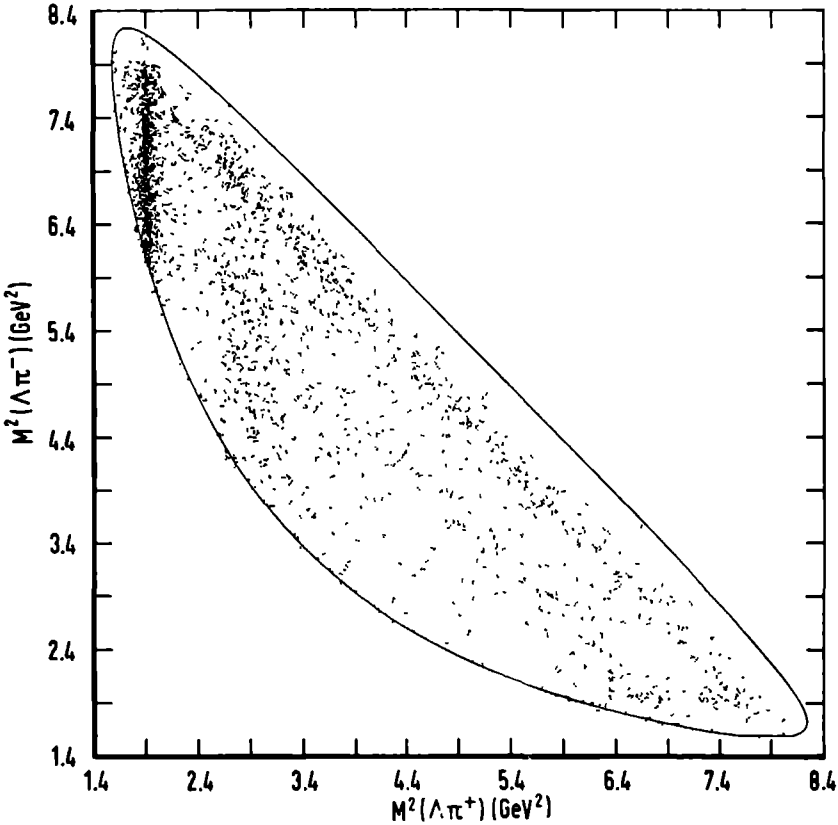

Fig.IV.1. Dalitz plot for the channel $K^-p \to \Lambda\pi^+\pi^-$.

final state are presented in section IV.2.3.

If there is a resonance produced, decaying into particles 1 and 2, the distribution of the effective mass of particles 1 and 2 can be parameterised by a so-called Breit-Wigner function:

$$BW(M_{12}) = \frac{C}{(M_{12} - M_o)^2 + \Gamma_o^2/4}$$

where C is a normalisation constant and M_o, Γ_o the central mass and width of the resonance respectively.

An estimate of the amount of resonance production and of the resonance parameters M_o and Γ_o can be obtained by a maximum likelihood fit to an incoherent sum of a Breit-Wigner distribution and a background distribution. The parameterisation of the background can take many forms, varying from a pure phase space distribution to an arbitrary n-th order polynomial distribution.

To fit a one-dimensional effective mass distribution the programme STK [St74] was used. The logarithm of the likelihood function $\mathcal{L}$ to be maximised was given by:

$$\ln\mathcal{L} = \sum_{j=1}^{N} W_j \ln \left[\sum_i f_i \, BW_i(M_{oi}, \Gamma_{oi}; M_j) + f_B \, BG(M_j) \right] \qquad \text{(IV.9a)}$$

where N is the total number of events used in the fit, W_j the weight factor, f_i the fraction of resonance i production, f_B the fraction of background events, BG a second order polynomial and M_j the effective mass of the particle combination under consideration; j labels the events and i the different Breit-Wigner channels. The parameters varied in the fit are the quantities f_i, the coefficients in the polynomial and (unless otherwise stated) M_{oi}, Γ_{oi}.

The programme OPTIME [Eb72] has been used to perform a fit, using the extended maximum likelihood method [Or58] , in the multidimensional space of the effective masses. Fitting in this space has the advantage of taking all 'reflections'

directly into account. The likelihood function used is now defined as:

$$\ln\mathcal{L} = \sum_{j=1}^{N} W_j \ln y_j - Y \qquad \text{(IV.9b)}$$

with:

$$y_j = \sum_i f_i \, BW_i(M_{oi}, \Gamma_{oi}; M_j) + f_p$$

Y is the integral of the distribution function y over the entire phase space; f_i and f_p are parameters in the fit which are related to the fraction of events in resonance i and the fraction of pure phase space events respectively.

IV.2. Resonance production.

IV.2.1. The channels $K^-p \to \Sigma^+\pi^-\pi^+\pi^-$ *and* $K^-p \to \Sigma^-\pi^+\pi^+\pi^-$.

The distributions of the effective mass $M(\pi^+\pi^-)$ from the channels (IV.1) and (IV.2) are shown in figure IV.2a and IV.2b respectively. One observes ρ production at a mass of $\sim$ 0.77 GeV.

The $\Sigma^+\pi^-$ and $\Sigma^-\pi^+$ mass distributions (figure IV.2c and IV.2d respectively) show very significant peaks corresponding to the production of Σ(1385) and Λ(1405) at a mass around 1.4 GeV, Λ(1520) and Y*(1670). Also the latter signal may contain several resonances with different isospin.

The distributions of $M(\Sigma^+\pi^-\pi^+)$ from channel (IV.1) and $M(\Sigma^-\pi^+\pi^+)$ from channel (IV.2) are given in figure IV.2e and IV.2f respectively. Clear enhancements are seen in the mass region around 1.66 GeV. The background level in this region, although somewhat larger in the $\Sigma^-\pi^+\pi^+\pi^-$ channel than in the $\Sigma^+\pi^-\pi^+\pi^-$ channel, is generally quite small. Part of this background is due to Λ(1520) production in the $\Sigma^{\pm}\pi^{\mp}$ combination,

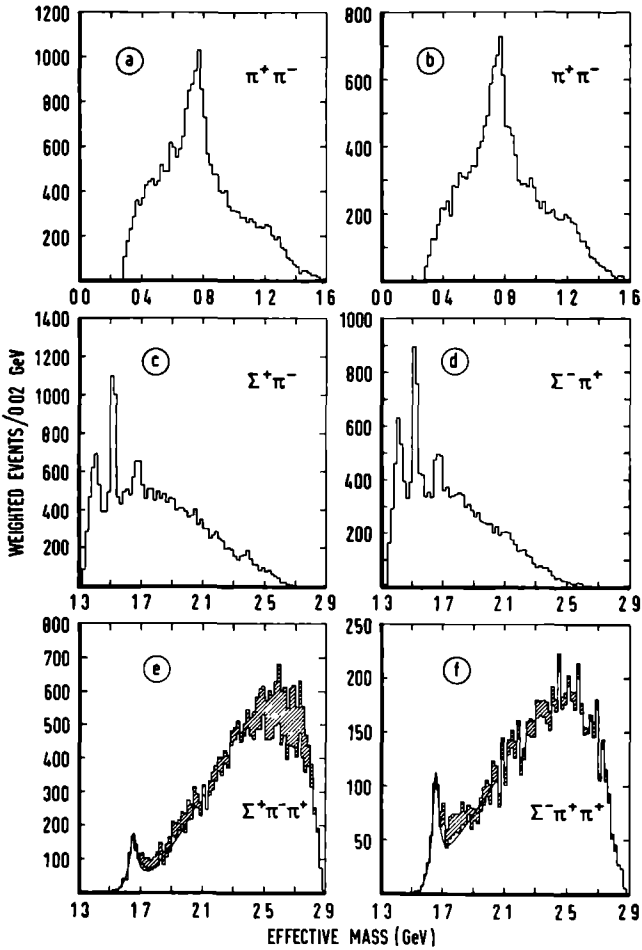

Fig.IV.2. Effective mass distributions: (a) $M(\pi^+\pi^-)$, (c) $M(\Sigma^+\pi^-)$, (e) $M(\Sigma^+\pi^-\pi^+)$ from the channel $K^-p \to \Sigma^+\pi^-\pi^+\pi^-$; (b) $M(\pi^+\pi^-)$, (d) $M(\Sigma^-\pi^+)$, (f) $M(\Sigma^-\pi^+\pi^+)$ from the channel $K^-p \to \Sigma^-\pi^+\pi^+\pi^-$. The shaded areas correspond to events in the $\Lambda(1520)$ - see text.

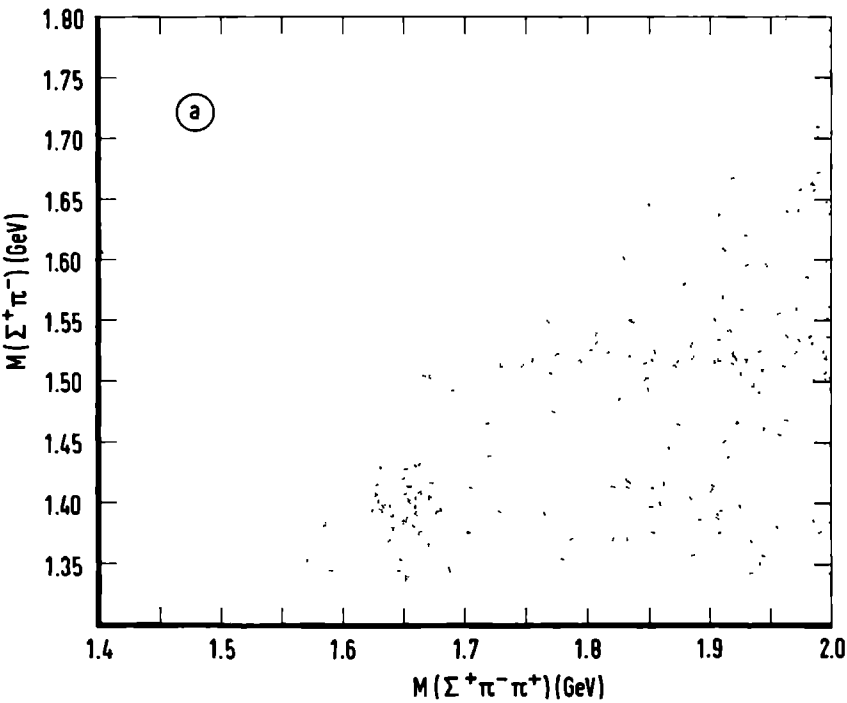

Fig.IV.3. (a) $M(\Sigma^+\pi^-)$ versus $M(\Sigma^+\pi^-\pi^+)$ for the channel $K^-p \to \Sigma^+\pi^-\pi^+\pi^-$; (b) $M(\Sigma^-\pi^+)$ versus $M(\Sigma^-\pi^+\pi^+)$ for the channel $K^-p \to \Sigma^-\pi^+\pi^+\pi^-$.

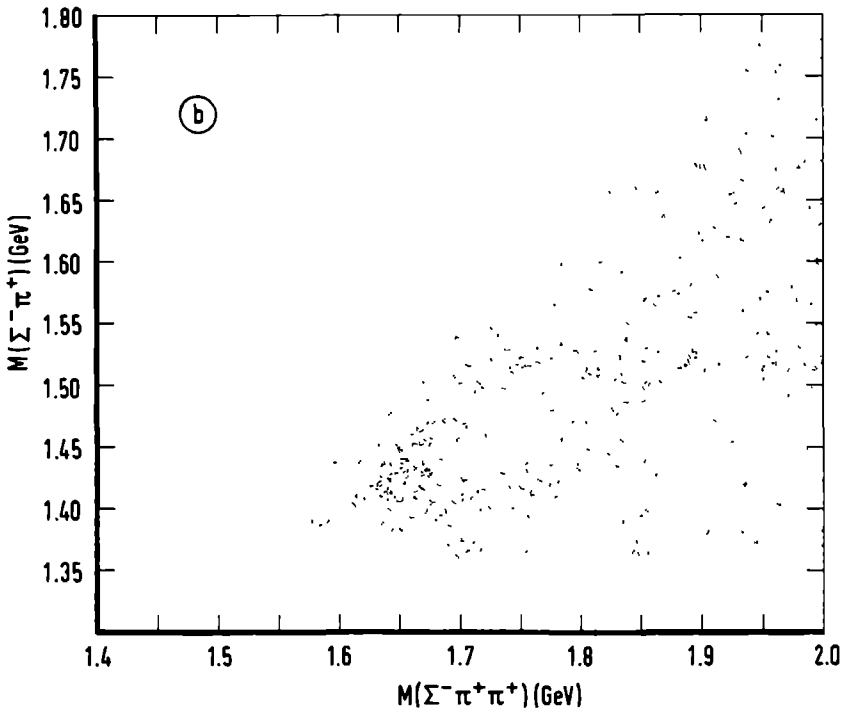

Fig. IV.3. Continued.

reflecting itself in the $M(\Sigma^{\pm}\pi^{\mp}\pi^{+})$ distribution. The threshold for this reflection into the $M(\Sigma\pi\pi)$ distribution is around 1.66 GeV (see figure IV.3). In the $\Sigma^{+}\pi^{-}\pi^{+}\pi^{-}$ channel we have eliminated this reflection by simply removing the events in the $\Lambda(1520)$ region (i.e. events having $1.50 < M(\Sigma^{+}\pi^{-}) < 1.54$ GeV). In the $\Sigma^{-}\pi^{+}\pi^{+}\pi^{-}$ channel however, both $\Sigma^{-}\pi^{+}$ mass combinations can be in the $\Lambda(1520)$ region. To remove the $\Lambda(1520)$ reflection in this final state, we have given the events in the $\Lambda(1520)$ region a statistical weight ½. This results in the non-shaded distributions of figure IV.2e and IV.2f.

In figure IV.4 we now plot the effective mass of $\Sigma^{+}\pi^{-}$ for events having $M(\Sigma^{+}\pi^{-}\pi^{+})$ in the $\Sigma(1660)$ region:

$$1.60 < M(\Sigma^{+}\pi^{-}\pi^{+}) < 1.72 \text{ GeV}$$

The shaded distribution is corrected for the background under the $\Sigma(1660)$. This correction is based on a linear background and is derived from interpolation between the numbers of events seen to the left and right of the resonance. The side mass bands used were (1.54 - 1.60) GeV and (1.72 - 1.78) GeV. The curve represents a phase space distribution. It is clear that the experimental distribution is <u>not</u> a phase space distribution but almost entirely $\Lambda(1405)$ (*).

We now require the $\Sigma^{\pm}\pi^{\mp}$ effective mass to lie in the $\Lambda(1405)$ mass region:

$$1.34 < M(\Sigma^{\pm}\pi^{\mp}) < 1.44 \text{ GeV}$$

The $M(\Sigma^{\pm}\pi^{\mp}\pi^{+})$ distributions of the events meeting the above $\Lambda(1405)$ mass selection are shown in figures IV.5a and IV.5b.

(*) The amount of $\Sigma(1385)\pi$ decay in these channels is very small (see section VI.1).

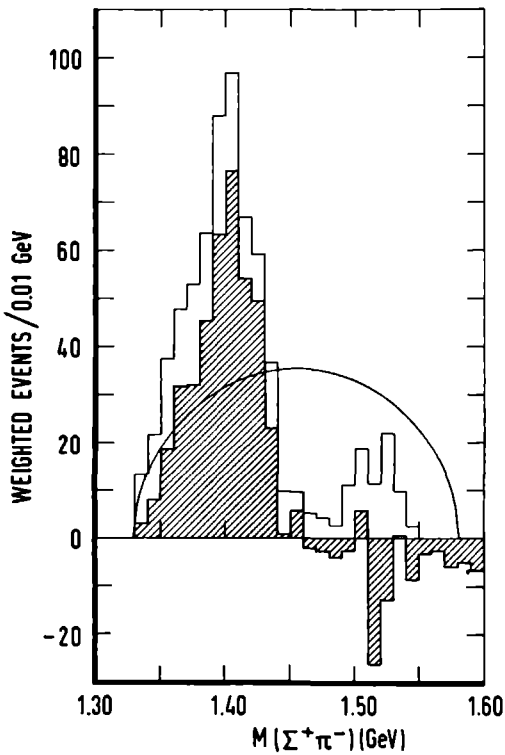

Fig. IV.4. Effective mass distribution $M(\Sigma^+\pi^-)$ for the channel $K^-p \to \Sigma^+\pi^-\pi^+\pi^-$ for events in the $\Sigma(1660)$ mass region: $1.60 < M(\Sigma^+\pi^-\pi^+) < 1.72$ GeV. The shaded distribution is obtained after subtraction of the background under the $\Sigma(1660)$ - see text.

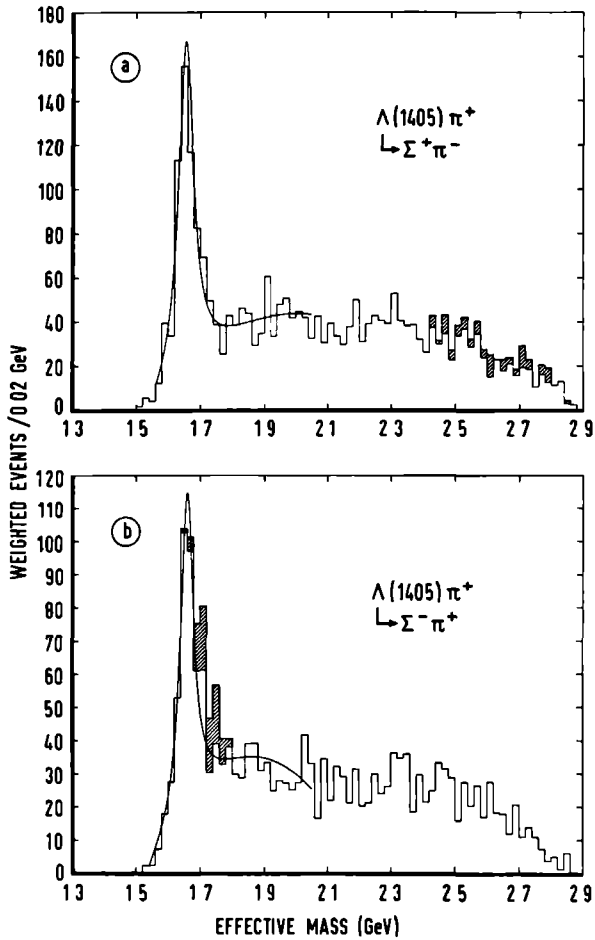

Fig. IV.5. Effective mass distributions: (a) $M(\Sigma^+\pi^-\pi^+)$ for the channel $K^-p \to \Sigma^+\pi^-\pi^+\pi^-$, where $1.34 < M(\Sigma^+\pi^-) < 1.44$ GeV and (b) $M(\Sigma^-\pi^+\pi^+)$ for the channel $K^-p \to \Sigma^-\pi^+\pi^+\pi^-$, where $1.34 < M(\Sigma^-\pi^+) < 1.44$ GeV. The shaded areas correspond to events in the $\Lambda(1520)$ - see text.

The non-shaded distributions are again obtained after the removal of the $\Lambda(1520)$ reflection. In both distributions we see pronounced signals at 1.66 GeV, which we attribute to the resonance $\Sigma(1660)$. The numbers of events in the $\Sigma(1660)$ peaks are not significantly different from those in figure IV.2e and IV.2f. The decay of $\Sigma(1660)$ into $\Sigma\pi\pi$ is thus consistent with being entirely $\Lambda(1405)\pi$.

We have performed maximum likelihood fits to the non-shaded $M(\Sigma\pi\pi)$ distributions of figures IV.2e, IV.2f, IV.5a and IV.5b. The fits were limited to the mass region below 2.05 GeV. The distribution function was parameterised as an incoherent sum of an s-wave Breit-Wigner function and a quadratic background term. From these fits we have obtained best values for the central value M_o, the width Γ_o and the number of events in the resonance. The results are given in table IV.1. The curves shown in the figures represent the results of these fits. We have done several fits to these mass spectra, with different parameterisations of the background and varying the mass regions considered. The errors in table IV.1. have been increased to reflect the variation observed between the results of these fits (the errors are typically increased by some 30%).

Table IV.1. Results of Fits to the Mass Distributions.

Decay Mode	M_o (MeV)	Γ_o (MeV)	Number of Events in the Resonance
$\Sigma^+\pi^-\pi^+$	1655 ± 3	57 ± 7	617 ± 50
$\Lambda(1405)\pi^+ \rightarrow \Sigma^+\pi^-\pi^+$	1655 ± 3	56 ± 7	586 ± 50
$\Sigma^-\pi^+\pi^+$	1659 ± 4	48 ± 7	315 ± 30
$\Lambda(1405)\pi^+ \rightarrow \Sigma^-\pi^+\pi^+$	1660 ± 4	48 ± 7	330 ± 30

The various values found for M_o and Γ_o are consistent. The fitted numbers of events for $\Sigma^+\pi^-\pi^+$ and $\Sigma^-\pi^+\pi^+$ agree with the numbers of events in these final states after the $\Lambda(1405)$ selection was included. It thus appears that the decay of $\Sigma^+(1660)$ into $(\Sigma\pi\pi)^+$ occurs entirely via $\Lambda(1405)\pi^+$. We return to this point in chapter VI, where we determine branching ratios for $\Sigma(1660)$.

However, there is one problem left: from isospin one expects equal numbers of $(\Sigma^+\pi^-)\pi^+$ and $(\Sigma^-\pi^+)\pi^+$ events, while experimentally this ratio is 1.8 ± 0.2. Similar values for this ratio have been obtained by other authors [Lo66,Eb67]. A part of this effect may be explained by a small difference in available phase space for the decays of $\Lambda(1405)$ into $\Sigma^+\pi^-$ and $\Sigma^-\pi^+$ respectively, caused by the $\Sigma^+ - \Sigma^-$ mass difference. Another possible cause is the interference between the two possible $\Lambda(1405)$ combinations in the decay chain $\Sigma^+(1660) \rightarrow \Lambda(1405)\pi^+ \rightarrow \Sigma^-\pi^+\pi^+$. The two $\Lambda(1405)$ bands overlap in the decay Dalitz plot(*) and must interfere because of Bose symmetry for the two identical pions (a further discussion of this interference effect will be presented in section V.5). However these two explanations together can not account for more than 5% of the effect. The largest part of the effect must therefore be due to other processes; the most likely candidate is an interference process between the $\Lambda(1405)\pi$ mode and a direct three-body $\Sigma\pi\pi$ mode.

(*) We do not have this difficulty with the two π^-'s in the $\Sigma^+\pi^-\pi^+\pi^-$ final state, since at our energy it is kinematically impossible for both $\Sigma^+\pi^-\pi^+$ mass combinations to lie below 2.05 GeV.

IV.2.2. The channels $K^-p \to \Sigma^0\pi^+\pi^-$ *and* $K^-p \to \Sigma^+\pi^0\pi^-$.

In figures IV.6a and IV.6b we present the effective mass distributions $M(\pi^+\pi^-)$ and $M(\Sigma^0\pi^-)$ from channel (IV.3). Clear peaks can be seen around 0.76 and 1.26 GeV in the $M(\pi^+\pi^-)$ distribution. These peaks correspond to production of the ρ^0 and f meson respectively. A small enhancement of events in the $(\Sigma^0\pi^-)$ mass distribution is visible around 1.66 GeV and may be attributed to production of $\Sigma^-(1660)$.

Our main interest lies in the $M(\Sigma^0\pi^+)$ distribution shown in figure IV.6c. In this distribution we observe a small peak at 1.39 GeV, corresponding to $\Sigma^+(1385)$ production, and a very significant peak at 1.66 GeV which is the result of strong $\Sigma^+(1660)$ production. There is also a small enhancement present at $\sim$ 1.46 GeV. A study of the decay angular distributions of the Σ^0 shows however, that there is a large contamination of $\Lambda\pi^+\pi^-$ events in this mass region due to the abundant production of $\Sigma^+(1385)$ in $\Lambda\pi^+$. Misidentification of about 3% of the events of channel (IV.5) (while having a negligible influence on the rest of the $M(\Sigma^0\pi^+)$ distribution) could account for this effect.

We have performed a maximum likelihood fit to an s-wave Breit-Wigner function plus a quadratic background in the $M(\Sigma^0\pi^+)$ region from 1.52 to 2.10 GeV. Results from this fit on the mass and width of the $\Sigma(1660)$ and the total number of events in the resonance are presented in table IV.2. The curve shown in figure IV.6c represents the result of this fit.

The effective mass distributions of all three two-particle combinations of the channel $K^-p \to \Sigma^+\pi^0\pi^-$ are shown in figures IV.7a, b, and c. As explained in section I.3, only events with Σ^+ decaying into $n\pi^+$ were used. One observes a

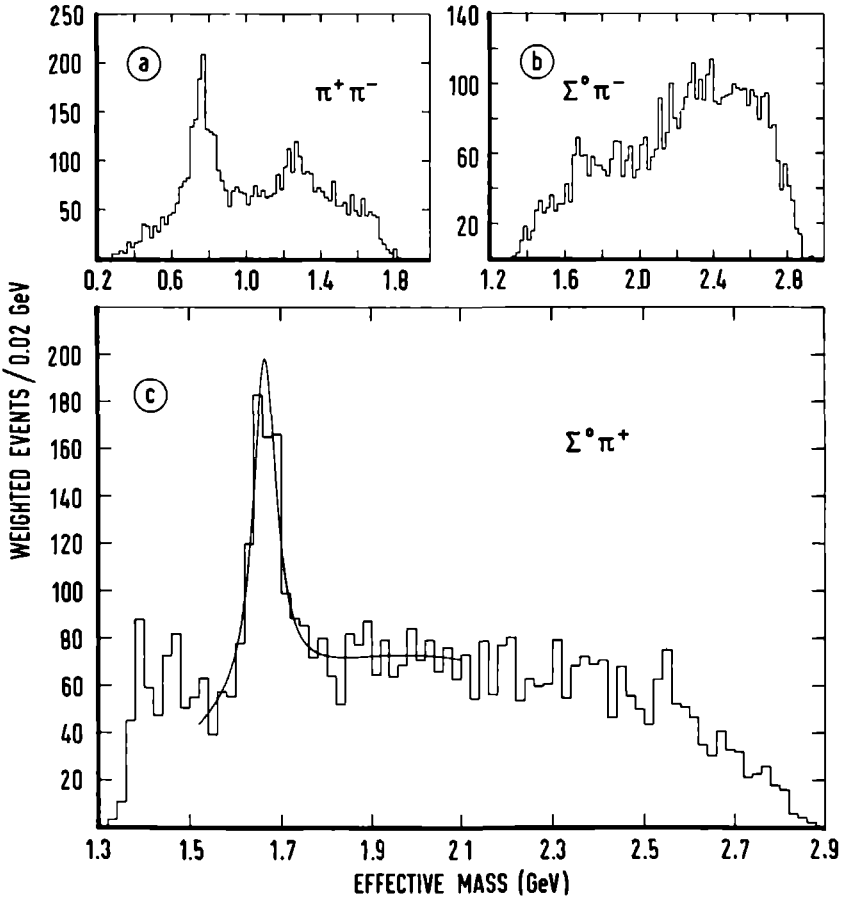

Fig. IV. 6. Effective mass distributions from the channel $K^-p \to \Sigma^o\pi^+\pi^-$: (a) $M(\pi^+\pi^-)$, (b) $M(\Sigma^o\pi^-)$ and (c) $M(\Sigma^o\pi^+)$.

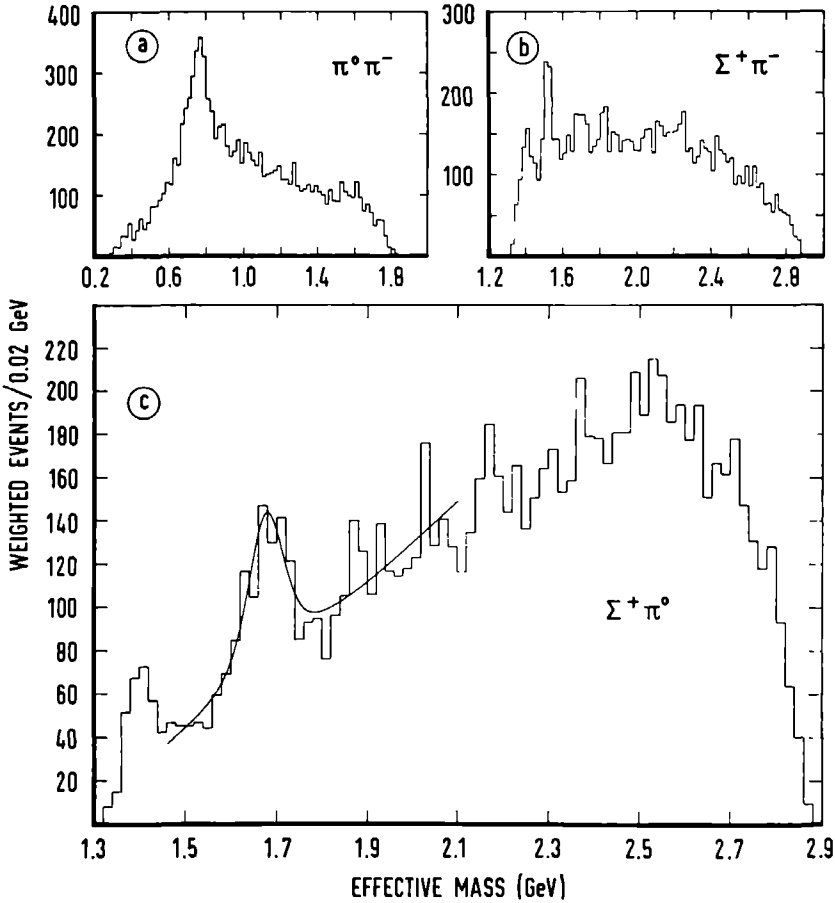

Fig. IV.7. Effective mass distributions from the channel $K^-p \to \Sigma^+\pi^0\pi^-$: (a) $M(\pi^+\pi^-)$, (b) $M(\Sigma^+\pi^-)$ and (c) $M(\Sigma^+\pi^0)$.

broad peak around 0.77 GeV in the $\pi^-\pi^o$ effective mass distribution, which is due to production of ρ^-. In the $M(\Sigma^+\pi^-)$ distribution one observes the production of $\Sigma(1385)/\Lambda(1405)$, $\Lambda(1520)$ and some Y^*'s around 1.66 GeV. Finally, the $\Sigma^+\pi^o$ effective mass plot shows that $\Sigma(1385)$ and also $\Sigma(1660)$ are produced. The width of the $\Sigma(1660)$ enhancement is larger than in the $M(\Sigma^o\pi^+)$ distribution; this is due to the poorer mass resolution in the $\Sigma^+\pi^o\pi^-$ final state. In the $\Sigma(1660)$ mass region (1.56 - 1.76) GeV the resolution is measured to be 55 MeV in the $\Sigma^+\pi^o\pi^-$ final state as compared to 12 MeV in the $\Sigma^o\pi^+\pi^-$ final state [Ga76-2] . Since the resolution in the $\Sigma^+\pi^o$ mass is comparable to the width of the resonance, we have folded this resolution into the fitted distribution function. The maximum likelihood fit was done to an incoherent sum of an s-wave Breit-Wigner function and a quadratic background in the mass region (1.46 - 2.10) GeV. The results of this fit are also given in table IV.2 and are shown in figure IV.7c.

Table IV.2. Results of the Fits to the $M(\Sigma^o\pi^+)$ and $M(\Sigma^+\pi^o)$ Distributions.

Decay Mode	M_o (MeV)	Γ_o (MeV)	Number of Events in the Resonance
$\Sigma^o\pi^+$	1665 ± 3	62 ± 9	635 ± 50
$\Sigma^+\pi^o$	1677 ± 7	63 ± 17	451 ± 60

The mass and width are in good agreement with the values obtained in the fit to the $M(\Sigma^o\pi^+)$ distribution. One can further do a consistency check using the numbers of $\Sigma(1660)$ events found in these fits. On the basis of isospin one

expects equal numbers of events decaying into $\Sigma^o\pi^+$ and $\Sigma^+\pi^o$. Let us calculate the expected number of events in the $\Sigma^o\pi^+$ decay mode from the observed number of events in the $\Sigma^+\pi^o$ decay mode. We then have to apply the following corrections to the observed number of Σ^+ events:

a. a correction for not using the events in which the Σ^+ decayed into $p\pi^o$; this yields a correction factor of 2.07.

b. a correction for the non-observation of the $n\pi^o$ decay mode of the Λ; this leads to a correction factor of 0.642.

c. a correction for the difference in the processing efficiency between the topologies 201 and 210+; this yields a factor of 1.18.

Using these numbers we expect to find 700 ± 90 events in the $\Sigma^o\pi^+$ decay mode. This is in good agreement with the result given in table IV.2.

IV.2.3. The channel $K^-p \to \Lambda\pi^+\pi^-$.

The Dalitz plot $M^2(\Lambda\pi^-)$ versus $M^2(\Lambda\pi^+)$ for this channel was already shown in figure IV.1. In this plot as well as in the projections (figure IV.8b,c) one clearly sees production of the $\Sigma(1385)$ in both the $\Lambda\pi^-$ and $\Lambda\pi^+$ mass combinations. In the $\pi^+\pi^-$ effective mass distribution (figure IV.8a) one observes very significant peaks at 0.76 GeV and at 1.26 GeV. These peaks correspond to the production of the ρ^o and f meson respectively.

The $M(\Lambda\pi^+)$ distribution is shown in figure IV.8c. We see a broad enhancement at a mass value of 1.7 GeV. For reasons which will be explained in chapter VI it is very unlikely that

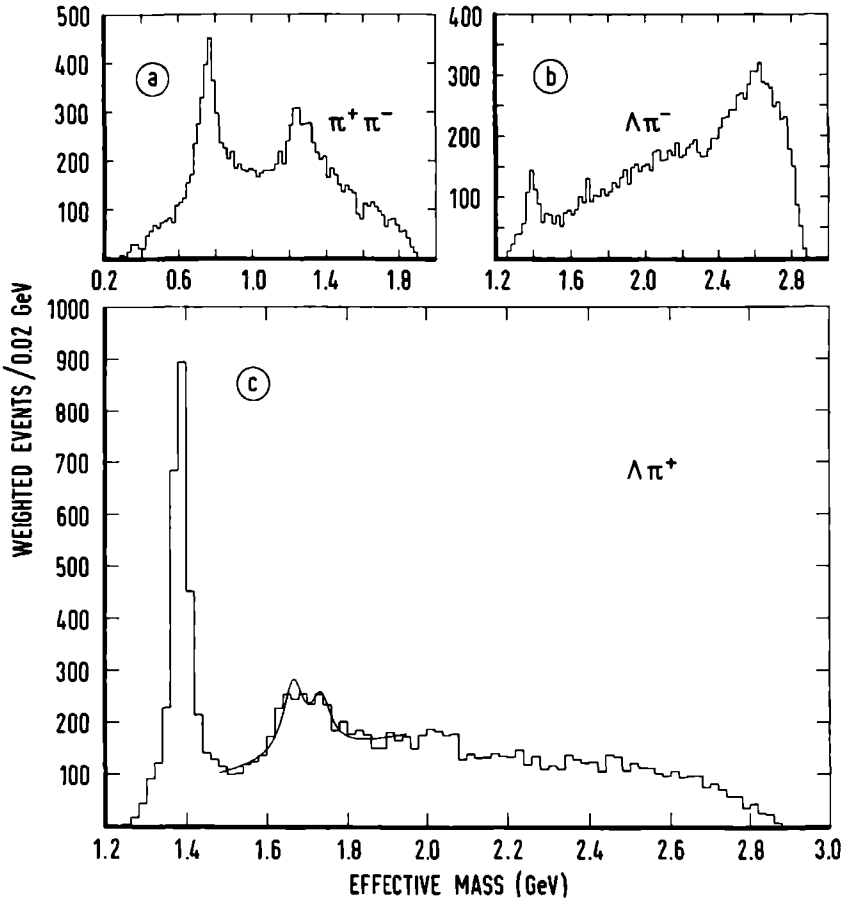

Fig. IV.8. Effective mass distributions from the channel $K^-p \to \Lambda\pi^+\pi^-$: (a) $M(\pi^+\pi^-)$, (b) $M(\Lambda\pi^-)$ and (c) $M(\Lambda\pi^+)$.

this enhancement is due to just one resonance. To estimate an upper limit for the amount of $\Sigma(1660)$ production in this channel we performed a maximum likelihood fit in the mass region (1.48 - 1.95) GeV to an incoherent sum of two s-wave Breit-Wigners and a linear background term. For one Breit-Wigner we kept the mass and width fixed to the values obtained from the fit to the $M(\Sigma^{o}\pi^{+})$ distribution, i.e. 1665 and 62 MeV respectively. For the second Breit-Wigner we fixed the width at 60 MeV. This fixed width was chosen to maximise the number of events in the $\Sigma(1660)$ while still giving a good fit to the entire region. The free parameters in the fit were the mass of the second resonance, the slope of the background and the fractions of the events in the two resonances. The curve representing the result of this fit is displayed on figure IV.8c and shows good agreement with the data. The maximum number of events in the $\Sigma(1660)$ resonance amounts to 600 ± 70.

IV.2.4. The channel $K^{-}p \rightarrow p\bar{K}^{o}\pi^{-}$.

Abundant $K^{*}(890)$ production is present in this channel, as can be seen from the distribution of the $\bar{K}^{o}\pi^{-}$ effective mass in figure IV.9a. In addition one observes an enhancement of events in the region around 1.42 GeV, corresponding to the production of $K^{*}(1420)$. The $M(p\pi^{-})$ distribution (figure IV.9b) shows three peaks at mass values of approximately 1.24, 1.50 and 1.68 GeV. The first peak is due to the $\Delta(1236)$ resonance, while the other two may be assigned to the $N^{*}(1520)$ and $N^{*}(1670)$. The distribution of the $p\bar{K}^{o}$ effective mass (figure IV.9c) shows little structure. There is a small enhancement around 1.78 GeV, due to production of $\Sigma(1765)$. However, there is certainly no evidence for the production of $\Sigma(1660)$. This

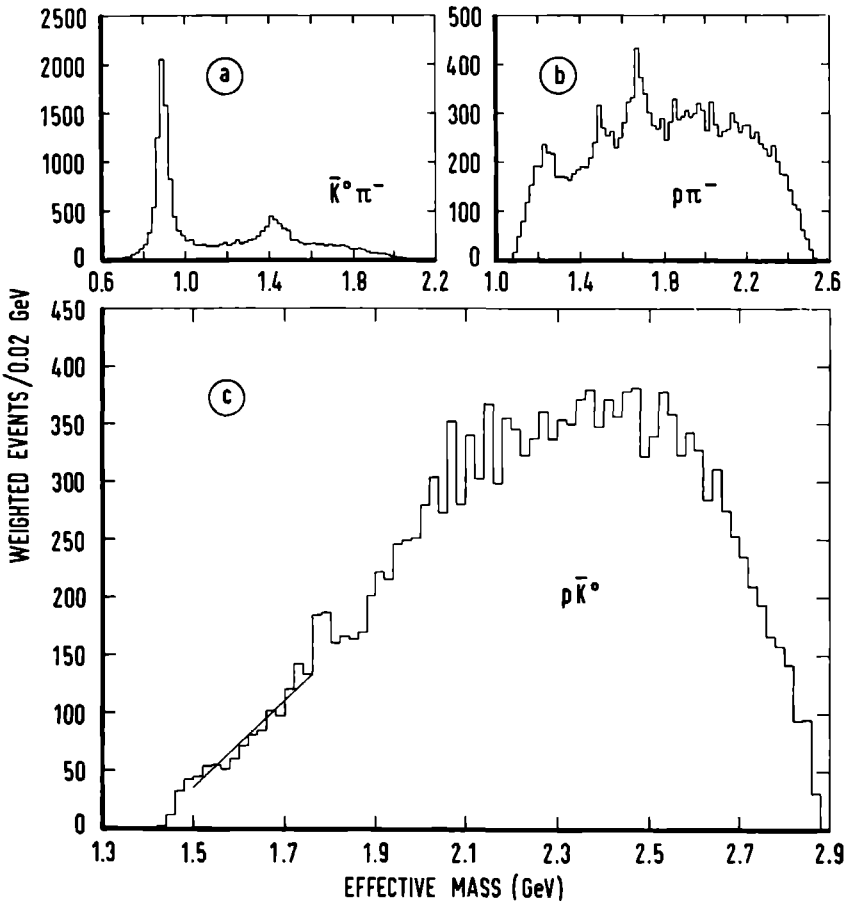

Fig. IV.9. Effective mass distributions from the channel $K^-p \to p\bar{K}^0\pi^-$: (a) $M(\bar{K}^0\pi^-)$, (b) $M(p\pi^-)$ and (c) $M(p\bar{K}^0)$.

is an important finding, because the $\Sigma(1660)$ resonance observed in formation experiments is known to decay into $N\bar{K}$ (see chapters III and VI).

The curve shown in figure IV.9c is the result of a maximum likelihood fit to an incoherent sum of an s-wave Breit-Wigner and a linear background in the mass region between 1.50 and 1.76 GeV. The mass and width of the resonance were fixed at the values obtained from the fit to the $M(\Sigma^{o}\pi^{+})$ distribution. The likelihood function reaches its maximum value for zero events in the $\Sigma(1660)$ resonance. Even in very elaborate studies of this channel there has been no indication of the production of $\Sigma(1660)$ decaying into $p\bar{K}^{o}$ [Ti74, En76].

IV.2.5. The channel $K^{-}p \rightarrow \Lambda\pi^{+}\pi^{o}\pi^{-}$.

Many resonances are produced in this channel as may be seen from the effective mass distributions shown in figures IV.10a-j. One observes the production of the ρ meson in the two-pion effective mass plots (figures IV.10a, b, c) and some f meson production in $M(\pi^{+}\pi^{-})$ (figure IV.10b). In the $M(\pi^{+}\pi^{-}\pi^{o})$ spectrum (figure IV.10d) one sees clear peaks at 0.55 and 0.78 GeV and an enhancement around 1.00 GeV, corresponding to the production of the η, ω and Φ mesons respectively. Significant production of $\Sigma(1385)$ is present in all three $\Lambda\pi$ effective mass distributions (figures IV.10 e, f, g). There is also a small peak visible in the $M(\Lambda\pi^{+}\pi^{-})$ distribution (figure IV.10i) due to some $\Lambda(1520)$ production.

Looking for production of $\Sigma^{+}(1660)$, we now concentrate on the effective mass distribution of the $\Lambda\pi^{+}\pi^{o}$ combination, shown in figure IV.10h. There is a broad structure present in the mass region between 1.60 and 1.80 GeV. The background in

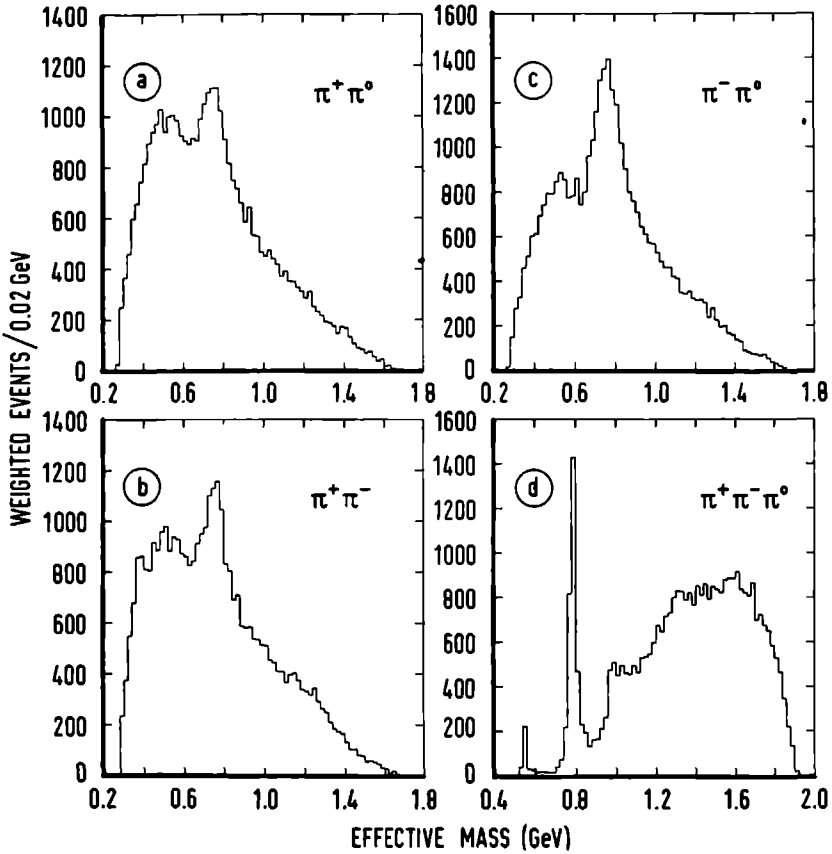

Fig. IV.10. Effective mass distributions from the channel $K^-p \to \Lambda\pi^+\pi^o\pi^-$: (a) $M(\pi^+\pi^o)$, (b) $M(\pi^+\pi^-)$, (c) $M(\pi^-\pi^o)$, (d) $M(\pi^+\pi^-\pi^o)$, (e) $M(\Lambda\pi^+)$, (f) $M(\Lambda\pi^o)$, (g) $M(\Lambda\pi^-)$, (h) $M(\Lambda\pi^+\pi^o)$, (i) $M(\Lambda\pi^+\pi^-)$ and (j) $M(\Lambda\pi^-\pi^o)$.

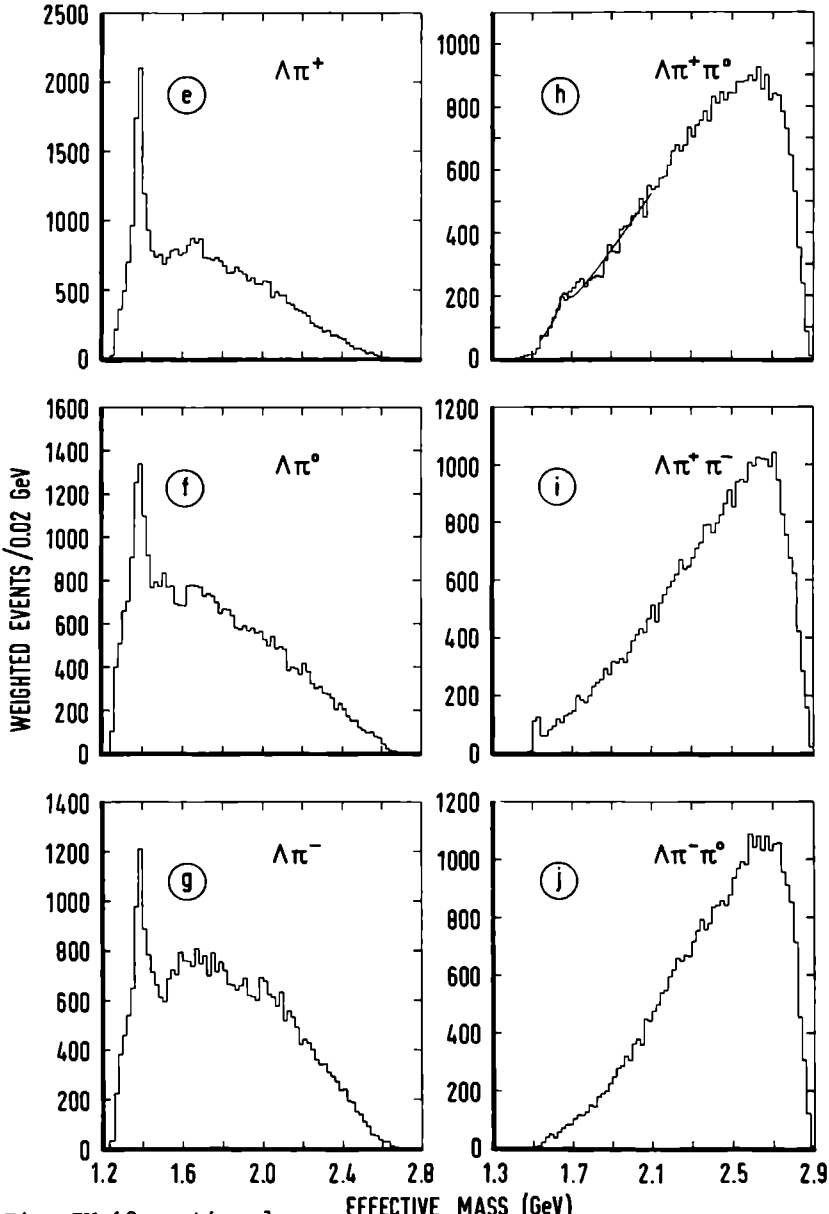

Fig. IV.10 continued.

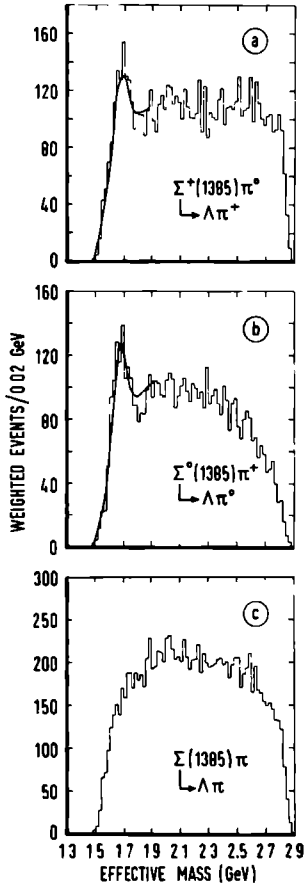

Fig. IV.11. Effective mass distribution $M(\Lambda\pi^+\pi^o)$ from the channel $K^-p \to \Lambda\pi^+\pi^o\pi^-$, where: (a) $1.34 < M(\Lambda\pi^+) < 1.44$ GeV; (b) $1.34 < M(\Lambda\pi^o) < 1.44$ GeV; (c) either $M(\Lambda\pi^+)$ or $M(\Lambda\pi^o)$ lies in the mass interval (1.34-1.44) GeV.-The curves in (a) and (b) are the result of a multidimensional maximum likelihood fit in which no $\Sigma(1660) \to \Sigma(1385)\pi$ decay was parameterised.

this mass region is large and rising. It is very difficult to extract reliable resonance parameters from this effective mass distribution. Again we have only estimated an upper limit for the production of $\Sigma^+(1660)$ decaying into $\Lambda\pi^+\pi^o$. In the maximum likelihood fit to an s-wave Breit-Wigner plus a quadratic background we fixed the mass and width at the values found in the fit of the $\Lambda(1405)\pi^+$ spectrum (1655 and 56 MeV respectively). The fit has been restricted to the mass region (1.54 - 2.10) GeV. The curve resulting from this fit is also shown in figure IV.10h. The maximum number of events in the resonance is found to be 228 ± 47.

We now investigate the possible decay of $\Sigma(1660)$ into $\Sigma(1385)\pi$. We therefore require the $\Lambda\pi^{\pm o}$ effective mass to lie in the $\Sigma(1385)$ region:

$$1.34 < M(\Lambda\pi^{\pm o}) < 1.44 \text{ GeV}$$

The $M(\Lambda\pi^+\pi^o)$ distributions with the $\Sigma(1385)$ mass cut imposed on the $\Lambda\pi^+$ and $\Lambda\pi^o$ combination respectively, are shown in figure IV.11a,b . Both figures show an enhancement of events in the mass region around 1.66 GeV. These enhancements could indicate a possible decay of $\Sigma(1660)$ into $\Sigma(1385)\pi$. On the other hand, if we plot the $\Lambda\pi^+\pi^o$ effective mass with the restriction that <u>either</u> $M(\Lambda\pi^+)$ <u>or</u> $M(\Lambda\pi^o)$ satisfies the $\Sigma(1385)$ mass selection, we do not observe a $\Sigma(1660)$ at all (figure IV.11c). The peak in the former two distributions can therefore be explained as a reflection of $\Sigma(1385)$ production in the 'other' $\Lambda\pi$ combination. This is illustrated in figure IV.12 where we display $M(\Lambda\pi^+)$ versus $M(\Lambda\pi^+\pi^o)$ for events having $M(\Lambda\pi^o)$ in the $\Sigma(1385)$ mass region. As can be seen in this figure, the presence of $\Sigma(1385)$ in $\Lambda\pi^+$ reflects as an enhancement of events in the $M(\Lambda\pi^+\pi^o)$ distribution around 1.66 GeV.

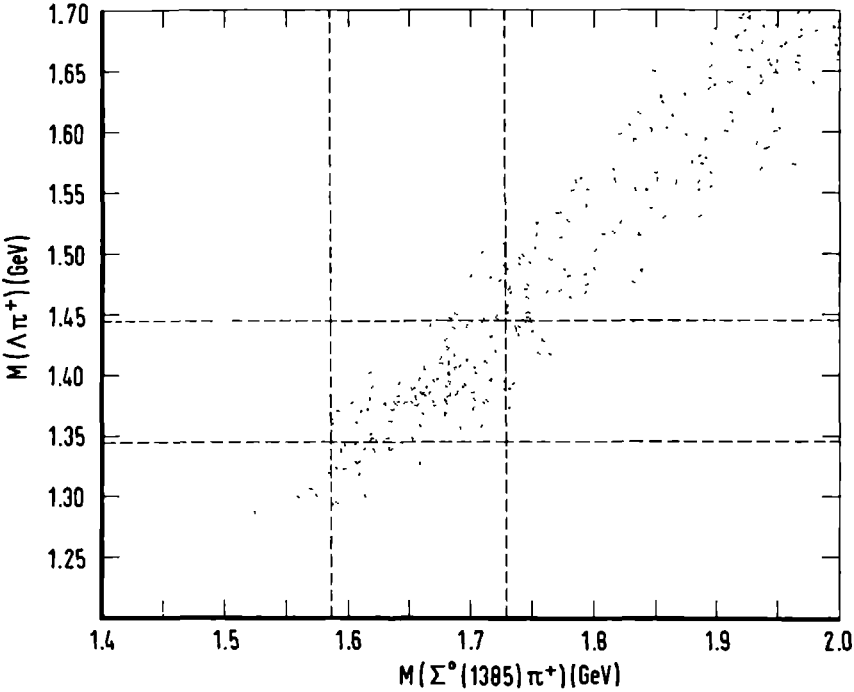

Fig. IV.12. $M(\Lambda\pi^+)$ versus $M(\Lambda\pi^+\pi^0)$ for the channel $K^-p \to \Lambda\pi^+\pi^0\pi^-$, where $1.34 < M(\Lambda\pi^0) < 1.44$ GeV.

This explanation of the effect is also confirmed by an OPTIME fit to an incoherent sum of Breit-Wigners and phase space, not including the possibility of the decay of $\Sigma(1660)$ into $\Sigma(1385)\pi$. Only events having $M(\Lambda\pi^+\pi^0) < 1.9$ GeV were used in this fit. The curves resulting for the $M(\Sigma^0(1385)\pi^+)$ distributions are also shown in figure IV.11a,b. It is clear that our data do not require a (substantial) decay of $\Sigma(1660)$ into $\Sigma(1385)\pi$. The number of $\Sigma(1660)$ events decaying into

$\Lambda\pi^+\pi^o$ is found to be 271 ± 41, in good agreement with the result obtained from the one-dimensional fit to the $\Lambda\pi^+\pi^o$ effective mass distribution.

While the above explanation of the data is clearly the simplest one, it is a different question whether we can also exclude the possibility of a $\Sigma(1385)\pi$ decay mode. The answer to this question is no. Any genuine $\Sigma(1385)\pi$ decay mode would populate the distributions considered in exactly the same way. For branching ratio considerations we will therefore have to accept the possibility of a $\Sigma(1385)\pi$ decay mode and consider the number of $\Sigma(1660)$ events found in the $\Lambda\pi^+\pi^o$ mass fit as a possible upper limit for this mode.

IV.3. Production angular distributions.

In this section we examine the production angular distribution of the $\Sigma(1660)$ in the reaction $K^-p \to \Sigma^+(1660)\pi^-$. We define the production angle θ^* in the reaction centre-of-mass system as the angle between the target proton and the $\Sigma(1660)$ system (see figure IV.13), i.e. $\cos\theta^* = \hat{\Sigma}(1660)\cdot\hat{p}$.

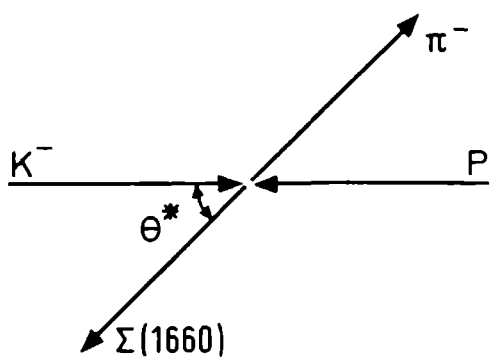

Fig. IV.13. Definition of the $\Sigma(1660)$ production angle.

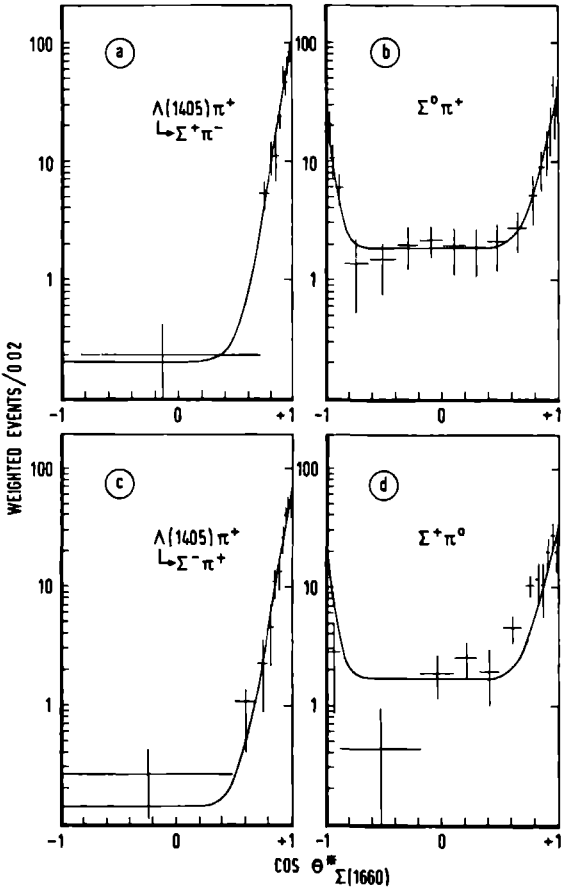

Fig. IV.14. Production angular distributions in the overall c.m.s. with background subtracted: (a) for $\Sigma(1660) \rightarrow \Lambda(1405)\pi^+ \rightarrow \Sigma^+\pi^-\pi^+$ from the channel $K^-p \rightarrow \Sigma^+\pi^-\pi^+\pi^-$, (b) for $\Sigma(1660) \rightarrow \Sigma^0\pi^+$ from the channel $K^-p \rightarrow \Sigma^0\pi^+\pi^-$, (c) for $\Sigma(1660) \rightarrow \Lambda(1405)\pi^+ \rightarrow \Sigma^-\pi^+\pi^+$ from the channel $K^-p \rightarrow \Sigma^-\pi^+\pi^+\pi^-$, (d) for $\Sigma(1660) \rightarrow \Sigma^+\pi^0$ from the channel $K^-p \rightarrow \Sigma^+\pi^0\pi^-$.

We have not used the channels IV.5 and IV.7 in this study of the production angle distribution, because for these channels it is difficult to separate the $\Sigma(1660)$ from the relatively large background and/or neighbouring resonances. Furthermore the channels IV.2 and IV.4 will only be used to make qualitative checks on the characteristics observed in the channels $K^-p \to \Sigma^+\pi^-\pi^+\pi^-$ and $K^-p \to \Sigma^o\pi^+\pi^-$ respectively.

The distribution of $\cos\theta^*$ for $\Sigma^+(1660)$ events from channel (IV.1) ($1.60 < M(\Sigma^+\pi^-\pi^+) < 1.66$ GeV and $1.34 < M(\Sigma^+\pi^-) < 1.44$ GeV) is shown in figure IV.14a. In this distribution the background under the $\Sigma(1660)$ signal has been substracted; this subtraction was based on the control regions (1.54 - 1.60) and (1.72 - 1.78) GeV and assumed a linear behaviour of the background. Figure IV.14b shows the production angular distribution for events from channel (IV.3) having $M(\Sigma^o\pi^+)$ between 1.60 and 1.72 GeV. Again the background was substracted. One immediately notices a striking difference between the two distributions. While the distribution for $\Sigma^+(1660) \to \Lambda(1405)\pi^+ \to \Sigma^+\pi^-\pi^+$ is sharply peaked in the forward direction and contains hardly any event for $\cos\theta^* < 0.7$, the distribution for $\Sigma^+(1660) \to \Sigma^o\pi^+$ not only has a forward peak, it contains events at all production angles and has a significant backward peak.

We have performed maximum likelihood fits to these distributions using an isotropic term and one (or two) exponential(s):

$$c + a\, e^{\alpha \cos\theta^*} \; (+\, b\, e^{-\beta \cos\theta^*})$$

The curves resulting from these fits are shown on figure IV.14. The best estimates for the 'slopes' of the distributions (i.e. the coefficients α, β in the exponentials) are given in table IV.3. In this table we also present the corresponding slopes

for the t' distribution of again the $\Lambda(1405)\pi^+$ decay mode and for the t' and u' distribution of the $\Sigma^o\pi^+$ decay mode.
The quantities t' and u' are defined as:

$$t' = t - t_{min}$$

$$u' = u - u_{min}$$

where t(u) is the 4-momentum transfer between the $\Sigma(1660)$ and the target proton (beam particle) and t_{min} (u_{min}) the 'minimal' value of this quantity, i.e. its value in the most forward (backward) direction $\cos\theta^* = +1$ ($\cos\theta^* = -1$).

Table IV.3. Slopes of the $\cos\theta^*$ and t' and u' Distribution.

Decay Mode	$\cos\theta^*$		t' (in GeV^{-2})	u' (in GeV^{-2})
	Forward (α)	Backward (β)		
$\Lambda(1405)\pi^+$ $\hookrightarrow \Sigma^+\pi^-$	12.9 ± 0.8	-	4.7 ± 0.3	-
$\Sigma^o\pi^+$	11.6 ± 1.5	19 ± 4	4.3 ± 0.6	7.0 ± 1.5

We have also demonstrated this difference in production angular distribution in figure IV.15, where we show the effective mass spectra $M(\Lambda(1405)\pi^+)$ from channel (IV.1) and $M(\Sigma^o\pi^+)$ from channel (IV.3) for the following three $\cos\theta^*$ intervals:

$0.7 < \cos\theta^* \leq 1.0$ (figs. (a), (d))
$-0.8 < \cos\theta^* \leq 0.7$ (figs. (b), (e))
$-1.0 \leq \cos\theta^* \leq -0.8$ (figs. (c), (f))

In the $M(\Lambda(1405)\pi^+)$ distributions we only observe production of $\Sigma(1660)$ in the forward production angular region. However, in the $M(\Sigma^o\pi^+)$ distributions a $\Sigma(1660)$ signal is present in all three $\cos\theta^*$ regions.

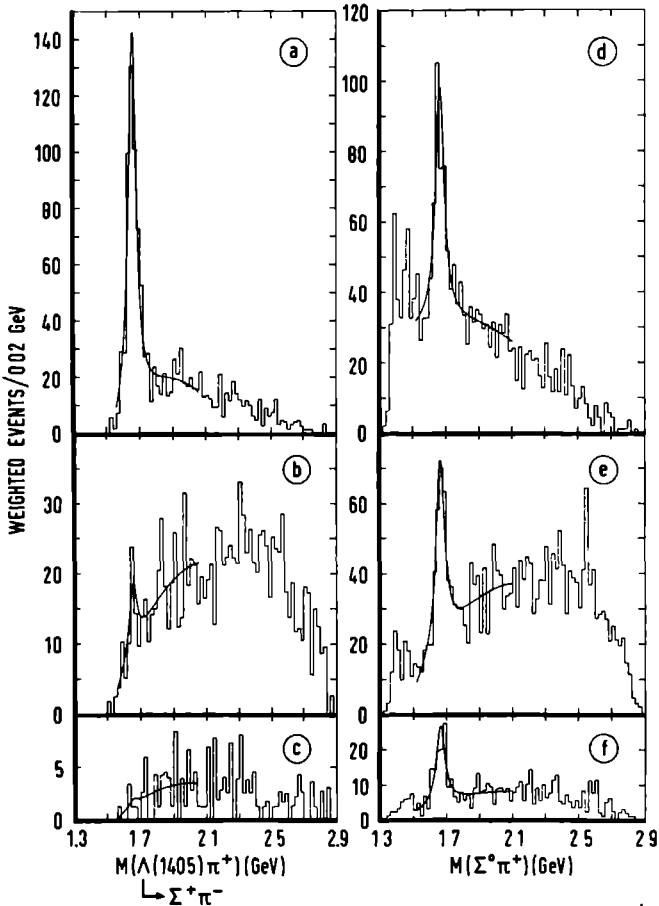

Fig. IV.15. Effective mass distributions: $M(\Lambda(1405)\pi^+)$ for the channel $K^-p \to \Sigma^+\pi^-\pi^+\pi^-$ in the production angular regions: (a) $0.7 < \cos\theta^* \leqslant 1.0$, (b) $-0.8 < \cos\theta^* \leqslant 0.7$, (c) $-1.0 \leqslant \cos\theta^* \leqslant -0.8$; $M(\Sigma^o\pi^+)$ for the channel $K^-p \to \Sigma^o\pi^+\pi^-$ and for the same $\cos\theta^*$ intervals ((d), (e) and (f) respectively). The curves are the result of fits described in chapter VI.

The production angular distributions (after background subtraction) of $\Sigma^+(1660) \to \Lambda(1405)\pi^+ \to \Sigma^-\pi^+\pi^+$ and of $\Sigma^+(1660) \to \Sigma^+\pi^o$ are shown in figures IV.14c,d (for figure (d) the $\Sigma(1660)$ region was taken as (1.60 - 1.74) GeV and the control regions were (1.50 - 1.57) GeV and (1.77 - 1.84) GeV). The curves represent the results of the fits to the $\Sigma(1660)$ production angular distributions from channel (IV.1) and (IV.3) respectively, but normalised to the number of events in the distribution under consideration. The $\Sigma^+(1660) \to \Sigma^-\pi^+\pi^+$ shows a behaviour similar to the $\Sigma^+(1660)$ of channel (IV.1) and the $\Sigma^+(1660) \to \Sigma^+\pi^o$ production angular distribution is in qualitative agreement with the distribution of $\Sigma^+(1660) \to \Sigma^o\pi^+$. The fact that we do not see a backward peak in the $\Sigma^+\pi^o$ case is probably due to the poorer resolution in the $\Sigma^+\pi^o\pi^-$ channel.

This striking difference in production angular distribution for the $\Lambda(1405)\pi^+$ and $(\Sigma\pi)^+$ decay modes has been observed in several experiments at different beam momenta [Eb69,Ag70, NA71,Cl73,Ap74,Es74]. It strongly suggests that in production experiments there exist two $\Sigma(1660)$ resonances with approximately the same mass and width but different production characteristics.

IV.4. Cross sections.

On the basis of the numbers of events found in the fits to the effective mass distributions of $\Sigma^{\pm}\pi^{\mp}\pi^+$, $\Sigma^+\pi^o$, $\Lambda\pi^+$, $p\bar{K}^o$ and $\Lambda\pi^+\pi^o$, we can calculate the cross section for the various decay modes of the $\Sigma^+(1660)$. It is not useful to calculate the total reaction cross section for $K^-p \to \Sigma^+(1660)\pi^-$ since we are dealing with (at least) two resonances.

In order to compensate for losses and for cuts applied to the data, several corrections must be made to the bare numbers of events found in the mass fits. Most of these corrections have already been mentioned in chapter II, such as corrections for rejected events, scan efficiency, unseen decay modes and a cut on the fit probability. We use weighted numbers of events to correct for decay length losses and for small decay angle losses. In addition to the correction for unseen or unused decay modes of semi-stable particles (Λ, $\bar{K}^o$, Σ^+) we must still correct for the undetected and/or unused decay modes of resonances ($\Lambda(1405)$, $\Sigma(1385)$). These corrections are either given by Clebsch-Gordan coefficients or by the branching fractions of the particular resonance. For the latter we have taken the values from the Particle Data Group listings [Pd76].

The results for the cross sections of the various decay modes of $\Sigma(1660)$, together with the applied correction factors are summarised in table IV.4. In figure IV.16 we display the cross section for the $\Lambda(1405)\pi^+$ and $(\Sigma\pi)^+$ decay modes of $\Sigma^+(1660)$ as a function of the beam momentum. Where appropriate the reported values are multiplied by a factor 3/2 or 3 to account for unused $\Lambda(1405)\pi^+ \to \Sigma^o\pi^o\pi^+$ and $\Lambda(1405)\pi^+ \to \Sigma^-\pi^+\pi^+$ decay modes. One can see that our result at 4.2 GeV/c is in agreement with the value one expects from a smooth momentum dependence of the cross section. The unusually large $\Lambda(1405)\pi^+$ cross section observed by Aguilar-Benitez et al. at 3.9 GeV/c [Ag70] is either due to an s-channel resonance effect or more likely an erroneous measurement.

Table IV.4. Cross Sections of $K^- p \to \Sigma^+(1660)\pi^-$ for Various Decay Modes of the $\Sigma(1660)$.

Decay Mode	$\Lambda(1405)\pi^+ \hookrightarrow \Sigma^+\pi^-$	$\Lambda(1405)\pi^+ \hookrightarrow \Sigma^-\pi^+$	$\Sigma^o\pi^+$	$\Sigma^+\pi^o$	$\Lambda\pi^+$	$p\bar{K}^o$	$\Sigma(1385)\pi$
Number of Events	586 ± 50	330 ± 30	635 ± 50	451 ± 60	< 600 ± 70	< 22	< 228 ± 47
Correction Factors:							
. for branching ratios	1.0	1.0	1.56	2.07	1.56	2.91	1.77(**)
. for probability cuts	1.01	1.01	1.05	1.08	1.01	1.01	1.12
Total	1.01	1.01	1.64	2.23	1.57	2.94	1.98
μb - equiv.	58.7 ± 0.5	60.2 ± 0.5	64.2 ± 0.4	56.1 ± 0.5	64.2 ± 0.4	64.2 ± 0.4	64.2 ± 0.4
Cross Section(*) (μb)	10 ± 2	6 ± 1	16 ± 2	18 ± 4	< 15 ± 3	< 1	< 7 ± 2

(*) The errors quoted contain systematic contributions.

(**) This factor becomes 1.56 if one assumes the decay to be $\Lambda\pi^+\pi^o$ and not $\Sigma(1385)\pi$.

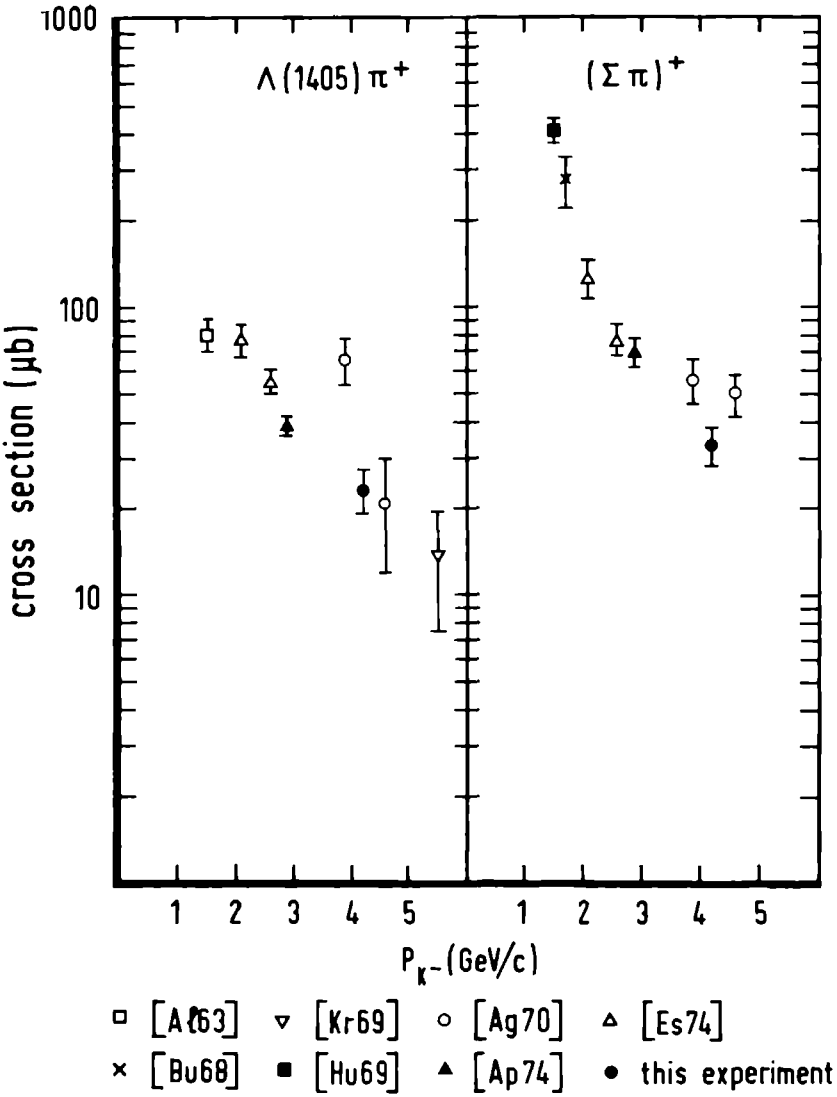

Fig. IV.16. Cross sections of the $\Lambda(1405)\pi^+$ and $(\Sigma\pi)^+$ decay modes of $\Sigma^+(1660)$ at various beam momenta.

CHAPTER V.

S P I N - P A R I T Y A N A L Y S I S O F Σ(1660).

Information on the spin-parity of a baryon resonance comes in general from its decay angular distribution and the polarisation distribution of the final baryon. In formation experiments these distributions are analysed in terms of partial wave amplitudes. By varying the beam momentum, these amplitudes can then be studied as a function of the total energy. The amplitude in which a resonant effect occurs, determines directly the spin and the parity of the resonance. Ambiguities in the relations between the experimental distributions and the partial wave amplitudes can cause complications. The spin itself can however in principle be determined uniquely from the decay angular distribution, because - in formation experiments - the resonance is produced in a known mixture of pure spin states. In various formation experiments was the spin-parity of the Σ(1660) established to be $3/2^-$ [Ar69,Ga70,Bu71,Ki71,La72,Ho72,Pr74,Ba75,Ho75,Po75]. In production experiments however, the experimental situation is less clear. Information on the spin of a resonance still comes from its decay angular distribution only. However, in production experiments the resonance is in general produced in an a priori unknown mixture of pure spin states. The decay angular distribution therefore contains a number of unknown parameters, the elements of the so-called 'spin density matrix' [Fa57]. Only in some very special cases can the decay angular distribution be written in a form with no unknown parameters. A direct spin determination is then in principle possible. An example of such a special case is the sample of events ob-

tained after the data selection connected with the so-called Adair method.

In production experiments so far, the Adair method has been used to determine the spin for $\Sigma^+(1660) \to \Lambda(1405)\pi^+$ [Eb67,Ap74]. General methods allow for the presence of a priori unknown spin density matrix elements; examples are the analysis in terms of moments of the decay angular distribution or more complex, the so-called Byers-Fenster method. A Byers-Fenster analysis of the $\Sigma^o\pi^+$ decay of $\Sigma(1660)$ has been performed by Button-Shafer [Bu68]. For a given J, parity determinations are possible by looking at interference effects. An example is the Dalitz-Miller analysis, which has been applied to the $\Sigma\pi\pi$ decay of the $\Sigma(1660)$ [Eb67].

In this chapter we describe all these methods in some detail and present the results obtained for the spin-parity of the $\Sigma(1660)$ in applying them. In the moments analyses (general and Byers-Fenster) and in the Adair analysis, we have only used the $\Lambda(1405)\pi^+$ and $\Sigma^o\pi^+$ decay modes. This restriction is made, since in these channels the separation of $\Sigma(1660)$ from the background is more reliable, as we have seen in chapter IV. The Dalitz-Miller analysis for the determination of the parity is applied to the $\Sigma^-\pi^+\pi^+$ decay mode only.

V.1. Reference frames.

The decay angular distribution of a resonance is given with respect to a coordinate system defined in its rest system. The normal $\hat{n}$ to the production plane is always taken as one of the axes of the coordinate triad. We have used the following systems (figure V.1):

a) Helicity frames. The normal to the production plane

is chosen as the y-axis. For the t-channel helicity (TH) or Jackson frame one takes as z-axis the direction of the incoming proton in the resonance rest frame. In the s-channel helicity (SH) frame the z-axis is the direction of the resonance in the overall centre-of-mass system.

b) Transversity frames. The normal to the production plane is taken as the z-axis. The x-axis of the s-channel transversity (ST) frame is the z-axis of the s-channel helicity frame and the x-axis of the t-channel transversity (TT) frame is the z-axis of the t-channel helicity frame.

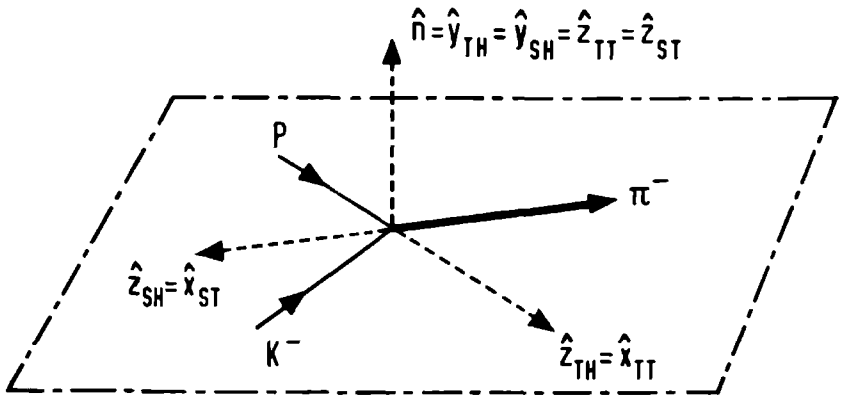

Fig. V.1. Reference frames in the rest system of the $\Sigma(1660)$ for the reaction $K^-p \to \Sigma^+(1660)\pi^-$. $\hat{n}$ is the normal to the production plane.

V.2. Moments analysis in terms of the spherical harmonics Y_L^M.

The angular distribution for the parity conserving decay of $\Sigma(1660)$ into a spin 1/2 baryon and a spinless meson is given by:

$$F(\cos\Theta,\varphi) = \sum_{\substack{L=0 \\ (L \text{ even})}}^{2J} \sum_{M=-L}^{+L} a_{LM}\, Y_L^{M*}(\Theta,\varphi) \qquad (V.2.1)$$

where J is the spin of $\Sigma(1660)$ and a_{LM} parameters related to elements of the spin density matrix of $\Sigma(1660)$ (*).

From the measurement of the parameters a_{LM} in (V.2.1), one can set a lower limit for the spin J: any non-zero coefficient a_{LM} for L = L', requires J to be at least $\frac{L'}{2}$ (since L runs from 0 to 2J).

Estimates of the parameters a_{LM} may be obtained by the method of moments. The moment $\langle Y_L^M \rangle$ of the spherical harmonic Y_L^M is defined by:

$$\langle Y_L^M \rangle = \int Y_L^M(\Theta,\varphi)\, F(\cos\Theta,\varphi)\, d\cos\Theta\, d\varphi$$

Experimentally, the moments $\langle Y_L^M \rangle$ are obtained by calculating the average of the function Y_L^M over the data sample:

$$\overline{Y_L^M} = \frac{1}{N} \sum_{i=1}^{N} Y_L^M(\Theta_i,\varphi_i) \qquad (V.2.2)$$

Instead of the moments (V.2.2) one frequently plots the 'summed moments': $N.\overline{Y_L^M}$; these quantities have the advantage that, in a graph of a 'summed moment' versus, e.g. the effective mass of the particles involved, the significance of the moment with respect to the background can be estimated directly.

(*) The distribution function is obtained from Eq.(13a) of appendix B after the substitution:

$$D_{M0}^{L}(\varphi,\Theta,0) = \sqrt{\frac{4\pi}{2L+1}}\; Y_L^{M*}(\Theta,\varphi)$$

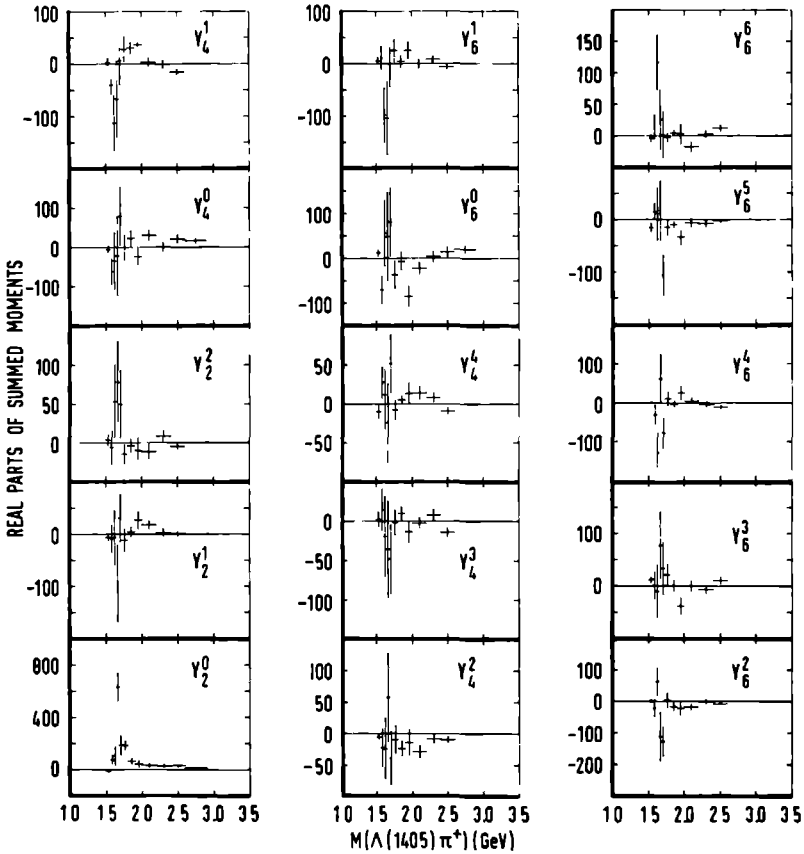

Fig. V.2. Real parts of the summed moments $N.\langle Y_L^M \rangle$ of the $\Lambda(1405)\pi^+$ system versus $M(\Lambda(1405)\pi^+)$ for final state $K^-p \to \Sigma^+\pi^-\pi^+\pi^-$ in the t-channel helicity frame and for events with $\cos\theta^* > 0.9$.

In figure V.2 we have plotted the 'summed moments' of the spherical harmonics (for L values up to 6) as a function of $M(\Sigma^+\pi^-\pi^+)$ for the decay mode $\Sigma(1660) \rightarrow \Lambda(1405)\pi^+ \rightarrow \Sigma^+\pi^-\pi^+$. To reduce the background in the $\Sigma(1660)$ region, the production angle $\cos\theta^*$ was required to be larger than 0.9. The angles Θ_i and φ_i are evaluated in the t-channel helicity frame (see section V.1). Only the real parts of the moments are plotted, since parity conservation in the production of $\Sigma(1660)$ requires the imaginary parts to be identically zero. There is a very significant $\langle Y_2^0 \rangle$ moment in the $\Sigma(1660)$ region, which establishes that the spin J of $\Sigma(1660)$ is $\geqslant 3/2$. Inspection of the other moments shows, that with the possible exception of $\langle Y_6^2 \rangle$, there is no other significant structure present in the $\Sigma(1660)$ region. The χ^2 probability for the $\langle Y_6^2 \rangle$ moment, averaged over the $\Sigma(1660)$ mass band (1.60 - 1.72 GeV), to be zero is 6%. The probability of all L=6 moments being identically zero is 20%.

We now turn our attention to the decay $\Sigma^+(1660) \rightarrow \Sigma^0\pi^+$. Figures V.3a, b, c show the 'summed moments' of the spherical harmonics as a function of $M(\Sigma^0\pi^+)$ for the production angular regions $0.7 < \cos\theta^* \leqslant 1.0$, $-0.8 < \cos\theta^* \leqslant 0.7$ and $-1.0 \leqslant \cos\theta^* \leqslant -0.8$ respectively. The angles Θ_i and φ_i are again taken in the t-channel helicity frame. As before, we observe significant structure in the $\Sigma(1660)$ region for the L=2 moments, especially in the backward region (c), where the signal to background ratio is larger (see figure IV.15). The presence of significant L=2 moments leads to the conclusion that also $\Sigma^+(1660) \rightarrow \Sigma^0\pi^+$ has spin $J \geqslant 3/2$.

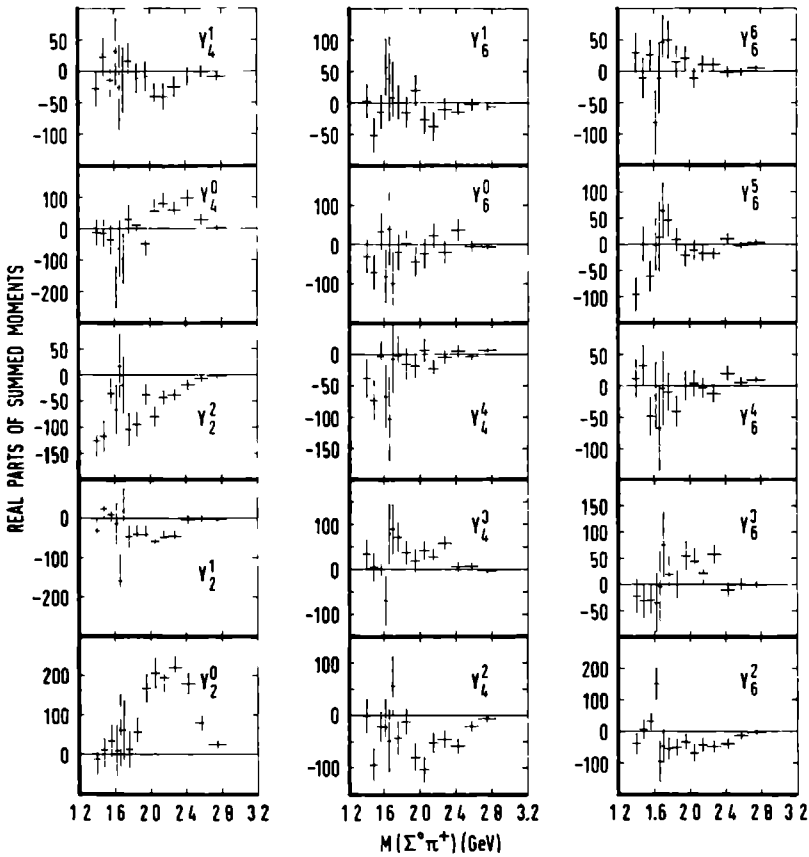

Fig. V.3. Real parts of the summed moments $N.\langle Y_L^M \rangle$ of the $\Sigma^o\pi^+$ system versus $M(\Sigma^o\pi^+)$ for final state $K^-p \to \Sigma^o\pi^+\pi^-$ in the t-channel helicity frame for the production angle intervals:
(a) $0.7 < \cos\theta^* \leqslant 1.0$; (b) $-0.8 < \cos\theta^* \leqslant 0.7$;
(c) $-1.0 \leqslant \cos\theta^* \leqslant -0.8$.

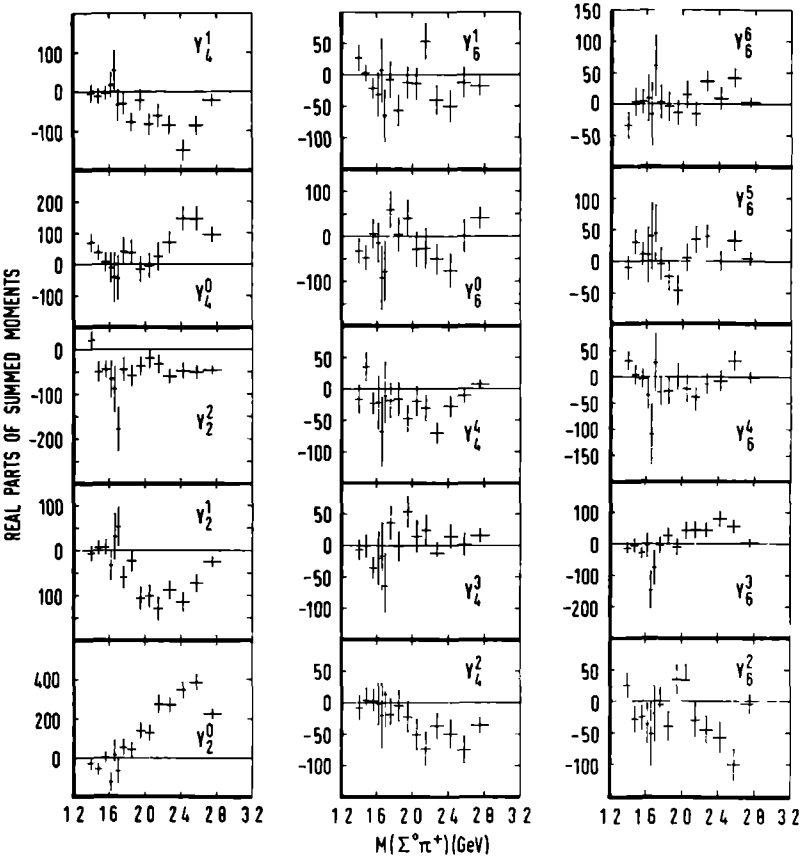

Fig. V.3b.

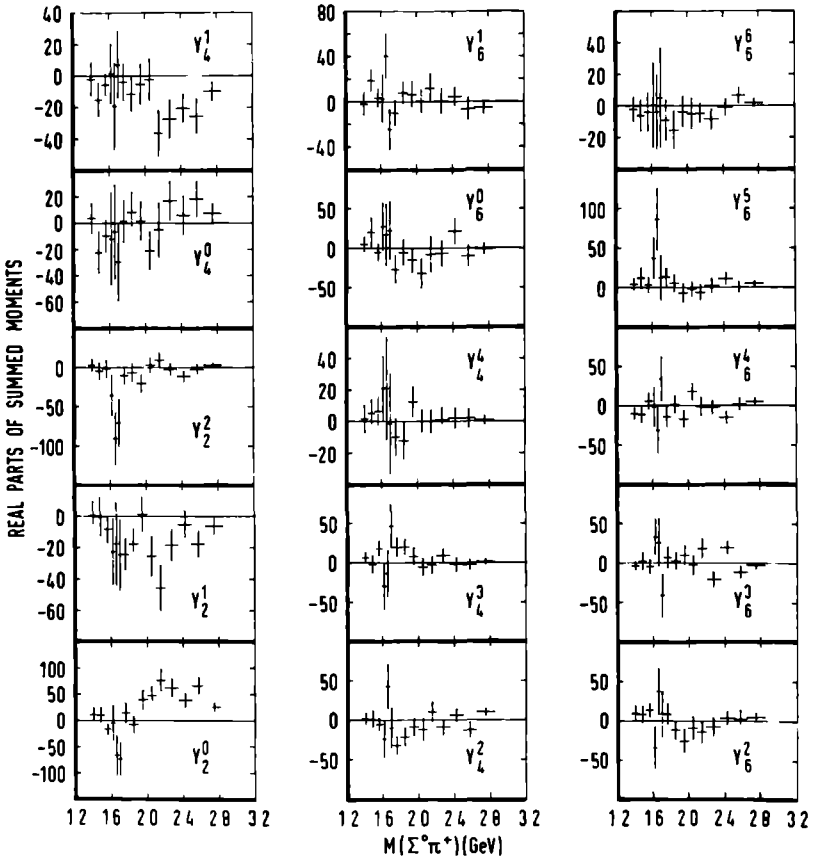

Fig. V.3c.

V.3. Adair analysis.

It was pointed out by R.K. Adair [Ad55] more than twenty years ago, that in a reaction of the type MESON (spin 0) + PROTON → X + MESON (spin 0) configurations where X is produced at or near 0° with respect to the incoming beam direction, are well suited for the determination of the spin of particle X. Consider for example the reaction $K^{-}p \rightarrow \Sigma^{+}(1660)\pi^{-}$. Let the quantisation axis be the direction of the incoming proton. Since the K^{-} has spin 0 and the proton has spin 1/2 the projection of the total angular momentum of the initial state has to be $\pm$ 1/2. If $\Sigma^{+}(1660)$ is produced at 0°, the projection of the orbital angular momentum of the final state must be zero. Hence, since the π^{-} is also spinless, the spin projection of $\Sigma(1660)$ will be $\pm$ 1/2. The population of the magnetic substates of $\Sigma(1660)$ is therefore uniquely determined and this leads to a definite prediction for the decay angular distribution of $\Sigma(1660)$. We present these distributions for J values up to 7/2, in table V.1.

Table V.1. Distribution of the Adair Angle for Half-Integer Spins.

J	Distribution function
1/2	1
3/2	$1/2\ (1 + 3\cos^2\theta)$
5/2	$3/4\ (1 - 2\cos^2\theta + 5\cos^4\theta)$
7/2	$1/16\ (9 + 45\cos^2\theta - 165\cos^4\theta + 175\cos^6\theta)$

In practice however, the number of events produced at or very close to 0^{o} (or 180^{o}) is very small. In order to have sufficient statistics, one has to relax the requirement on the production angle and accept all events within a finite production angle interval. This interval should however be kept small enough so as to ensure that all particles are produced in the $|J, \pm 1/2>$ state.

We have tested the spin hypotheses 1/2, 3/2, 5/2 and 7/2 in various $\cos\theta^*$ intervals using a maximum likelihood method. The results of these tests for the $(\Sigma^+\pi^-)\pi^+$ decay mode ($1.60 < M(\Sigma^+\pi^-\pi^+) < 1.72$ GeV and $1.34 < M(\Sigma^+\pi^-) < 1.44$ GeV) are given in table V.2. For the $\cos\theta^*$ interval (0.95 - 1.0) the results are also displayed in figure V.4. From the table one sees that in the intervals (0.8 - 1.0), (0.9 - 1.0) and even (0.95 - 1.0) there is overwhelming evidence for spin 3/2.

States other than $|J, \pm 1/2>$ are associated with $M \neq 0$ orbital angular momentum states; they can give non-negligible contributions to the production angular distribution up to angles $\theta^* \gtrsim \frac{1}{L}$. If one assumes that the range of the interaction is given by the Compton wavelength of the π-meson ($\sim$ 1 Fermi $= 10^{-13}$ cm) and uses this value as the maximum impact parameter of the collision, one finds that the maximum L value is given by:

$$L_{max} = \frac{P_{inc}^{CM}}{m_{\pi}}$$

where P_{inc}^{CM} is the momentum of the incoming particle in the centre-of-mass system and m_{π} the mass of the π-meson. At our energy $P_{inc}^{CM} = 1.31$ GeV/c and $L_{max} \simeq 10$. Therefore to apply the Adair analysis safely, the production angle cosine $\cos\theta^*$ should be larger than

$$\cos\left(\frac{1}{L_{max}}\right) \simeq 0.995$$

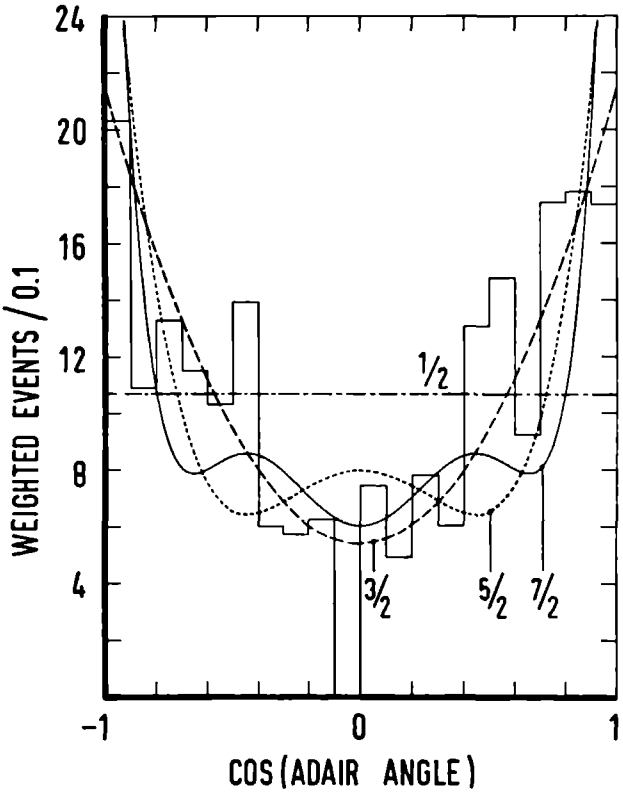

Fig. V.4. Adair angular distribution for $\Sigma(1660) \rightarrow \Lambda(1405)\pi^+$ in the final state $K^-p \rightarrow \Sigma^+\pi^-\pi^+\pi^-$ for events with $\cos\Theta^* > 0.95$.

Table V.2. Results of an Adair Analysis on $\Sigma(1660)^+ \rightarrow \Lambda(1405)\pi^+ \rightarrow \Sigma^+\pi^-\pi^+$ for Various Production Angle Intervals.

$\cos\theta^*$	number of events	$2.\Delta(\ln\mathcal{L})$ (*)			
		J = 1/2	J = 3/2	J = 5/2	J = 7/2
> 0.800	303	68.6	0	42.6	42.8
> 0.900	233	46.4	0	27.4	24.6
> 0.950	142	34.6	0	27.6	26.8
> 0.980	75	11.6	1.2	4.6	0
> 0.990	38	10.0	1.2	3.4	0
> 0.995	14	10.8	3.4	3.2	0

(*) Twice the decrease in the natural logarithm of the likelihood function in going from the most probable hypothesis to the hypothesis under consideration (= the number of standard deviations in case of a normal distribution) ; 0 indicates the most probable hypothesis.

In view of this limitation, the preference observed for J=3/2 in the first three $\cos\theta^*$ intervals of table V.2 could be fortuitous. In the last three intervals limited statistics prevents any real discrimination between the J=3/2, 5/2 and 7/2 hypotheses. However the fact that all solutions, when moving from the larger $\cos\theta^*$ intervals to the extreme forward region, show the smooth behaviour expected for the gradual reduction of statistics, and in particular the fact that the J=3/2 solution remains a good one up to the last interval, gives some confidence to the assignment J=3/2 for the spin of $\Sigma(1660) \to \Lambda(1405)\pi$ (*).

V.4. Byers-Fenster analysis.

V.4.1. Three-step decay angular distribution.

Byers and Fenster have developed a formalism for the determination of the spin and the parity of a baryon B_1, produced in a reaction of the type

$$K^- + p \to B_1 + m_1$$

where m_1 is a spinless meson [By63,By67]. This method is based on a measurement of the so-called multipole moments of the decay angular distribution and the polarisation distribution of the decay hyperon in the two-step decay:

(*) We have also tried the Adair analysis on the $\Sigma^0\pi^+$ final state in the forward as well as in the backward production angular regions ($\cos\theta^* > 0.9$ and $\cos\theta^* < -0.9$ respectively). Large background in the forward region and few events in the region $\cos\theta^* < -0.9$ (58 events) prevented us from drawing any conclusion on the spin of $\Sigma(1660) \to \Sigma\pi$.

$$B_1 \rightarrow \begin{cases} B_2 + m_2 \\ \hookrightarrow B_3 + m_3 \end{cases}$$

where B_1 is a baryon witn arbitrary spin-parity, B_2 and B_3 baryons with spin 1/2 and m_2 and m_3 spin zero mesons. To be useful the second decay must be parity violating, so as to allow a polarisation measurement of B_2.

In this type of analysis one implicitely assumes, that the production amplitude of B_1 is the only important one and that final state interactions between the decay products of B_1 and the particle(s) produced in association with B_1 are negligible. In other words one assumes that there is no background.

The starting point of the method is the joint angular distribution function F_{23}, giving the probability for finding B_2 emitted in a solid angle $d\Omega_2$ in the B_1 rest frame and B_3 emitted in a solid angle $d\Omega_3$ in the B_2 rest frame. Since B_2 has spin 1/2, this correlation function F_{23} should be of the general form [Le57] :

$$F_{23} = \frac{1}{4\pi} (I_2 + \alpha_2 I_2 \vec{P}_2 \cdot \hat{q}_3) \qquad (V.4.1)$$

where I_2 is the angular distribution for B_1 decaying into B_2 and m_2 (in the B_1 rest frame), $\vec{P}_2$ the polarisation vector of B_2, α_2 the asymmetry parameter of the decay of B_2 and $\hat{q}_3$ a unit vector specifying the direction of B_3 in the B_2 rest frame (see figure V.5).

The expressions for the intensity and polarisation distributions are given by (see appendix B):

$$I_2(\Theta_2,\varphi_2) = \frac{1}{4\pi} \sum_{L=0}^{2J_1} (E_L + \alpha_1 O_L) \sum_{M=-L}^{+L} Z_L^M \, D^L_{M0}(\varphi_2,\Theta_2,0) \qquad (V.4.2a)$$

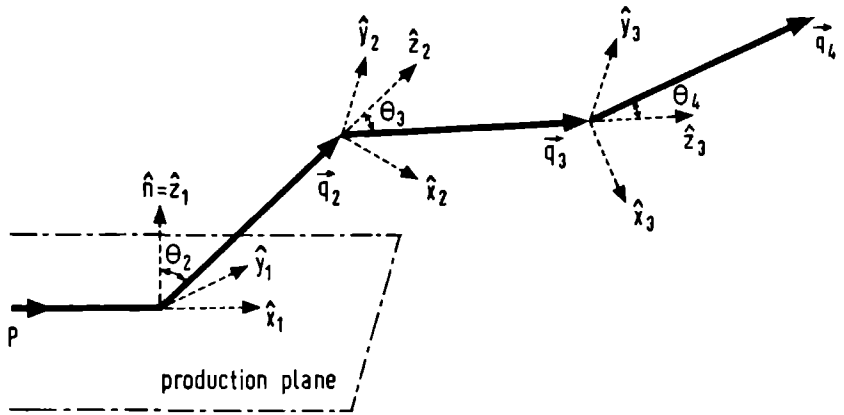

Fig.V.5. Reference frames in the three-step decay chain of B_1.

$$I_2\vec{P}_2\cdot\hat{q}_2 = I_2\vec{P}_2\cdot\hat{z}_2 = \frac{1}{4\pi}\sum_{L=0}^{2J_1}(\alpha_1 E_L + O_L)\sum_{M=-L}^{+L} Z_L^M\, D_{M0}^L(\varphi_2,\theta_2,0) \tag{V.4.2b}$$

$$I_2\vec{P}_2\cdot(\hat{x}+i\hat{y}_2) = -\frac{1}{4\pi}(2J_1+1)\sqrt{1-\alpha_1^2}\, e^{-i\Phi_1}\cdot$$

$$\sum_{L=0}^{2J_1}\frac{O_L}{\sqrt{L(L+1)}}\sum_{M=-L}^{+L} Z_L^M\, D_{M1}^L(\varphi_2,\theta_2,0) \tag{V.4.2c}$$

where: . for L even : $E_L = 1$, $O_L = 0$;

. for L odd : $E_L = 0$, $O_L = 1$;

. J_1 is the spin of B_1;

. α_1, Φ_1 are the decay parameters of B_1 (*) (see appendix B);

. $D^L_{MN}(\varphi,\Theta,\xi) = e^{-iM\varphi}\, d^L_{MN}(\cos\Theta)\, e^{-iN\xi}$ are the Wigner rotation functions; for properties see Rose [Ro57].

The parameters Z^M_L describe the spin orientation of B_1. They are related to the spin multipole parameters or statistical tensors t^M_L through:

$$Z^M_L = (-)^{J_1-\frac{1}{2}} \sqrt{(2J_1+1)(2L+1)}\, C(JJL;\ \tfrac{1}{2},\ -\tfrac{1}{2})\ t^M_L \qquad (V.4.3)$$

where C is a Clebsch-Gordan coefficient.

The t^M_L are defined by the expansion of the spin density matrix in terms of the spherical tensor operators T^M_L (see appendix B for their definition):

$$\rho = \frac{1}{2J+1} \sum_{L=0}^{2J} \sum_{M=-L}^{+L} (2L+1)\ t^{M*}_L\ T^M_L \qquad (V.4.4)$$

Θ_2 and φ_2 in (V.4.2a) are the angles of B_2 measured in a B_1 rest system S_1 defined independently of the decay of B_1. Equations (V.4.2b) and (V.4.2c) give the components of the polarisation vector of B_2 in a reference frame S_2 obtained

---

(*) In a parity conserving B_1 decay is $\cos\Phi_1 = \pm 1$ and determines the parity of B_1:

$$\cos\Phi_1 = \pm 1 \text{ for } P_{B_1} = P_{B_2}\, P_{m_2}\, (-)^{J_1 \mp \frac{1}{2}}$$

where P_{B_1}, P_{B_2} and P_{m_2} are the parities of B_1, B_2 and m_2 respectively.

from S_1 by a rotation through the Euler angles $(\varphi_2, \Theta_2, 0)$.

If the decay of B_2 is parity conserving (i.e. $\alpha_2 = 0$), one sees from (V.4.1) that adding this second decay does not yield any new information. If however there is a third decay:

$$B_3 \rightarrow B_4 + m_4$$

(where again B_4 has spin 1/2 and m_4 is spinless), and if this decay happens to be weak, we do obtain additional information by including this third step in our analysis. It is the latter situation which we encounter in the decay chain

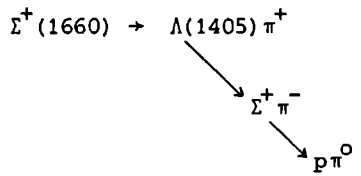

The correlation function F_{234} for such a three-step decay chain is then written as:

$$F_{234} = \frac{1}{(4\pi)^2} I_2[1 + \alpha_3 \vec{P}_3 \cdot \hat{q}_4] \qquad (V.4.5)$$

where: α_3 is the asymmetry parameter of the B_3 decay;

$\vec{P}_3$ is the polarisation vector of B_3;

$\hat{q}_4$ is the direction of B_4 in the B_3 rest frame.

The polarisation vector $\vec{P}_3$ of B_3 is in this case given by the expression [Le57-2]:

$$\vec{P}_3 = (\vec{P}_2 \cdot \hat{q}_3)\, \hat{q}_3 + \hat{q}_3 \times (\vec{P}_2 \times \hat{q}_3) \qquad (V.4.6)$$

$\vec{P}_3$ is defined in the rest frame of B_3 obtained by a Lorentz-transformation along $\hat{q}_3$ from the reference frame S_2 defined above (cf. appendix B). The dependence of F_{234} on the six

decay angles is then found to be:

$$F_{234}\,(\cos\Theta_2,\,\varphi_2,\,\cos\Theta_3,\,\varphi_3,\,\cos\Theta_4,\,\varphi_4) =$$

$$\frac{1}{(4\pi)^3}\sum_{L=0}^{2J_1}\sum_{M=-L}^{+L}\Bigg[(E_L + C_Z\,O_L)\,Z_L^M\,D_{M0}^L(\varphi_2,\Theta_2,0) + O_L\,\frac{2J_1+1}{\sqrt{L(L+1)}}\,\{C_A\,\mathrm{Re}\,[Z_L^M\,D_{M1}^L(\varphi_2,\Theta_2,\Phi_1+\varphi_3)] + C_B\,\mathrm{Im}\,[Z_L^M\,D_{M1}^L(\varphi_2,\Theta_2,\Phi_1+\varphi_3)]\}\Bigg] \qquad (V.4.7)$$

where: $C_Z = \alpha_3(\cos\Theta_3\cos\Theta_4 - \sin\Theta_3\sin\Theta_4\cos\varphi_4)$

$C_A = -\alpha_3(\sin\Theta_3\cos\Theta_4 + \cos\Theta_3\sin\Theta_4\cos\varphi_4)$

$C_B = -\alpha_3\,\sin\Theta_4\sin\varphi_4$

E_L = 1 for L even and = 0 for L odd;

O_L = 0 for L even and = 1 for L odd.

A complete derivation of the correlation function F_{234} for the general case is given in appendix B. Equation (V.4.7) is obtained from the general expression (B.21) by substitution of $\alpha_1 = \alpha_2 = \Phi_2 = 0$.

The above result has been derived for all m_i being spinless mesons. However the formalism can also be used for the case where B_2 is a Σ^o, decaying (electromagnetically) into Λ and a (spin 1) photon. The Σ^o decay is isotropic ($\alpha_2 = 0$) and the polarisation of the Λ is (see e.g. Feld [Fe69]):

$$\vec{P}_3 = -\,(\vec{P}_2\cdot\hat{q}_3)\hat{q}_3 \qquad (V.4.8)$$

Equation (V.4.5) then reads:

$$F_{234} = \frac{1}{(4\pi)^2}\,[I_2 - \alpha_3(\hat{q}_3\cdot\hat{q}_4)(I_2\vec{P}_2\cdot\hat{q}_3)] \qquad (V.4.9)$$

which is equivalent to the two-step decay distribution (V.4.1) with α_2 replaced by $-\alpha_3(\hat{q}_3 \cdot \hat{q}_4)$.

V.4.2. Procedures and results.

The three-step decay angular distribution (V.4.7) is a function of the parameters α_3 and Φ_1, the spin value J_1 of B_1 and the multipole parameters Z_L^M describing the spin density matrix of B_1. In this analysis we are primarily interested in the spin and parity of the baryon B_1 (i.e. J_1 and Φ_1). We therefore use values for α_3 as reported in the Particle Data Group tables [Pd76]:

$$\alpha_3 = -0.979 \text{ for the decay } \Sigma^+ \to p\pi^o;$$
$$\alpha_3 = \ \ 0.647 \text{ for the decay } \Lambda \ \to p\pi^-.$$

Byers and Fenster [By63] have shown that estimates for the unknown parameters Z_L^M, J_1 and Φ_1 may be obtained by the calculation of the moments of certain (judiciously chosen) functions. The moment $\langle G \rangle$ of a function G of the six decay angles Θ_i, φ_i is defined by:

$$\langle G \rangle = \int d\Omega_2 \, d\Omega_3 \, d\Omega_4 \, F_{234} \, G \qquad \text{(V.4.10)}$$

where $d\Omega_i$ is an element of the solid angle in the rest frame of baryon B_{i-1}. Experimentally $\langle G \rangle$ is estimated by the average of G over all events:

$$\bar{G} = \frac{1}{N} \sum_{i=1}^{N} G(\Theta_{2i}, \varphi_{2i}, \Theta_{3i}, \varphi_{3i}, \Theta_{4i}, \varphi_{4i}) \qquad \text{(V.4.11)}$$

The general definitions of the above mentioned moment functions are again given in appendix B (equation B.22). For the special case of baryons B_1 and B_2 being a $\Sigma(1660)$ and $\Lambda(1405)$ respectively, these definitions are as follows:

. for L even:

$$G_E(L,M) = (2L+1)\, D^{L*}_{M0}(\varphi_2,\Theta_2,0) \qquad (V.4.12)$$

. for L odd:

$$G_{O0}(L,M) = \frac{3(2L+1)}{\alpha_3}\,(\cos\Theta_3\cos\Theta_4 - \sin\Theta_3\sin\Theta_4\cos\varphi_4)\, D^{L*}_{M0}(\varphi_2,\Theta_2,0)$$

and

$$G_{O1}(L,M) = -\frac{3(2L+1)}{\alpha_3}\sqrt{L(L+1)}\,.\,(\sin\Theta_3\cos\Theta_4 + \cos\Theta_3\sin\Theta_4\cos\varphi_4 + i\,\sin\Theta_4\sin\varphi_4)\, D^{L*}_{M1}(\varphi_2,\Theta_2,\varphi_3)$$

Performing the integrations (V.4.10) for the above functions then yields:

$$\langle G_E(L,M)\rangle = Z^M_L \qquad (V.4.13a)$$

$$\langle G_{O0}(L,M)\rangle = Z^M_L \qquad (V.4.13b)$$

$$\langle G_{O1}(L,M)\rangle = Z^M_L\,.\,(2J_1+1)\,e^{-i\Phi_1} \qquad (V.4.13c)$$

Note that equations (V.4.13b) and (V.4.13c) contain the same (odd-L) Z^M_L. Hence, from the ratio of these two odd-L moments one can in principle determine both the spin and the parity of B_1:

$$(2J_1+1)\,e^{-i\Phi_1} = \frac{\langle G_{O1}(L,M)\rangle}{\langle G_{O0}(L,M)\rangle} \qquad (V.4.14)$$

a) $\Lambda(1405)\pi^+$ decay.

In table V.3 we present the Z^M_L -values resulting from the calculation of the $\langle G\rangle$ moments for the decay $\Sigma(1660) \to \Lambda(1405)\pi^+$; values up to L=7 were considered. The B_1 rest frame was chosen to be the t-channel transversity frame of B_1. In order to have a clear $\Sigma(1660)$ signal we required $\cos\Theta^*$ to be larger than 0.7. Since the decay asymmetry parameter α

of the $\Sigma^+ \to n\pi^+$ decay is small (+ 0.066 ± 0.016), we have only used the $\Sigma^+ \to p\pi^o$ decays (155 events) in the evaluation of the odd-L moments. The even-L moments on the other hand are calculated from the two-step decay only, using both the $p\pi^o$ and the $n\pi^+$ decay modes (328 events in total).

Since $\Sigma(1660)$ is produced in a reaction with unpolarised target and the Z_L^M are evaluated in the t-channel transversity frame, the "checkerboard" theorem of Capps [Ca61] is applicable. This implies that all odd-M moments should be zero. Inspection of table V.3 shows that two odd-M moments (Z_4^1 and Z_4^3) deviate from zero by approximately 2.5σ . Although this could be an indication of some interference contribution, the deviation could be just as well a statistical fluctuation of the data. The probability of finding out of 18 odd-M moments with $L \leq 4$, 2 moments that deviate from zero by 2.5 standard deviations is 2%. The overall behaviour of the odd-M moments is consistent with the hypothesis of all being zero (χ^2 test probability is 30%).

Further it can be seen in this table, that all the odd-L, even-M moments are within two standard deviations consistent with zero. We conclude that the $\Sigma(1660)$ is produced with little or no spin alignment. The Byers-Fenster test (V.4.14) is thus inconclusive with respect to the spin-parity determination of the $\Sigma(1660)$.

The even-L, even-M moments confirm the observations made from the moments of the spherical harmonics evaluated in the t-channel helicity frame (section V.2): there are two very significant L=2 moments present (5 and 4 standard deviations respectively), while all the other moments are (within 2σ) consistent with being zero.

Table V.3 - Moments of the Sequential Decay $\Sigma^+(1660)\to\Lambda(1405)\to\Sigma^+\to p$ for $\cos\theta^* > 0.7$.

		M=0		M=1		M=2		M=3		M=4		M=5		M=6		M=7	
		Re	Im	Re	Im	Re	Im	Re	Im	Re	Im	Re	Im	Re	Im	Re	Im
L=1	L	-0.11 ±0.31		-0.08 ±0.29	-0.04 ±0.20												
	T	0.43 ±0.46	0.66 ±0.50	-0.40 ±0.40	-0.51 ±0.41												
L=2		-0.61 ±0.13		-0.10 ±0.11	0.09 ±0.09	0.45 ±0.11	-0.20 ±0.12										
L=3	L	0.01 ±0.51		0.69 ±0.37	-0.20 ±0.28	-0.35 ±0.42	0.14 ±0.36	-0.09 ±0.39	-0.06 ±0.38								
	T	0.8 ±1.5	-2.3 ±1.5	0.5 ±1.5	-1.8 ±1.8	-1.0 ±1.7	-3.5 ±1.7	-2.8 ±1.8	2.5 ±1.7								
L=4		-0.00 ±0.18		0.38 ±0.14	0.00 ±0.13	0.03 ±0.13	0.03 ±0.14	-0.37 ±0.15	0.35 ±0.14	-0.15 ±0.16	-0.04 ±0.16						
L=5	L	0.94 ±0.57		-0.26 ±0.48	0.31 ±0.41	-0.35 ±0.49	-0.21 ±0.39	0.25 ±0.46	-0.89 ±0.42	-0.48 ±0.52	-0.16 ±0.50	0.11 ±0.49	-0.52 ±0.46				
	T	3.1 ±3.0	2.8 ±3.3	-2.2 ±2.7	-1.7 ±3.4	-0.2 ±3.3	-0.4 ±3.3	4.2 ±3.5	-3.0 ±3.1	1.7 ±3.9	-4.6 ±3.2	-1.9 ±3.5	5.0 ±3.6				
L=6		-0.05 ±0.22		-0.21 ±0.17	0.09 ±0.15	-0.19 ±0.16	0.09 ±0.17	0.06 ±0.18	-0.15 ±0.16	-0.17 ±0.17	-0.06 ±0.17	0.21 ±0.19	0.10 ±0.18	0.12 ±0.20	0.33 ±0.18		
L=7	L	-0.37 ±0.71		0.17 ±0.54	-0.03 ±0.44	-0.02 ±0.57	-0.40 ±0.46	0.39 ±0.56	0.06 ±0.52	0.22 ±0.51	-0.01 ±0.51	-0.43 ±0.48	-0.77 ±0.63	-0.21 ±0.60	-0.25 ±0.61	0.00 ±0.57	-1.2 ±0.5
	T	1.1 ±4.9	-5.5 ±5.2	0.2 ±4.5	-2.3 ±4.9	3.5 ±5.0	3.9 ±5.3	0.4 ±5.7	0.9 ±4.9	-2.9 ±5.3	1.6 ±5.0	1.9 ±5.4	0.0 ±5.7	-5.3 ±5.8	6.6 ±5.8	0.6 ±6.1	1.1 ±5.5

For the type of reactions we are analysing, Doncel et al. [Do72] have derived spin tests based on the multipole parameters t_L^M. These tests follow from conditions on the rank of the spin density matrix. If B_1 is produced in a reaction

$$\text{spin } 0 + \text{spin } 1/2 \rightarrow B_1 \text{ (spin J)} + \text{spin } 0$$

then the rank of the spin density matrix ρ of B_1 can be at most 2. This is essentially due to the fact that the unpolarised initial state is determined by two and only two independent spin states (namely the two possible polarisation states of the initial spin 1/2 particle) and that the recoil particle in the final state has spin 0(*).

Consider now ${}^{(E)}\rho$, the so-called even projection of the spin density matrix ρ. ${}^{(E)}\rho$ is obtained from ρ, by setting all odd-L t_L^M in ρ equal to zero. The matrix ${}^{(E)}\rho$ is, like ρ, Hermitian, positive definite and of trace 1. Since the rank of ρ is at most 2, ${}^{(E)}\rho$ is of rank ≤ 4.

Doncel et al. have now shown, that if all even-L t_L^M are zero for $L > 2$, then:

$$\text{rank of } {}^{(E)}\rho = 2J \pm 1 \qquad \text{(V.4.15)}$$

In addition, for each J they derive a relation which then should hold for the L=2 t_L^M's. As the rank of ${}^{(E)}\rho$ is ≤ 4, eq. (V.4.15) sets an upper limit on the spin J, i.e. $J \leq 5/2$. Our data are consistent with all even-L t_L^M for $L > 2$ being identically zero as required by the model. It thus follows that the spin of the $\Sigma(1660)$ decaying into $\Lambda(1405)\pi$ has to be 3/2 or 5/2. Our measured values of the t_L^M agree with both the

---

(*) Strictly speaking this argument is only true at a fixed production angle.

J=3/2 and J=5/2 constraint relation. We can therefore not discriminate between J=3/2 and J=5/2. However, the data of table V.3 are also in agreement with the assumption of all odd-L statistical tensors being zero. The latter implies that $^{(E)}\rho$ is identical to ρ and hence the rank of $^{(E)}\rho$ is 2. From (V.4.15) we can then conclude, that the spin J of $\Sigma(1660)$ must be 3/2.

For J=3/2, the above-mentioned constraint equation reads (in terms of Z_L^M's):

$$(Z_2^0)^2 + 2.|Z_2^2|^2 = 1 \qquad \text{(V.4.16)}$$

Substitution of the measured Z_L^M values gives a left-hand-side value for this equation of 0.9 ± 0.3, which is in good agreement with the required right-hand-side value of 1.

b) Σ^o decay.

We have also applied the Byers-Fenster moments analysis to the $\Sigma^o\pi^+$ decay mode of $\Sigma(1660)$. The three-step distribution function is now given by (V.4.9). The definitions of the moment functions become:

. for L even:

$$G_E(L,M) = (2L+1)D^{L*}_{M0}(\varphi_2,\theta_2,0) \qquad \text{(V.4.17)}$$

. for L odd:

$$G_{OO}(L,M) = -\frac{9(2L+1)}{\alpha_3}\cos\theta_3\cos\theta_4\, D^{L*}_{M0}(\varphi_2,\theta_2,0)$$

and

$$G_{O1}(L,M) = \frac{9(2L+1)}{\alpha_3}\sqrt{L(L+1)}\sin\theta_3\cos\theta_4\, D^{L*}_{M1}(\varphi_2,\theta_2,\varphi_3)$$

As before, the multipole parameters Z_L^M are obtained by the integration of the moment functions over the six decay angles,

the results of which are given by (V.4.13).

We have calculated the above moments for events in the $\Sigma(1660)$ production angular region $-1.0 \leqslant \cos\theta^* \leqslant -0.8$. Here too, the t-channel transversity frame was chosen as the $\Sigma(1660)$ restframe. The results for L-values up to 7 are presented in table V.4. The odd-M moments have to be zero, because of parity conservation in the production process. In fact there are three odd-M moments (Im Z_3^3, Re Z_4^1 and Re Z_6^1) which have a 2σ deviation from zero. As in the $\Lambda(1405)\pi$ case, this is not alarming; the probability for having these three moments deviating from zero by 2σ (out of 36 odd-M moments with $L \leqslant 6$) is 15%. The odd-L even-M moments are all consistent with zero with the exception of Re Z_3^2 and Re Z_5^2. The data are however not inconsistent with the hypothesis that all odd-L even-M moments are zero. A χ^2 test of the hypothesis that all of the L=3, even-M moments are zero, gives a probability of 25%. The hypothesis that all L=5, even-M moments are zero has a χ^2 probability of 8%.

We have also evaluated the moments for events in the central ($-0.8 < \cos\theta^* \leqslant 0.7$) and forward ($0.7 < \cos\theta^* \leqslant 1.0$) production angular regions. No significantly non-zero odd-L even-M moment was found. We conclude that also the $\Sigma(1660)$ which decays into $\Sigma^0\pi^+$ is produced with little or no spin alignment. The Byers-Fenster test on the spin-parity is therefore again inconclusive.

Returning to the backward region, table V.4 also shows, that there is only one even-L moment significantly different from zero: Z_2^0 shows a four standard deviation effect. This of course, we have already seen in the moments of the spherical harmonics in section V.2. So, also in this decay mode, we find that the data are consistent with only L=2 non-zero moments.

Table V.4. - Moments of the Sequential Decay $\Sigma^{+}(1660) \to \Sigma^{0} \to \Lambda \to p$ for $\cos\theta^{*} < -0.8$.

	M=0 Re	M=0 Im	M=1 Re	M=1 Im	M=2 Re	M=2 Im	M=3 Re	M=3 Im	M=4 Re	M=4 Im	M=5 Re	M=5 Im	M=6 Re	M=6 Im	M=7 Re	M=7 Im
L=1 L	-0.04 ±1.22		0.10 ±0.57	-0.26 ±0.58												
L=1 T	0.10 ±0.88	-0.45 ±1.10	-1.96 ±1.30	-0.92 ±1.43												
L=2	1.21 ±0.29		0.32 ±0.21	-0.07 ±0.18	0.16 ±0.16	-0.20 ±0.14										
L=3 L	0.87 ±1.57		-1.26 ±1.42	-0.81 ±1.07	-0.57 ±0.92	-0.29 ±1.15	-0.77 ±0.69	-0.05 ±0.77								
L=3 T	0.48 ±5.50	0.05 ±6.55	-1.34 ±5.21	3.31 ±5.28	-12.6 ± 5.2	-6.28 ±3.89	-1.37 ±3.18	7.04 ±3.50								
L=4	0.19 ±0.38		0.61 ±0.30	-0.14 ±0.29	0.29 ±0.27	0.13 ±0.27	-0.23 ±0.22	-0.07 ±0.22	0.10 ±0.23	-0.13 ±0.15						
L=5 L	1.21 ±1.74		-2.33 ±1.66	1.53 ±1.44	-3.42 ±1.71	-0.93 ±1.44	0.13 ±1.48	0.04 ±1.06	-1.99 ±1.39	-0.28 ±0.81	-0.81 ±0.70	1.32 ±0.96				
L=5 T	0.9 ±11.0	14.4 ±12.2	-12.4 ±10.5	10.5 ±13.4	-28.8 ± 9.7	-6.1 ±10.4	-14.7 ± 8.6	13.9 ±10.3	-3.00 ±7.17	2.66 ±7.62	3.10 ±5.44	-4.79 ±6.20				
L=6	-0.35 ±0.47		0.67 ±0.32	0.29 ±0.35	-0.19 ±0.36	0.63 ±0.35	-0.10 ±0.32	0.19 ±0.33	-0.10 ±0.31	-0.08 ±0.25	-0.16 ±0.25	0.10 ±0.25	-0.10 ±0.22	-0.25 ±0.22		
L=7 L	3.90 ±2.42		0.30 ±1.46	1.02 ±1.58	-1.58 ±2.09	1.10 ±1.75	0.04 ±2.19	-0.04 ±1.45	0.03 ±1.68	-0.33 ±1.38	0.94 ±1.08	1.06 ±1.56	0.30 ±1.14	0.43 ±1.38	1.16 ±0.81	-0.63 ±1.03
L=7 T	2.1 ±17.7	- 1.1 ±17.4	8.0 ±16.7	16.7 ±21.2	-20.7 ±16.8	-14.3 ±21.5	5.2 ±14.2	26.9 ±16.9	-4.5 ±14.7	12.6 ±16.9	3.9 ±13.4	8.1 ±11.7	2.3 ±9.3	-4.6 ±11.3	-8.0 ±8.2	-0.3 ±9.4

The same reasoning about the rank of the spin density matrix as in the $\Lambda(1405)$ mode, yields that the spin of the $\Sigma(1660)$ which decays into $\Sigma\pi$ is 3/2. From table V.4 we now find that the left-hand-side of (V.4.16) amounts to 1.6 ± 0.7. The constraint equation for J=3/2 is therefore again satisfied, although the error is now rather large.

The statistical errors on the L=2 moments in the forward production angular region are too large to be used in an analogous test.

V.5. Dalitz-Miller analysis of $\Sigma^+(1660) \to \Sigma^-\pi^+\pi^+$.

We have used the events of final states (IV.2) in a Dalitz-Miller analysis [Da61] . This analysis is based on the interference effects in the $\Sigma^-\pi^+\pi^+$ decay, caused by the presence of the two identical pions. Mathematically this interference is introduced by symmetrising the decay matrix element for the exchange of the two pions. If we assume the decay of $\Sigma(1660)$ into $\Sigma^-\pi^+\pi^+$ to proceed completely through $\Lambda(1405)$ (see chapter IV), the distribution of the points in the Dalitz-plot is given by [Ja65,Le65]:

$$dN \sim [p_2^{2\ell}|G_1|^2 + p_1^{2\ell}|G_2|^2 + 2\,\mathrm{Re}(G_1^* G_2) p_1^{\ell} p_2^{\ell} P_{\ell}(\cos\theta_{12})]\, dE_1\, dE_2 \qquad (V.5.1)$$

where the symbols used have the following definitions:

$G_j = \dfrac{\Gamma}{M_o - M(\Sigma^-\pi_j^+) - i\frac{\Gamma}{2}}$ is the Breit-Wigner line shape

$M(\Sigma^-\pi_j^+)$ the effective mass of Σ^- and π_j^+ ,

M_0, Γ the mass and width of $\Lambda(1405)$,

p_j the momentum of π_j^+ in the $\Sigma^-\pi^+\pi^+$ rest frame,

ℓ the orbital angular momentum of the $\Lambda(1405)$-π^+ system,

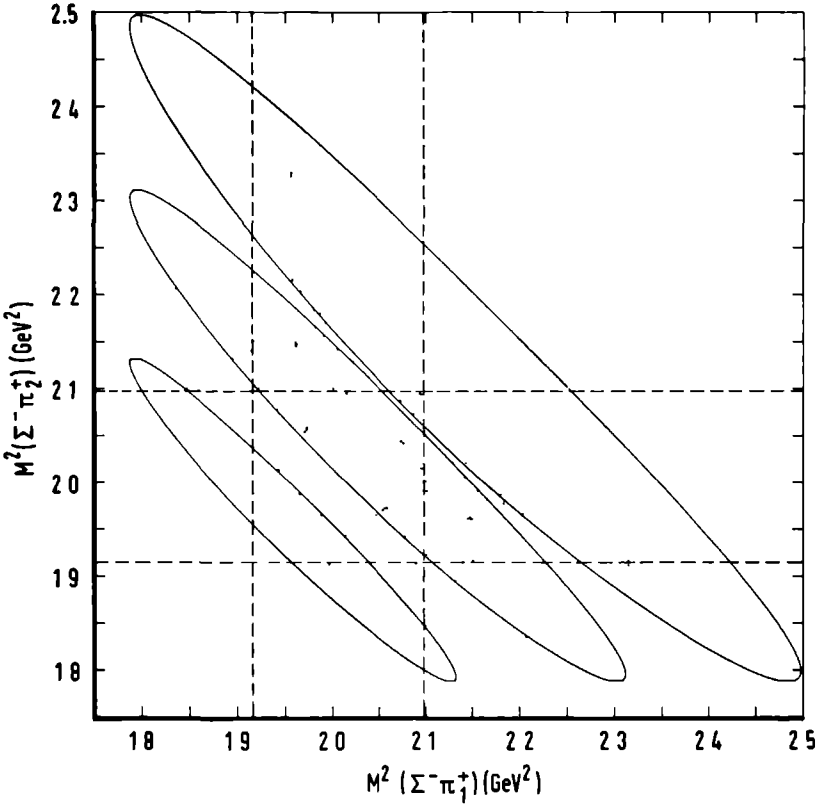

Fig.V.6. Dalitz plot for the $\Sigma^-\pi^+\pi^+$ system in the $\Sigma(1660)$ mass region for $\cos\theta^* > 0.9$; the contours correspond to $\Sigma(1660)$ masses of 1.60, 1.66 and 1.72 GeV respectively; also indicated are 2 Γ- wide $\Lambda(1405)$ mass bands.

P_ℓ the Legendre polynomial of order ℓ.

$\cos\theta_{12}=\hat{p}_1\cdot\hat{p}_2$ the angle between the two pions in the $\Sigma^-\pi^+\pi^+$ rest frame.

Figure V.6 shows the $\Sigma^-\pi^+\pi^+$ Dalitz plot for events having $M(\Sigma^-\pi^+\pi^+)$ between 1.60 and 1.72 GeV. Also shown in this figure are the two $\Lambda(1405)$ bands and the Dalitz plot boundaries for three values of the $\Sigma^-\pi^+\pi^+$ invariant mass (1.60, 1.66 and 1.72 GeV respectively). The data points have been symmetrised by letting each event enter twice. As can be seen from this plot, there is a large area where interference effects between the two $\Lambda(1405)$'s can take place. It is also clear, that this interference can be large only on the low-mass side of the $\Sigma(1660)$. In addition, the background under the $\Sigma(1660)$ is smaller on the low-mass side. Therefore, to be more sensitive to the interference term in (V.5.1) and hence to the value of ℓ, we have restricted the analysis to events satisfying

$$1.60 < M(\Sigma^-\pi^+\pi^+) < 1.66 \text{ GeV}.$$

In addition we required the $\Sigma^-\pi^+\pi^+$ CM-production-angle cosine to be larger than 0.9. The amount of background left after these selections is estimated to be very small ($\lesssim 5\%$).

We have obtained a 'best' value of ℓ by means of maximum likelihood fits to the Dalitz plot. The likelihood function used in the fit was the Dalitz plot density function (V.5.1) multiplied by a Breit-Wigner function accounting for the $\Sigma^-\pi^+\pi^+$ mass dependence. Fits were performed with the $\Lambda(1405)$ and $\Sigma(1660)$ resonance parameters fixed (i.e. with ℓ as the only free parameter), with only the mass and width of $\Lambda(1405)$ left free and finally with both the $\Lambda(1405)$ and $\Sigma(1660)$ parameters left free. The results, for ℓ=1, 2 and 3, are presented in table V.5. The ℓ=0 hypothesis was a priori strongly excluded by the decay angle spherical harmonics (see section V.2). One observes that there is a strong preference for

ℓ=1. With the $\Sigma(1660)$ resonance parameters fixed and those of $\Lambda(1405)$ left free, the decrease in the natural logarithm of the likelihood $\mathcal{L}$ for ℓ=2 amounts to 13.7. One expects a priori the decrease to be smaller with additional free parameters (M_o and Γ of $\Sigma(1660)$), but even in this case the difference in $\ln\mathcal{L}$ is 5.6 or larger. A χ^2 comparison between the projections resulting from the fits and the experimental projected distributions shows that the curves for ℓ=1 fit the data reasonably well, while at least one of the projections for ℓ=2 and ℓ=3 do not give a good fit to the data.

The $M(\Sigma^-\pi^+)$ and $\cos\theta_{12}$ projections (together with the projections from the fits with the $\Lambda(1405)$ parameters left free but the $\Sigma(1660)$ parameters kept fixed) are shown in figure V.7.

Since the $\Lambda(1405)$ has $J^P=1/2^-$, the value ℓ=1 implies that the $\Sigma(1660)$ has $J^P=3/2^-$ or $1/2^-$. However, J=1/2 is strongly excluded by the moments of the spherical harmonics (see section V.2). The Dalitz-Miller analysis thus conclusively establishes that the $\Sigma(1660) \rightarrow \Lambda(1405)\pi$ has spin-parity $3/2^-$.

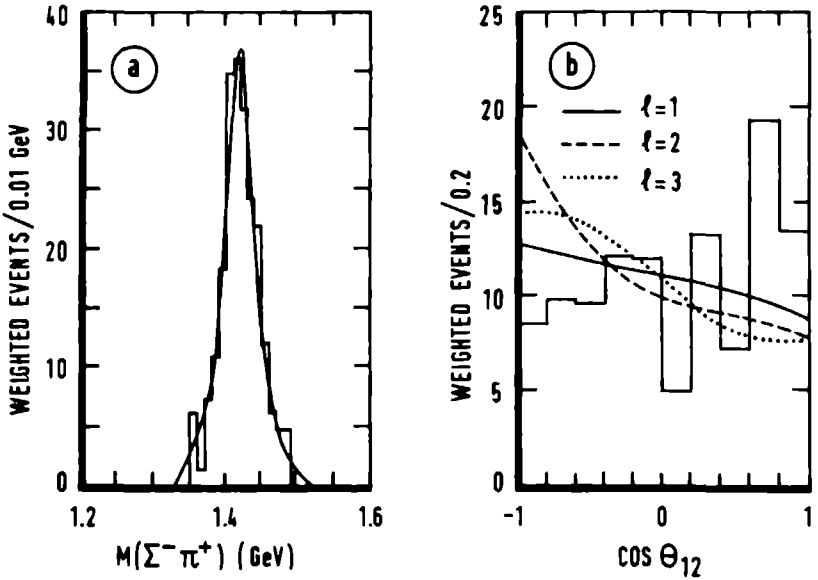

Fig. V.7. (a) Effective mass distribution $M(\Sigma^-\pi^+)$ for $\Sigma(1660)$ events; the curve is the result of a maximum likelihood fit to the Dalitz plot for $\ell=1$.

(b) Distribution of the cosine of the angle between the two π^+'s in the $\Sigma^-\pi^+\pi^+$ rest frame. The curves show the result of maximum likelihood fits to the Dalitz plot for $\ell=1$, 2 and 3 respectively.

Table V.5. Results of Dalitz-Miller Analysis of $\Sigma^-\pi^+\pi^+$ Events Having $1.6 < M(\Sigma^-\pi^+\pi^+) < 1.66$ GeV and $\cos\theta^* > 0.9$ (91 events).

ℓ	Resonance parameters				$\ln\mathcal{L}$	χ^2/ND of projected distributions		
	$\Lambda(1405)$		$\Sigma(1660)$					
	M_o	Γ	M_o	Γ		$M(\Sigma^-\pi^+)$	$M(\Sigma^-\pi^+\pi^+)$	$\cos\theta_{12}$
1	fixed at				37.8	23/12	0.6/5	9/9
2	1.405	0.040	1.657	0.053	12.3	38/12	5.7/5	18/7
3					-4.1	85/14	13/4	31/8
1	1.416 ± .005	0.032 ± .006	fixed at		47.1	3.7/10	2.4/5	6.1/6
2	1.419 ± .003	0.025 ± .003	1.657	0.053	33.4	3.4/10	8.8/5	16/6
3	1.423 ± .004	0.022 ± .004			29.8	12/10	19/5	14/6
1	1.416 ± .005	0.032 ± .006	1.650 ± .007	0.052 ± .015	48.0	4.8/10	0.9/5	4.5/6
2	1.420 ± .004	0.025 ± .005	1.644 ± .008	0.075 ± .029	39.1	7.2/9	1.1/5	15/6
3	1.424 ± .004	0.022 ± .006	1.671 ± .054	0.044 ± .091	42.4	15/10	33/5	13/6

CHAPTER VI.

B R A N C H I N G R A T I O S O F $\Sigma(1660)$.

As shown in chapter III, there is a large discrepancy between the decay rates of the $\Sigma(1660)$'s observed in formation and in production experiments. We have also established that in production experiments one observes (at least) two $\Sigma(1660)$ resonances, one of which has a large $\Lambda(1405)\pi$ decay mode. In this final chapter, we present results on the relative decay rates of the $\Sigma(1660)$ observed in our experiment and compare them with formation experiments. Comparisons with predictions from SU(3)- and SU(6)-fits are also made.

VI.1. Experimental results.

The presence of $\Sigma(1660)$ in the various channels has been examined in chapter IV. For the channels $K^-p \to \Sigma^+\pi^-\pi^+\pi^-$ and $K^-p \to \Sigma^o\pi^+\pi^-$ we determined, through maximum likelihood fits to the effective mass spectra, the numbers of $\Sigma(1660)$ events both for the entire production angular region and for three different subregions of the $\Sigma(1660)$ production angle: (a) $0.7 < \cos\theta^* \leq 1.0$, (b) $-0.8 < \cos\theta^* \leq 0.7$, (c) $-1.0 \leq \cos\theta^* \leq -0.8$. In the latter fits, we kept the mass and the width fixed at the values obtained in the fits to the total production angular region. The curves derived from these fits were shown in figure IV.15. The results obtained for the channels $K^-p \to \Lambda\pi^+\pi^-$, $K^-p \to p\bar{K}^o\pi^-$ and $K^-p \to \Lambda\pi^+\pi^o\pi^-$ performing the same type of fits are shown in figures VI.1, VI.2 and VI.3 respectively. It may be recalled that the $M(\Lambda\pi^+)$ distribution was fitted to an incoherent sum of two Breit-Wigner functions plus a linear background. The reason for doing this

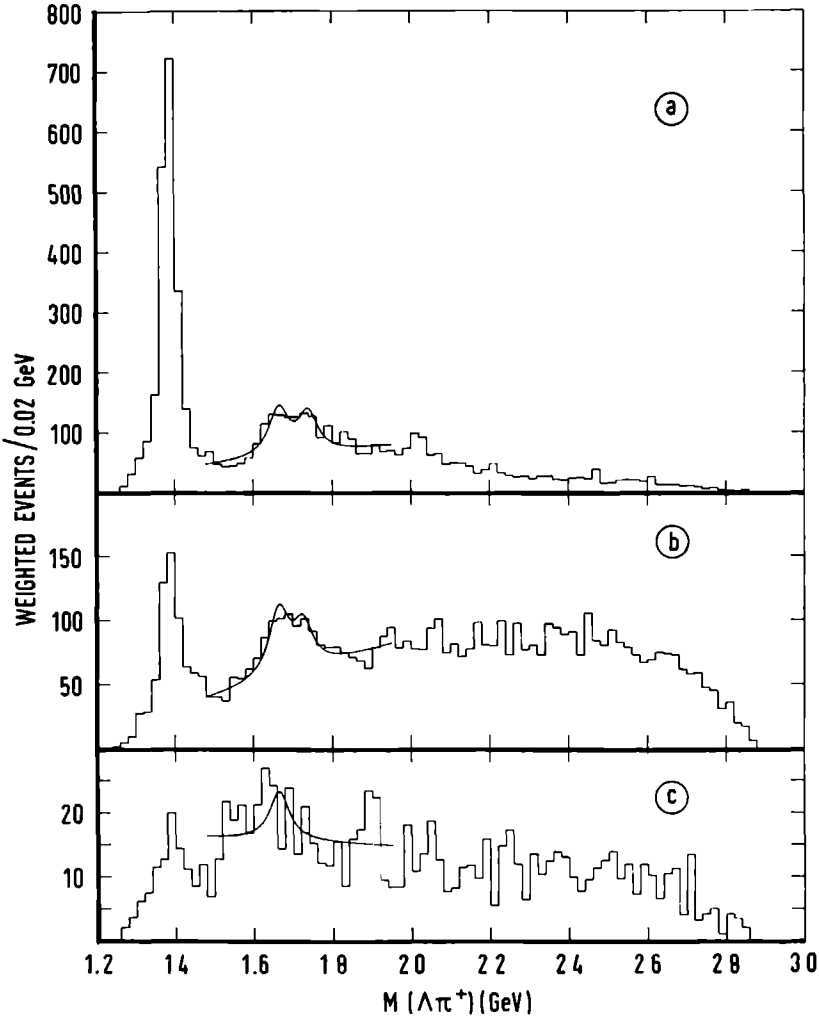

Fig.VI.1. Effective mass distribution $M(\Lambda\pi^+)$ for the channel $K^-p \to \Lambda\pi^+\pi^-$ in the production angular regions: (a) $0.7 < \cos\theta^* \leq 1.0$, (b) $-0.8 < \cos\theta^* \leq 0.7$, (c) $-1.0 \leq \cos\theta^* \leq -0.8$.

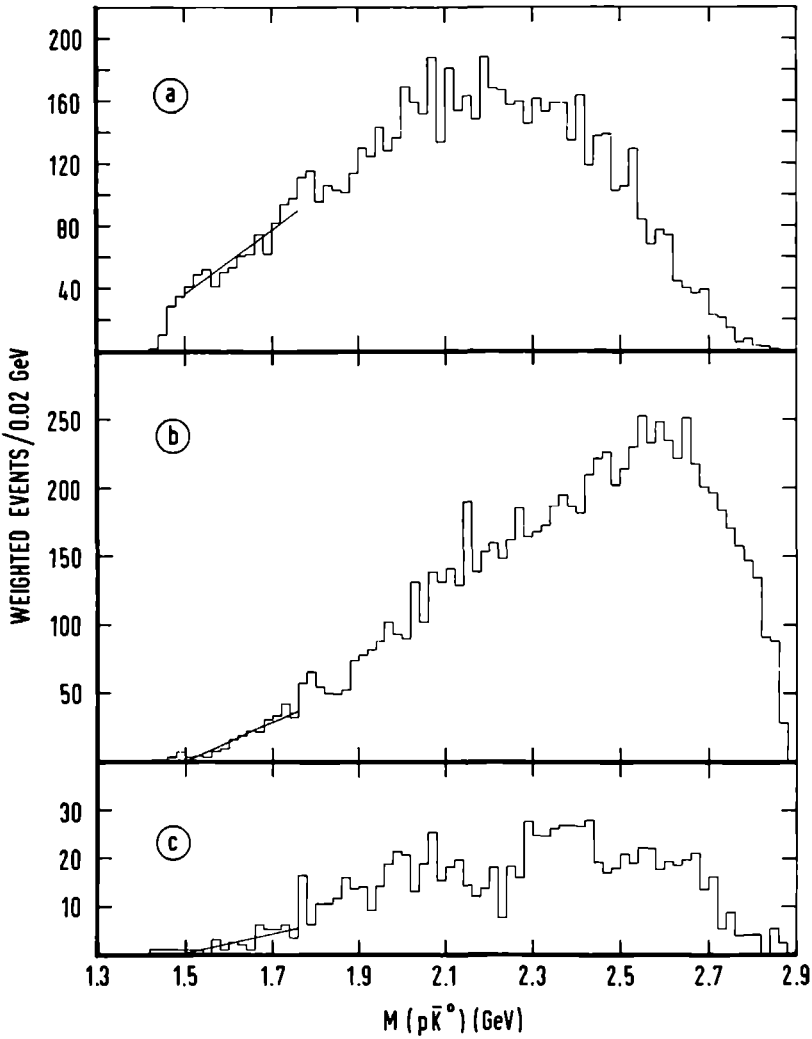

Fig.VI.2. Effective mass distribution $M(p\bar{K}^0)$ for the channel $K^-p \to p\bar{K}^0\pi^-$ in the production angular regions: (a) $0.7 < \cos\theta^* \leqslant 1.0$, (b) $-0.8 < \cos\theta^* \leqslant 0.7$, (c) $-1.0 \leqslant \cos\theta^* \leqslant -0.8$.

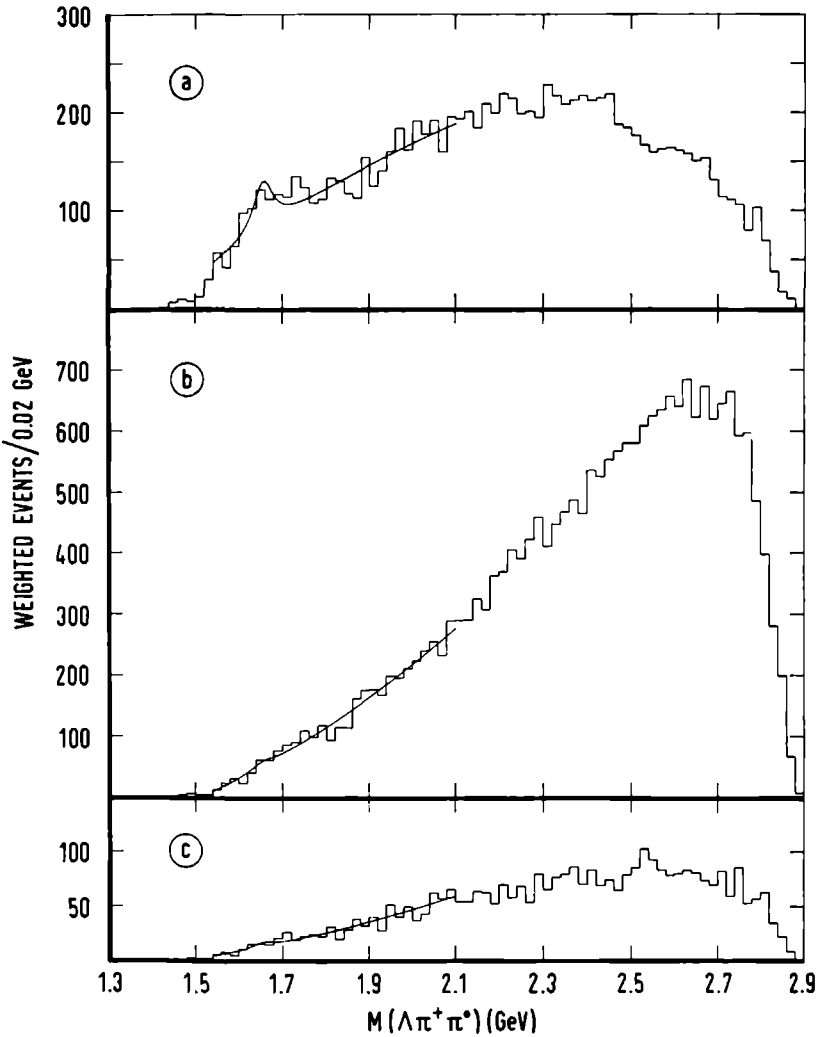

Fig.VI.3. Effective mass distribution $M(\Lambda\pi^+\pi^o)$ for the channel $K^-p \to \Lambda\pi^+\pi^o\pi^-$ in the production angular regions: (a) $0.7 < \cos\theta^* \leq 1.0$, (b) $-0.8 < \cos\theta^* \leq 0.7$, (c) $-1.0 \leq \cos\theta^* \leq -0.8$.

can be seen in figure VI.1. The broad enhancement at 1.7 GeV stays equally broad in all three production angular regions, but shifts to a lower central mass value in the backward region ($\cos\theta^* \leq -0.8$). The enhancement can thus not be due to just a single resonance.

The numbers of events in the $\Sigma(1660)$ obtained from the different fits are given in table VI.1. A consistency check is supplied by the observation that the numbers of events in the 'total' fits agree well with the sum of the numbers of events in the three angular regions separately.

Table VI.1. Number of Events in $\Sigma^+(1660)$ for the Various Decay Modes and Production Angular Regions.

$\cos\theta^*$ interval	$\Lambda(1405)\pi^+$ $\hookrightarrow\Sigma^+\pi^-$	$\Sigma^o\pi^+$	$\Lambda\pi^+$	$p\bar{K}^o$	$\Lambda\pi^+\pi^o$
(-1.0,1.0)	586 ± 50	635 ± 50	<600 ± 70	<22	<228 ± 47
(0.7,1.0)	526 ± 30	301 ± 36	<350 ± 52	<18	<186 ± 36
(-0.8,0.7)	38 ± 17	240 ± 30	<228 ± 43	<25	< 37 ± 17
(-1.0,-0.8)	2 ± 6	98 ± 16	< 16 ± 23	<10	< 14 ± 12

In order to calculate the branching ratio $\Lambda(1405)\pi/\Sigma\pi\pi$, we have fitted the $\Sigma^+\pi^-\pi^+$ mass spectrum for $\cos\theta^* > 0.7$ (see figure VI.4). Again, the mass and width in this fit were kept fixed at the values obtained in the fit to the complete spectrum. The number of $\Sigma(1660)$ events found in this fit was 545 ± 35. We thus obtain for the branching ratio:

$$\frac{\Sigma(1660) \rightarrow \Lambda(1405)\pi}{\Sigma(1660) \rightarrow \Sigma\pi\pi} = 0.97 \pm 0.08$$

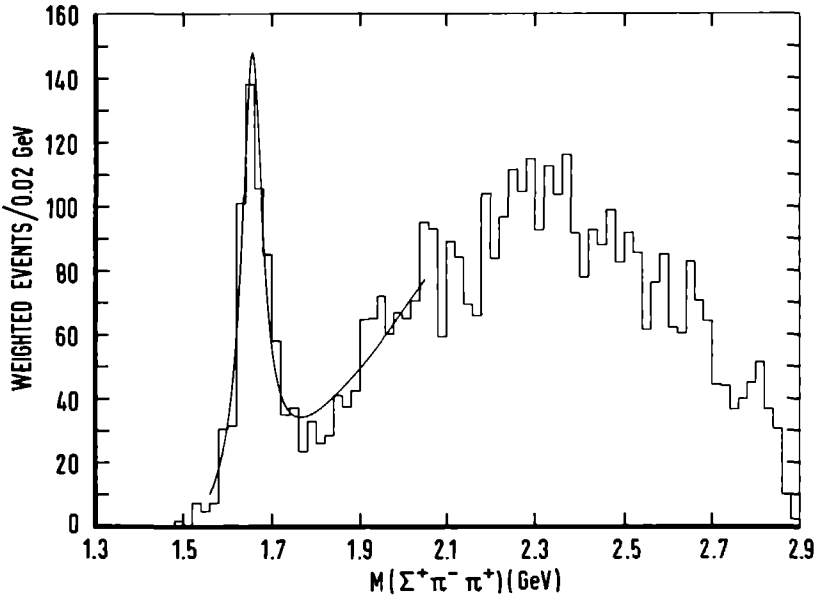

Fig.VI.4. Effective mass distribution $M(\Sigma^+\pi^-\pi^+)$ for the channel $K^-p \to \Sigma^+\pi^-\pi^+\pi^-$ in the production angular region $0.7 < \cos\theta^* \leq 1.0$.

Although we have always assumed that the decay of $\Sigma(1660) \to \Sigma\pi\pi$ was entirely $\Lambda(1405)\pi$ decay, there is a priori considerable overlap between $\Sigma(1385)$ and $\Lambda(1405)$ in the $M(\Sigma\pi)$ distribution. From the results for the $\Lambda\pi^+\pi^0$ decay mode, we can make an estimate of the $\Sigma(1385)\pi$ contribution to the decay $\Sigma^+(1660) \to \Sigma^+\pi^-\pi^+$ (*). Let us assume that all of the decay $\Sigma(1660) \to \Lambda\pi\pi$ indeed proceeds via $\Sigma(1385)\pi$. Then correc-

(*) $\Sigma(1385)$ decays into $\Lambda\pi$ and $\Sigma\pi$; $\Lambda(1405)$ can only decay into $\Sigma\pi$.

ting for the (known) $\Lambda\pi/\Sigma\pi$ branching ratio of the $\Sigma(1385)$ decay, for the isospin Clebsch-Gordan coefficients of the $\Sigma\pi$ decay mode and for the relative detection efficiency of the two topologies, one obtains an upper limit for the $\Sigma(1385)\pi^+$ contribution in the decay $\Sigma^+(1660) \rightarrow \Sigma^+\pi^-\pi^+$ of 12 ±3 events, a negligible contamination.

Using the numbers of events in table VI.1., the μb-equivalents and the total correction factors from table IV.4, we calculated the branching ratios given in table VI.2. Note once more, the dramatic change with the production angle of the $\Lambda(1405)\pi/\Sigma\pi$ branching ratio, change which is at the origin of the hypothesis that one observes (at least) two $\Sigma(1660)$ resonances in production experiments.

Table VI.2. Branching Ratios of $\Sigma(1660)$.

	all events	$0.7<\cos\theta^*\leq 1.0$	$-0.8<\cos\theta^*\leq 0.7$	$-1.0\leq\cos\theta^*\leq -0.8$
$\frac{N\bar{K}}{\Sigma\pi}$	< 0.03	< 0.05	< 0.09	< 0.09
$\frac{\Lambda\pi}{\Sigma\pi}$	< 0.45 ± 0.07	< 0.56 ± 0.11	< 0.46 ± 0.10	< 0.08 ± 0.11
$\frac{\Lambda(1405)\pi}{\Sigma\pi}$	0.93 ± 0.11	1.8 ± 0.3	0.16 ± 0.08	0.02 ± 0.07
$\frac{\Sigma(1385)\pi}{\Sigma\pi}^{(\dagger)}$	< 0.22 ± 0.05	< 0.37 ± 0.09	< 0.09 ± 0.05	< 0.09 ± 0.08

(†) This ratio is calculated assuming that the entire $\Lambda\pi\pi$ decay mode is $\Sigma(1385)\pi$.

VI.2. Comparison with results from formation experiments.

In formation experiments one obtains the resonance parameters through a partial wave analysis. This yields the ampli-

tudes T_{1k} for the scattering process of channel 1 to channel k. The Breit-Wigner approximation to these amplitudes may be written as:

$$T_{1k} = (x_1 x_k)^{\frac{1}{2}} \cdot \frac{\Gamma/2}{M - E - i\Gamma/2} \qquad \text{(VI.1)}$$

where $\Gamma = \sum_k \Gamma_k$ and $x_k = \frac{\Gamma_k}{\Gamma}$. E is the centre-of-mass energy, M the resonance mass and Γ the total width of the resonance. Γ_k is the partial width of channel k; x_1, often written as x_e, is the so-called elasticity of the resonance. Magnitudes of the different $\Sigma(1660)$ amplitudes at resonance (i.e. $(x_e x_k)^{\frac{1}{2}}$) found in various formation experiments are summarised in table VI.3. There is good agreement between the different experiments, although additional measurements of the amplitudes for $\Sigma(1385)\pi$ and $\Lambda(1405)\pi$ are badly needed. Using the averaged values we determined the following branching ratios for the (formation experiment) $\Sigma(1660)$:

$$\text{B.R.} \left(\frac{N\bar{K}}{\Sigma\pi}\right) = 0.19 \pm 0.09$$

$$\text{B.R.} \left(\frac{\Lambda\pi}{\Sigma\pi}\right) = 0.17 \pm 0.09$$

$$\text{B.R.} \left(\frac{\Sigma(1385)\pi}{\Sigma\pi}\right) = 0.29 \pm 0.19$$

$$\text{B.R.} \left(\frac{\Lambda(1405)\pi}{\Sigma\pi}\right) < 0.15 \pm 0.06$$

Comparison of these branching ratios with the ratios found in our experiment (table VI.2), shows that there is reasonable agreement, except for the $\Lambda(1405)\pi/\Sigma\pi$ ratio. This suggests that the $\Sigma(1660)$ seen in production experiments and decaying into $\Sigma\pi$, $\Lambda\pi$ and possibly into $\bar{K}N$ and $\Sigma(1385)\pi$, may be identified with the $\Sigma(1660)$ observed in formation experiments. The other $\Sigma(1660)$ would then decay predominantly into $\Lambda(1405)\pi$.

Table VI.3. $\Sigma(1660)$ Amplitudes.

$\bar{K}N \to \bar{K}N$	$\bar{K}N \to \Lambda\pi$	$\bar{K}N \to \Sigma\pi$	$\bar{K}N \to \Sigma(1385)\pi$	$\bar{K}N \to \Lambda(1405)\pi$	Reference
0.09 ± 0.02				<0.06	Ar68,69-2
			<0.18 ± 0.02 (*)		Si68
0.08 ± 0.02		0.20 ± 0.01			Ar69
	0.09 ± 0.02	0.18 ± 0.06			Ga70
				<0.08 ± 0.02 (*)	Br70
	0.165 ± 0.01 (†)				Bu71
0.10 ± 0.03	0.13 ± 0.03	0.23 ± 0.05			La72
0.09 ± 0.03	0.09 ± 0.02	0.22 ± 0.02			Ho72,75
			0.11 ± 0.03		Pr74
	0.08 ± 0.01				Po75
	0.065 ± 0.02				Ba75
0.09 ± 0.02	0.08 ± 0.02	0.20 ± 0.02	0.11 ± 0.04	<0.08 ± 0.02	Average (§)

(§) The errors given on the averages are based on a typical systematic amplitude error of 0.05 [Fa72].

(†) This value has not been included in the average, because it is inconsistent with the majority of the other values.

(*) Derived from published result for $(x_e x_k)$.

VI.3. Comparison with predictions from SU(3) and SU(6) fits.

The SU(3) classification scheme for strongly interacting particles groups the particles into multiplets of dimension 1, 8 and 10 respectively. Pure SU(3) symmetry would predict that all of the particles within a multiplet have the same mass and the same coupling constant for decays into (different) members of the same multiplets. Within this model the partial decay rates can thus be calculated up to an a priori unknown SU(3) invariant coupling constant. Fits to partial decay rates of resonances in various SU(3) multiplets have been performed by many authors, most recently by Samios et al. [Sa74] . In calculating these decay rates, the amplitude for the two-particle decay of a resonance is written as a product of an SU(3) invariant reduced coupling constant and an SU(3) unitary spin coefficient (also called isoscalar factor). The partial width of the decay

$$x \to y + z$$

is then obtained by multiplying the square of the amplitude with an 'angular momentum barrier' factor and with a phase space factor, i.e.:

$$\Gamma_{x \to yz} = \left| A^{x}_{yz} \right|^{2} \cdot \left(\frac{p}{M}\right)^{2\ell} \cdot \left(\frac{p}{m}\right) \cdot M \qquad \text{(VI.3.1)}$$

where A^{x}_{yz} is the amplitude containing the SU(3) invariant amplitude, p the momentum of the decay particles in the rest frame of the resonance, m the mass of the decaying particle and ℓ the value of the orbital angular momentum of the decay. The arbitrary mass M(= 1 GeV) is introduced in order to have A^{x}_{yz} dimensionless. The above form for the kinematical factors is the one chosen by e.g. Samios et al.; however, different parameterisations of these factors are possible. A fit to the

decay rates does therefore not only test the validity of the SU(3) symmetry, but also the assumptions made for the kinematical factors. An additional assumption is that the reduced coupling constant is an SU(3) invariant, in spite of the fact that we know from the mass splittings within an SU(3) multiplet, that this symmetry is broken. The hope however is, that by using the physical masses in the calculation of the kinematical factors, the largest fraction of this symmetry-breaking will be taken into account.

Assuming the decay products y and z to belong to octet representations, the mother particle must belong to one of the representations of the following SU(3) 'Clebsch Gordan' series:

$$\{8\} \times \{8\} = \{1\} + \{8^S\} + \{8^a\} + \{10\} + \{\overline{10}\} + \{27\}$$

If x is a singlet or decimet member there is only one unknown amplitude and A^x_{yz} is simply written as:

$$A^x_{yz} = C_k \, A_k \quad (k = 1 \text{ or } = 10)$$

where C_k is a unitary spin coefficient and A_k an SU(3) invariant amplitude.

If x is an octet member, there are two possible couplings (symmetric and anti-symmetric) and thus two unknown invariant amplitudes: A_s and A_a. The amplitude A^x_{yz} is then given by

$$A^x_{yz} = C_s \, A_s + C_a \, A_a$$

A further complication arises from the fact that mixing may occur between the octet-isosinglet and any SU(3) singlet with the same spin-parity(*). If this so-called nonet structure is present, one has the following expressions for the amplitudes

---

(*) Other mixings are possible, but have not been used in previous analyses.

of the two physical iso-singlet particles x_1 and x_8:

$$A_{yz}^{x_1} = C_1 A_1 \cos\theta + (C_s A_s + C_a A_a) \sin\theta$$

$$A_{yz}^{x_8} = - C_1 A_1 \sin\theta + (C_s A_s + C_a A_a) \cos\theta$$

where θ is the mixing angle (the sign convention is that of Samios et al.). In this case there are thus 4 unknowns (A_1, A_s, A_a and θ).

For a $\Sigma(1660)$ belonging to an octet and decimet respectively, the amplitudes A_{yz}^{x} for octet-octet decay are given in table VI.4. Instead of using A_s and A_a, the amplitudes A_{yz}^{x} are expressed in terms of the amplitude A_8 and the parameter α. A_8 is proportional to the decay rate $N \to N\pi$ and α is the well known F/(F+D) ratio between the anti-symmetric (F) and the symmetric (D) amplitudes(†). This definition implies:

$$A_8 = \frac{\sqrt{15}}{10} A_s + \frac{\sqrt{3}}{6} A_a$$

$$\alpha = \frac{\sqrt{3}}{6} \frac{A_a}{A_8}$$

Table VI.4. Decay Amplitudes for $\Sigma(1660)$(*).

Decay Mode	Octet	Decimet
$N\bar{K}$	$\sqrt{2}\ (2\alpha-1)\ A_8$	$-\frac{\sqrt{6}}{6}\ A_{10}$
$\Lambda\pi$	$\frac{2}{\sqrt{3}}\ (1-\alpha)\ A_8$	$-\frac{1}{2}\ A_{10}$
$\Sigma\pi$	$2\sqrt{2}\ \alpha\ A_8$	$\frac{\sqrt{6}}{6}\ A_{10}$

(*) Isoscalar factors taken from the Particle Data Group tables [Pd76] (adapted from J.J. de Swart [Sw63]).

(†) In the literature one sometimes finds α defined as the D/(D+F) ratio.

The fit of Samios et al. to the $J^P = 3/2^-$ nonet, assumed to consist of $N^*(1520)$, $\Lambda(1520)$, $\Lambda(1690)$ and $\Sigma(1660)$ (†), yielded the values $\alpha = 0.72 \pm 0.15$ and $|A_8| = 41.1 \pm 1.6$. The resulting branching ratios

$$\text{B.R.}\ \left(\frac{N\bar{K}}{\Sigma\pi}\right) = 0.07 \pm 0.07$$

and

$$\text{B.R.}\ \left(\frac{\Lambda\pi}{\Sigma\pi}\right) = 0.09 \pm 0.14$$

are in reasonable agreement with our results and with those of the formation experiments.

In 1964 Gell-Mann [Ge64] and Zweig [Zw64] proposed that the strongly interacting particles are built from a triplet of fundamental particles, called quarks, and a triplet of their corresponding antiparticles (antiquarks). These two triplets would be the basic triplets for the representations of SU(3); mesons would be bound quark-antiquark states, baryons bound three-quark states. Within SU(3) the possible spin of the quarks is not considered. If we assume that the quarks are spin 1/2 particles, we have (in a non-relativistic description) six basic quark states, the basic multiplet of SU(6). These six states ([6]) form the components of a six-dimensional spinor. Higher multiplets may be obtained by forming direct products of the basic spinors. Possible SU(6) baryon multiplets are then given by the 'product':

$$[6] \times [6] \times [6] = [20] + [56] + [70] + [70]$$

(†) The Ξ candidate for this multiplet is assumed to be $\Xi^*(1820)$. Since the available experimental data for this resonance were poor, they were not included in the fit.

The total quark spin is either 1/2 (configuration $\uparrow\downarrow\uparrow$) or 3/2 (configuration $\uparrow\uparrow\uparrow$). In addition to spin, the quark-states have a total orbital angular momentum L. The lowest lying baryon states will be three-quark states with total orbital angular momentum L=0. The low-lying $1/2^+$ octet (16 states) and $3/2^+$ decimet (40 states) belong to the [56] representation with L=0 and total parity +, denoted by $[56,0^+]$. Excited states may be associated with three-quark states having a total angular momentum $L \neq 0$. Negative parity baryon states, such as the $\Sigma(1660)$, must be due to odd-L states; the simplest assumption is that these states are L=1 excitations of the three-quark system. The experimental evidence for the existence of the $1/2^-$ and $3/2^-$ nonets and a $5/2^-$ octet, all lying in a similar mass range, suggests to accomodate these low-lying negative parity baryons in the $[70,1^-]$ multiplet(*). The SU(3) decomposition of this multiplet is given by

$$[70] = [\{1\},1/2] + [\{8\},1/2] + [\{8\},3/2] + [\{10\},1/2]$$

where { } denotes the SU(3) multiplet and 1/2 (3/2) represents the total spin of the three quarks. Combining the total quark spin with the orbital angular momentum L=1 we expect the following SU(3) multiplets within the $[70,1^-]$ multiplet of SU(6): two singlets, two octets and two decimets, each with J=1/2 and J=3/2 respectively and three octets with J=1/2, 3/2 and 5/2 respectively. The SU(6) predictions for the α parameter of the octets are:

(*) The above notation implies that we are classifying excited states according to SU(6)xO(3) and not merely SU(6).

	octet 1	octet 2
J = 1/2 :	α = 0.625	α = -0.5
J = 3/2 :	α = 0.625	α = -0.5
J = 5/2 :		α = -0.5

where octet 1(2) is the octet with total quark spin 1/2 (3/2).

Fits of the entire [70,1^-] multiplet to the experimental partial widths for decay into a pseudoscalar meson and either a $J^P = 1/2^+$ baryon (octet) or a $J^P = 3/2^+$ baryon (decimet) have been done by Faiman and Plane [Fa72] and by Hey et al. [He75] . The input data for the fits come from formation experiments. The authors use a 'relativistic' version of SU(6), so-called $SU(6)_W$ [Li65] . This symmetry is a relativistically invariant spin symmetry for single particle states in motion.

In the fit of Faiman and Plane the agreement between the predicted and the experimental values for the different decay amplitudes of the $\Sigma(1660)$ resonance was very good (see first two lines in table VI.5). However, since no other Σ resonances were assigned to the remaining $3/2^-$ octet and decimet, part of this success may be due to the presence of two independent, adjustable mixing parameters. In the fit of Hey et al. two newly discovered Σ resonances, $\Sigma(1580)$ and $\Sigma(1940)$, were assigned to the two remaining $J^P = 3/2^-$ multiplets, thereby imposing more constraints to the fit. The agreement between predicted and experimental values for the amplitudes was again satisfactory.

Let us reconsider now the two $\Sigma(1660)$'s as observed in our production experiment. One $\Sigma(1660)$ (decaying into $\Sigma\pi$, $\Lambda\pi$ and $\Lambda\pi\pi$) was identified with the $\Sigma(1660)$ seen in formation experiments. If this hypothesis is true it must have spin-parity $3/2^-$. The second $\Sigma(1660)$ decaying predominantly into $\Lambda(1405)\pi$ was

established to have $J^P = 3/2^-$. Neglecting the multiplet assignment for the $\Sigma(1580)$ and the $\Sigma(1940)$, one can ask the question, whether the 'second' $\Sigma(1660)$ belongs to either the second octet ($\alpha = -0.5$) or to the decimet of the $[70,1^-]$ multiplet.

A first remark is that the 'second' $\Sigma(1660)$ cannot be a member of an unmixed decimet, since a decimet does not couple to $\Lambda(1405)\pi$ ($\Lambda(1405)$ is in an SU(3) singlet).

We calculated the partial decay widths of $\Sigma(1660)$ as if it was a member of the unmixed octet with $\alpha = -0.5$. The results, using the coupling constants obtained in the fit to the $[70,1^-]$ multiplet by Faiman and Plane, are given in table VI.5 (line 3). A large partial width is predicted for the $\Sigma(1385)\pi$ mode (38.6 MeV). The sum of the partial widths for $N\bar{K}$, $\Sigma\pi$, $\Lambda\pi$ and $\Sigma(1385)\pi$ amounts to 44 ± 9 MeV. Using our measured value of Γ for the decay mode $\Sigma(1660) \rightarrow \Lambda(1405)\pi^+ \rightarrow \Sigma^+\pi^-\pi^+$ as an estimate of the <u>total</u> width of the $\Sigma(1660)$, we thus predict an upper limit for the $\Lambda(1405)\pi/\Sigma(1385)\pi$ branching ratio of (0.32 ± 0.34). This value is in strong disagreement with our measured lower limit of (4.2 ± 1.0) (cf. table VI.2). We thus conclude that the 'second' $\Sigma(1660)$ cannot be a member of the unmixed, $\alpha = -0.5$, $3/2^-$ octet.

We have also calculated the partial decay widths, allowing for various mixings between the three $J^P = 3/2^-$ multiplets. If we assume one Σ to be mixed as found in the fit by Faiman and Plane and further accept only the minimal amount of mixing between the other octet and the decimet resulting from this assumption, we again find a large partial width for the $\Sigma(1385)\pi$ decay mode and thus once more a $\Lambda(1405)\pi/\Sigma(1385)\pi$ branching ratio in disagreement with our observed lower limit. If however we allow maximal mixing between the $\alpha = -0.5$ octet and the

decimet (lines 6-11 of table VI.5), one can obtain a $\Sigma(1660)$ for which the partial width of the $\Sigma(1385)\pi$ decay is so small that it cannot be ruled out by our measured $\Lambda(1405)\pi/\Sigma(1385)\pi$ branching ratio. Only in the latter case could the $\Sigma(1660)$ decaying into $\Lambda(1405)\pi$, be a member of the $SU(6)_W$ $[70,1^-]$ multiplet.

Table VI.5. Partial widths (in MeV) of $\Sigma(1660)$ decay modes. $\Sigma_1, \Sigma_2, \Sigma_3$ denote the physical $J^P = 3/2^-$ Σ states. Without mixing these states belong to the $\alpha = 0.625$ octet, the $\alpha = -0.5$ octet and the decimet respectively. The errors on the predicted values are typically of the order of 20%.

		$N\bar{K}$	$\Sigma\pi$	$\Lambda\pi$	$\Sigma(1385)\pi$	'Total	
1		3.6	18.2	4.6	0.1	26.5	Formation results
2	Σ_1	3.0	22.6	8.4	0.1	34.1	Results from Faiman and Plane fit
3	Σ_1	1.8	35.5	4.2	15.6	57.1	All three states unmixed
4	Σ_2	2.9	0.6	1.7	38.6	43.8	
5	Σ_3	1.8	1.4	4.2	62.4	69.8	
6	Σ_2	0.1	1.9	5.6	3.1	10.7	Octet with $\alpha = 0.625$ unmixed; maximum
7	Σ_3	4.6	0.1	0.3	97.9	102.9	mixing between $\alpha = -0.5$ octet and decimet
8	Σ_2	3.1	2.7	0.1	107.7	113.6	Σ_1 mixed as in fit of Faiman and Plane; Maximum mixing between remaining two states
9	Σ_3	0.6	12.9	1.9	8.8	24.2	
10	Σ_2	0.9	11.4	2.0	3.9	18.2	
11	Σ_3	2.8	4.2	0.0	112.6	119.6	

Appendix A.

P A R T I C L E P R O P E R T I E S.

In the table below we list some properties of elementary particles referred to in this thesis. The data are taken from the "Review of Particle Properties" by the Particle Data Group [Pd76] . The following symbols are used:
M=mass, τ=lifetime, Γ=width, B=baryonnumber, I=isospin, J=spin, P=parity.

Particle	M(MeV)	τ(sec)	B	I	J	P
γ	0	stable	0	0,1	1	-
π^+, π^-	139.6	2.6×10^{-8}	0	1	0	-
π^o	135.0	0.83×10^{-16}	0	1	0	-
K^+, K^-	493.7	1.2×10^{-8}	0	1/2	0	-
$K^o, \bar{K}^o$	497.7		0	1/2	0	-
K^o_S		0.89×10^{-10}	0	1/2	0	-
K^o_L		5.2×10^{-8}	0	1/2	0	-
p	938.3	stable	1	1/2	1/2	+
n	939.6	918	1	1/2	1/2	+
Λ	1115.6	2.6×10^{-10}	1	0	1/2	+
Σ^+	1189.4	0.80×10^{-10}	1	1	1/2	+
Σ^o	1192.5	$<1.0 \times 10^{-14}$	1	1	1/2	+
Σ^-	1197.4	1.5×10^{-10}	1	1	1/2	+
Ξ^o	1314.9	3.0×10^{-10}	1	1/2	1/2	+
Ξ^-	1321.3	1.7×10^{-10}	1	1/2	1/2	+
Ω^-	1672.2	1.3×10^{-10}	1	0	3/2	+

Particle	M(MeV)	Γ(MeV)	B	I	J	P
η	548.8	0.85×10^{-3}	0	0	0	-
ρ	773	152	0	1	1	-
ω	782.7	10.0	0	0	1	-
Φ	1019.7	4.1	0	0	1	-
f	1271	180	0	0	2	+
K*(890)	892.2	49.4	0	1/2	1	-
K*(1420)	1421	108	0	1/2	2	+
Δ(1236)	$\sim$1232	$\sim$115	1	3/2	3/2	+
Σ(1385)	$\sim$1385	$\sim$ 35	1	1	3/2	+
Λ(1405)	1405	40	1	0	1/2	-
Λ(1520)	1519	15	1	0	3/2	-

Appendix B.

D E C A Y A N G U L A R D I S T R I B U T I O N F O R A T H R E E - S T E P D E C A Y C H A I N.

The purpose is to find the (6 dimensional) decay angular distribution F_{234} for the decay chain:

$$\begin{array}{l} B_1 \to B_2 + m_2 \\ \qquad\searrow \\ \qquad\quad B_3 + m_3 \\ \qquad\qquad\searrow \\ \qquad\qquad\quad B_4 + m_4 \end{array} \qquad \text{(B.1)}$$

B_1 is a baryon having arbitrary spin J_1; B_2, B_3 and B_4 are baryons with spin ½; m_2, m_3 and m_4 are spinless mesons. The function F_{234} can be obtained by a generalisation of the two-step distribution function F_{23} derived by N. Byers [By67]. We repeat this derivation as a starting point.

B.1. Decay parameters.

Consider the decay $B_1 \to B_2 + m_2$. If a and b are the amplitudes for the final state having orbital angular momentum $\ell = J_1 - ½$ and $\ell = J_1 + ½$ respectively and if $A_{+½}$ and $A_{-½}$ are the amplitudes for finding B_2 in a helicity state $+½$ and $-½$ respectively, the decay parameters of B_1 can be defined as:

$$\alpha_1 = \frac{2\,\mathrm{Re}(a^* b)}{|a|^2 + |b|^2} = \frac{|A_{+½}|^2 - |A_{-½}|^2}{|A_{+½}|^2 + |A_{-½}|^2} \qquad \text{(B.2a)}$$

$$\beta_1 = \frac{2\,\mathrm{Im}(a^* b)}{|a|^2 + |b|^2} = \frac{2\,\mathrm{Im}(A_{+½}\, A^*_{-½})}{|A_{+½}|^2 + |A_{-½}|^2} \qquad \text{(B.2b)}$$

$$\gamma_1 = \frac{|a|^2 - |b|^2}{|a|^2 + |b|^2} = \frac{2\,\mathrm{Re}(A_{+\frac{1}{2}}\, A^*_{-\frac{1}{2}})}{|A_{+\frac{1}{2}}|^2 + |A_{-\frac{1}{2}}|^2} \qquad \text{(B.2c)}$$

β_1 and γ_1 can be written as:

$$\beta_1 = \sqrt{1-\alpha_1^2}\,\sin\Phi_1 \;;\; \gamma_1 = \sqrt{1-\alpha_1^2}\,\cos\Phi_1 \qquad \text{(B.3)}$$

Parity conservation in the decay implies that either a or b is zero, thus $\alpha_1 = \beta_1 = 0$ and $\gamma_1 = \pm 1$ ($\Phi_1 = 0$ or π).

B.2. Reference frames.

For each decay in the decay chain, we have two angles Θ and φ which specify the direction of the baryon B_{i+1} in the rest frame of the baryon B_i. The relative orientation of these rest frames can be seen in figure B.1. The choice of the rest frame of B_1 is arbitrary, as long as it is defined independently of the decay of B_1. The axes of two successive frames in the chain are related by:

$$\begin{aligned} \hat{z}_{i+1} &= \hat{q}_{i+1} \\ \hat{y}_{i+1} &= \hat{z}_i \times \hat{q}_{i+1} = \hat{z}_i \times \hat{z}_{i+1} \\ \hat{x}_{i+1} &= \hat{y}_{i+1} \times \hat{z}_{i+1} \end{aligned} \qquad \text{(B.4)}$$

where $\hat{q}_{i+1}$ is the direction of B_{i+1} in the rest frame of B_i. Since the polarisation vector of B_1 is perpendicular to the production plane, we choose the t-channel transversity frame (see section V.1) as the B_1 rest frame.
The decay angles of B_{i+1} in the rest frame of B_i are then defined by:

$$\left.\begin{aligned} \xi_{i+1} &\equiv \cos\Theta_{i+1} = \hat{q}_{i+1} \cdot \hat{z}_i \\ \varphi_{i+1} &= \operatorname{arctg}\left(\frac{\hat{q}_{i+1} \cdot \hat{y}_i}{\hat{q}_{i+1} \cdot \hat{x}_i}\right) \end{aligned}\right\} \quad (B.5)$$

With the above definitions the following relations can be shown to hold:

$$\left.\begin{aligned} \hat{q}_{i+1} \cdot \hat{x}_i &= \sqrt{1 - \xi_{i+1}^2}\ \cos\varphi_{i+1} \\ \hat{q}_{i+1} \cdot \hat{y}_i &= \sqrt{1 - \xi_{i+1}^2}\ \sin\varphi_{i+1} \end{aligned}\right\} \quad (B.6)$$

$$\left.\begin{aligned} \hat{x}_i \cdot \hat{x}_{i+1} &= \xi_{i+1} \cos\varphi_{i+1} \\ \hat{x}_i \cdot \hat{y}_{i+1} &= -\sin\varphi_{i+1} \\ \hat{x}_i \cdot \hat{z}_{i+1} &= \sqrt{1 - \xi_{i+1}^2}\cos\varphi_{i+1} \\ \hat{y}_i \cdot \hat{x}_{i+1} &= \xi_{i+1}\sin\varphi_{i+1} \\ \hat{y}_i \cdot \hat{y}_{i+1} &= \cos\varphi_{i+1} \\ \hat{y}_i \cdot \hat{z}_{i+1} &= \sqrt{1 - \xi_{i+1}^2}\sin\varphi_{i+1} \\ \hat{z}_i \cdot \hat{x}_{i+1} &= -\sqrt{1 - \xi_{i+1}^2} \\ \hat{z}_i \cdot \hat{y}_{i+1} &= 0 \\ \hat{z}_i \cdot \hat{z}_{i+1} &= \xi_{i+1} \end{aligned}\right\} \quad (B.7)$$

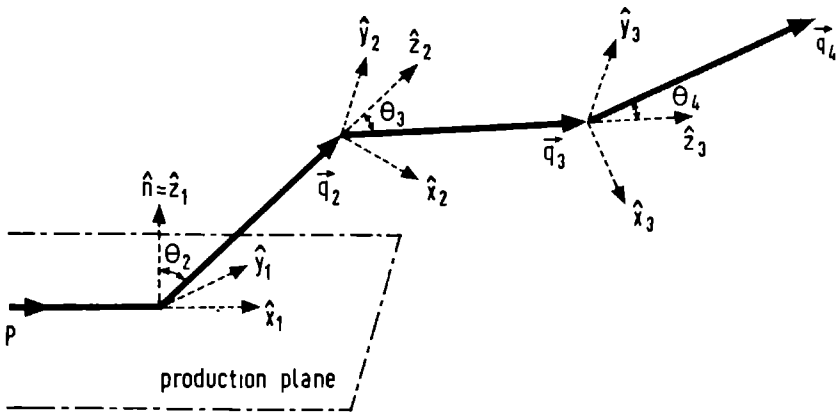

Fig. B.1. Definition of the reference frames in the three-step decay chain of B_1.

B.3. Two- and three-step decay angular distribution(*).

Consider the reaction $K^- + p \to B_1 + m_1$ and the decay $B_1 \to B_2 + m_2$, where B_1 has spin J_1, B_2 spin ½ and m_1, m_2 are spinless. The spin density matrix of B_2 can be written as:

$$\rho_2 = \frac{I_2}{2}\begin{pmatrix} 1 + P_{2z} & P_{2x} - i\,P_{2y} \\ P_{2x} + i\,P_{2y} & 1 - P_{2z} \end{pmatrix} \qquad (B.8)$$

where I_2 is the probability for finding B_2 in a solid angle

(*) The extension of the two-step decay angular distribution to an angular distribution for the three-step decay was first performed by J.P. Berge [Be72].

element $d\Omega_2$ in the B_1 rest frame and where P_{2x}, P_{2y} and P_{2z} are the components of the polarisation vector of B_2 in the B_2 rest frame (the helicity frame). ρ_2 is related to the spin density matrix ρ_1 of B_1 through

$$\rho_2 = S \ \rho_1 \ S^{\dagger}$$

where S is the transition matrix for this decay. The transition from the B_1 state with quantum numbers J_1,M into a two-particle state $B_2 + m_2$ with helicity λ is given by [Ja59]:

$$S_{\lambda M} = \sqrt{\frac{2J_1+1}{4\pi}} \ D^{J_1^*}_{M\lambda}(\varphi_2, \theta_2, 0) \ A_\lambda \qquad (B.9)$$

where A_λ is the amplitude for finding B_2 in a helicity λ. $D^J_{MN}(\varphi,\theta,\xi) = e^{-iM\varphi} d^J_{MN}(\cos\theta) e^{-iN\xi}$ are the Wigner rotation functions (see for properties Rose [Ro57]). Substitution of (B.9) into (B.8) and using for ρ_1 the expansion (V.4.4) yields:

$$(\rho_2)_{\lambda\lambda'} = \frac{A_\lambda A^*_{\lambda'}}{4\pi} \sum_{\substack{L \\ M\ M'}} \Sigma_{M''} \ (2L+1) t^{M''*}_L \ C(J_1 L J_1; M', M'') D^{J_1^*}_{M\lambda} \ D^{J_1}_{M'\lambda'} \qquad (B.10)$$

with $M = M' + M''$

In deriving the last expression we use the fact that with the normalisation:

$$\text{trace}(T^M_L \ T^{M'\dagger}_{L'}) = \delta_{LL'} \delta_{MM'} \ \frac{2J_1+1}{2L+1}$$

the matrix elements of the tensor operators T^M_L are given by the Clebsch-Gordan coefficients:

$$(T_L^{M''})_{MM'} = C(J_1 L J_1;\ M',\ M'') \text{ and } M = M' + M''$$

Substitution into (B.10) of

$$D^{J_1}_{M\lambda}\, D^{J_1 *}_{M'\lambda'} = D^{J_1}_{M\lambda}\, D^{J_1}_{-M'-\lambda'}\, (-)^{M'-\lambda'}$$

$$= \sum_{\ell} C(J_1 J_1 \ell;\ M,\ -M')\ C(J_1 J_1 \ell;\ \lambda,\ -\lambda')\,(-)^{M'-\lambda'} \qquad \text{(B.11)}$$

$$\times\ D^{\ell}_{M-M',\lambda-\lambda'}$$

and using:

$$C(J_1 L J_1;\ M', M'') = (-)^{J_1+M'} \sqrt{\frac{2J_1+1}{2L+1}}\ C(J_1 J_1 L; M, -M')$$

(with $M = M' + M''$)

together with the orthogonality of the Clebsch-Gordan coefficients gives:

$$(\rho_2)_{\lambda\lambda'} = (-)^{J_1-\lambda'} \sqrt{2J_1+1}\ \left(\frac{A_\lambda A^*_{\lambda'}}{4\pi}\right) \sum_{L,M} \sqrt{2L+1}\, C(J_1 J_1 L; \lambda, -\lambda')$$

$$\times\ t_L^{M *}\, D^{L *}_{M,\lambda-\lambda'}(\varphi_2, \Theta_2, 0) \qquad \text{(B.12)}$$

Substitution of (B.12) into (B.8) then leads to the following expressions for the decay angular and polarisation distributions:

$$I_2 = \frac{1}{4\pi} \sum_{L=0}^{2J_1} (E_L + \alpha_1 O_L) \sum_{M=-L}^{+L} Z_L^M\, D^L_{M0}(\varphi_2, \Theta_2, 0) \qquad \text{(B.13a)}$$

$$I_2 \vec{P}_2 \cdot \hat{q}_2 = \frac{1}{4\pi} \sum_{L=0}^{2J_1} (\alpha_1 E_L + O_L) \sum_{M=-L}^{+L} Z_L^M\, D^L_{M0}(\varphi_2, \Theta_2, 0) \qquad \text{(B.13b)}$$

$$I_2 \vec{P}_2 \cdot (\hat{x}_2 + i\,\hat{y}_2) = -\frac{1}{4\pi}(2J_1+1)\ \sqrt{1-\alpha_1^2}\, e^{-i\Phi_1} \qquad \text{(B.13c)}$$

$$\times \sum_{L=0}^{2J_1} \frac{O_L}{\sqrt{L(L+1)}} \sum_{M=-L}^{+L} Z_L^M\, D^L_{M1}(\varphi_2, \Theta_2, 0)$$

where $E_L = 1$ (=0) and $O_L = 0$ (=1) for L even (odd),

and $$Z_L^M = (-)^{J_1-\frac{1}{2}} \sqrt{(2J_1+1)(2L+1)}\, C(J_1 J_1 L; \tfrac{1}{2}, -\tfrac{1}{2})\, t_L^M.$$

The decay angular distribution F_{23} for the two-step decay is given by [Le57]:

$$F_{23} = \frac{1}{4\pi}\left[I_2 + \alpha_2 I_2 \vec{P}_2 \cdot \hat{q}_3\right] \qquad (B.14)$$

We may rewrite the last term in this expression as:

$$I_2\vec{P}_2\cdot\hat{q}_3 = (I_2\vec{P}_2\cdot\hat{x}_2)(\hat{x}_2\cdot\hat{q}_3) + (I_2\vec{P}_2\cdot\hat{y}_2)(\hat{y}_2\cdot\hat{q}_3)+(I_2\vec{P}_2\cdot\hat{z}_2)(\hat{z}_2\cdot\hat{q}_3) \qquad (B.15)$$

Using (B.6), (B.7), (B.13) and (B.14) we find:

$$F_{23} = \frac{1}{(4\pi)^2}\sum_{L=0}^{2J_1}\sum_{M=-L}^{+L}\Big[\{E_L(1+\alpha_1\alpha_2\xi_3)+O_L(\alpha_1+\alpha_2\xi_3)\}Z_L^M D_{M0}^L(\varphi_2,\theta_2,0) - O_L\frac{(2J_1+1)}{\sqrt{L(L+1)}}\alpha_2\sqrt{1-\alpha_1^2}\sqrt{1-\xi_3^2}\,\mathrm{Re}(Z_L^M D_{M1}^L(\varphi_2,\theta_2,\Phi_1+\varphi_3))\Big] \qquad (B.16)$$

If we extend the decay chain with a third decay, the angular distribution function becomes:

$$F_{234} = \frac{1}{(4\pi)^2}\left[I_2 + \alpha_2 I_2\vec{P}_2\cdot\hat{q}_3\right] \times \left[1 + \alpha_3\vec{P}_3\cdot\hat{q}_4\right] \qquad (B.17)$$

where $\vec{P}_3$ is the polarisation vector of B_3 in the B_3 rest frame defined by $(\hat{x}_3,\hat{y}_3,\hat{z}_3)$. $\vec{P}_3$ can be expressed in terms of the polarisation $\vec{P}_2$ and the decay parameters α_2, β_2 and γ_2 of the parent baryon B_2 as [Le57-2]

$$\vec{P}_3 = \frac{(\alpha_2 + \vec{P}_2\cdot\hat{q}_3)\hat{q}_3 + \beta_2(\vec{P}_2\times\hat{q}_3) + \gamma_2\hat{q}_3\times(\vec{P}_2\times\hat{q}_3)}{1+\alpha_2\vec{P}_2\cdot\hat{q}_3} \qquad (B.18)$$

$$= \frac{[\alpha_2 + (1-\gamma_2)\vec{P}_2\cdot\hat{q}_3]\hat{q}_3 + \beta_2(\vec{P}_2\times\hat{q}_3) + \gamma_2\vec{P}_2}{1+\alpha_2\vec{P}_2\cdot\hat{q}_3}$$

Substitution into (B.17) and re-arrangement of terms gives:

$$F_{234} = \frac{1}{(4\pi)^2}\,[\,(1 + \alpha_2\alpha_3\,\hat{q}_3\cdot\hat{q}_4)I_2 + \alpha_2\,I_2\vec{P}_2\cdot\,\hat{q}_3$$

$$+ \alpha_3\{(I_2\vec{P}_2\cdot\hat{q}_3)(\hat{q}_3\cdot\hat{q}_4) + \beta_2(I_2\vec{P}_2\times\hat{q}_3)\cdot\hat{q}_4 \qquad \text{(B.19)}$$

$$-\gamma_2(I_2\vec{P}_2\cdot\hat{q}_3)(\hat{q}_3\cdot\hat{q}_4) + \gamma_2\,I_2\vec{P}_2\cdot\hat{q}_4\}]$$

In the above expression there are two terms containing products of vectors defined in two different reference frames. They may be written in component form as:

$$(I_2\vec{P}_2\times\hat{q}_3)\cdot\hat{q}_4 = (I_2\vec{P}_2\cdot\hat{y}_3)(\hat{x}_3\cdot\hat{q}_4) - (I_2\vec{P}_2\cdot\hat{x}_3)(\hat{y}_3\cdot\hat{q}_4)$$

$$(I_2\vec{P}_2\cdot\hat{q}_4) = (I_2\vec{P}_2\cdot\hat{x}_3)(\hat{x}_3\cdot\hat{q}_4) + (I_2\vec{P}_2\cdot\hat{y}_3)(\hat{y}_3\cdot\hat{q}_4) \qquad \text{(B.20)}$$

$$+ (I_2\vec{P}_2\cdot\hat{z}_3)(\hat{z}_3\cdot\hat{q}_4)$$

with:

$$(I_2\vec{P}_2\cdot\hat{x}_3) = (I_2\vec{P}_2\cdot\hat{x}_2)(\hat{x}_2\cdot\hat{x}_3)+(I_2\vec{P}_2\cdot\hat{y}_2)(\hat{y}_2\cdot\hat{x}_3)+(I_2\vec{P}_2\cdot\hat{z}_2)(\hat{z}_2\cdot\hat{x}_3)$$

and similar expressions for $I_2\vec{P}_2\cdot\hat{y}_3$ and $I_2\vec{P}_2\cdot\hat{z}_3$.

Using (B.6), (B.7), (B.13), (B.15), (B.20) and substitution into (B.19) yields the complete three-step decay angular distribution

$$F_{234}\,(\cos\Theta_2,\varphi_2,\cos\Theta_3,\varphi_3,\cos\Theta_4,\varphi_4) =$$

$$\frac{1}{(4\pi)^3}\sum_{L=0}^{2J_1}\sum_{M=-L}^{+L}\Big[\{(C_U+\alpha_1C_Z)E_L+(\alpha_1C_U+C_Z)O_L\}Z_L^M\,D_{M0}^L(\varphi_2,\Theta_2,0)$$

$$+ O_L\,\frac{2J_1+1}{\sqrt{L(L+1)}}\,\sqrt{1-\alpha_1^2}\,\{C_A\mathrm{Re}[Z_L^MD_{M1}^L(\varphi_2,\Theta_2,\Phi_1+\varphi_3)]$$

$$+ C_B\mathrm{Im}[Z_L^MD_{M1}^L(\varphi_2,\Theta_2,\Phi_1+\varphi_3)]\}\Big] \qquad \text{(B.21)}$$

where: $C_U = 1+\alpha_2\alpha_3\cos\Theta_4$

$$C_Z = (\alpha_2+\alpha_3\cos\Theta_4)\cos\Theta_3-\alpha_3\sqrt{1-\alpha_2^2}\,\sin\Theta_3\sin\Theta_4\cos(\Phi_2+\varphi_4)$$

$$C_A = -(\alpha_2+\alpha_3\cos\Theta_4)\sin\Theta_3-\alpha_3\sqrt{1-\alpha_2^2}\,\cos\Theta_3\sin\Theta_4\cos(\Phi_2+\varphi_4)$$

$$C_B = -\alpha_3\sqrt{1-\alpha_2^2}\,\sin\Theta_4\sin(\Phi_2+\varphi_4)$$

Putting $\alpha_1 = \alpha_2 = \Phi_2 = 0$ we get the three-step decay angular distribution (V.4.7) for the decay chain $\Sigma(1660) \to \Lambda(1405) \to \Sigma \to p$.

To obtain the (six) single variable distributions, we integrate F_{234} over the other five variables. The resulting expressions are

$$F(\cos\Theta_2) = \tfrac{1}{2}\sum_{L=0}^{2J_1}(E_L + \alpha_1 O_L)\, Z_L^0\, d_{00}^L(\cos\Theta_2)$$

$$F(\varphi_2) = \frac{1}{2\pi}\{1+\sum_{L=1}^{2J_1}(E_L+\alpha_1 O_L)\sum_{M=1}^{L}(\cos M\varphi_2\ \mathrm{Re}Z_L^M+\sin M\varphi_2\ \mathrm{Im}Z_L^M)\, I_{M0}^L\}$$

$$F(\cos\Theta_3) = \tfrac{1}{2}(1 + \alpha_1\alpha_2\cos\Theta_3)$$

$$F(\varphi_3) = \frac{1}{2\pi}\left(1 - \frac{\pi}{8}(2J_1+1)\sqrt{1-\alpha_1^2}\,\alpha_2\cos(\Phi_1+\varphi_3)\cdot\right.$$
$$\left.\cdot\sum_{L=0}^{2J_1}\frac{O_L}{\sqrt{L(L+1)}}\, Z_L^0\, I_{01}^L\right)$$

$$F(\cos\Theta_4) = \tfrac{1}{2}(1 + \alpha_2\alpha_3\cos\Theta_4)$$

$$F(\varphi_4) = \frac{1}{2\pi}\left(1 - \frac{\pi^2}{16}\,\alpha_1\alpha_3\,\sqrt{1-\alpha_2^2}\cos(\Phi_2+\varphi_4)\right)$$

where I_{MN}^L is defined by

$$I_{MN}^L = \int_{-1}^{+1} d_{MN}^L(\cos\Theta_2)\, d\cos\Theta_2$$

Note that in the case of $\Sigma(1660) \to \Lambda(1405) \to \Sigma^+$, where both α_1 and α_2 are zero, the Θ_2 and φ_2 distributions contain only

even-L terms, while the remaining single-variable projections are flat. These projections can therefore not be used in a goodness-of-fit test concerning all the parameters.

B.4. Moments of the three-step decay angular distribution.

Given a function G of the six decay angles Θ_i, φ_i, one defines the moment $\langle G \rangle$ of the decay angular distribution F_{234} by

$$\langle G \rangle = \int d\Omega_2 \, d\Omega_3 \, d\Omega_4 \quad F_{234} \, G$$

where $d\Omega_i$ is an element of the solid angle in the rest frame of baryon B_{i-1}.

To estimate the parameters Z_L^M, J_1 and Φ_1 in the angular distribution function, the following moment functions are defined:

. for L even:

$$G_E(L,M) = \left[\frac{3\ (2L+1)}{3 + (\alpha_1\alpha_2)^2 + \alpha_3^2(\alpha_1^2 + \alpha_2^2 - \frac{2}{3}(\alpha_1\alpha_2)^2}\right] \cdot \cdot\ (C_U+\alpha_1 C_Z) D_{M0}^{L*}(\varphi_2,\Theta_2,0) \tag{B.22}$$

. for L odd:

$$G_{O0}(L,M) = \left[\frac{3\ (2L+1)}{3\ \alpha_1^2 + \alpha_2^2 + \alpha_3^2(1 - \frac{2}{3}\alpha_2^2 + (\alpha_1\alpha_2)^2}\right] \cdot \cdot\ (\alpha_1 C_U+C_Z) D_{M0}^{L*}(\varphi_2,\Theta_2,0)$$

and

$$G_{O1}(L,M) = \left[\frac{3\ (2L+1)}{\alpha_2^2 + \alpha_3^2(1 - \frac{2}{3}\alpha_2^2)}\right] \frac{\sqrt{L(L+1)}}{\sqrt{1 - \alpha_1^2}} \cdot (C_A+iC_B) D_{M1}^{L*}(\varphi_2,\Theta_2,\varphi_3)$$

with C_U, C_Z, C_A and C_B as defined in (B.21).
Again putting $\alpha_1 = \alpha_2 = \Phi_2 = 0$ yields the moment functions

(V.4.12) for the decay chain $\Sigma(1660) \rightarrow \Lambda(1405) \rightarrow \Sigma \rightarrow p$.

Performing the above integration for the moment functions then yields:

$$< G_{E} (L,M) > = Z_{L}^{M}$$

$$< G_{O0} (L,M) > = Z_{L}^{M}$$

$$< G_{O1} (L,M) > = Z_{L}^{M} . (2J_{1} + 1) \; e^{-i\Phi_{1}}$$

Appendix C.

MAXIMUM LIKELIHOOD FIT TO THE THREE-STEP DECAY ANGULAR DISTRIBUTION.

In section 4 of chapter V we described a procedure for obtaining the parameters Z_L^M of the three-step decay angular distribution by means of the moments method. In the case of the $\Lambda(1405)\pi^+$ decay mode we have also performed a maximum likelihood fit to estimate the Z_L^M parameters. The likelihood function, depending on the parameters Z_L^M, the spin J_1 and the parity through Φ_1, is defined by:

$$\ln\mathcal{L}(Z_L^M, J_1, \Phi_1) = \sum_{i=1}^{N} \ln F_{234}(\cos\Theta_{2i}, \varphi_{2i}, \cos\Theta_{3i}, \varphi_{3i}, \cos\Theta_{4i}, \varphi_{4i}) \qquad (C.1)$$

where F_{234} is the three-step decay angular distribution given in (V.4.7) and the summation runs over the experimental events. The decay angles $(\Theta_{2i}, \varphi_{2i})$ are defined in the t-channel transversity frame. Due to parity conservation in the production process of B_1, we expect all odd-M Z_L^M parameters to be equal to zero. To reduce the number of parameters in the fit, we have fixed the odd-M Z_L^M parameters at zero. We are then left with 1, 7 and 17 unknowns for the spin J_1 hypotheses 1/2, 3/2 and 5/2 respectively. The search for the maximum value of $\ln\mathcal{L}$ was done by the programme OPTIME [Eb72]. The 'best values' for the unknown parameters Z_L^M are presented in table C.1 for each of the spin-parity hypotheses $1/2^+$, $1/2^-$, $3/2^+$, $3/2^-$, $5/2^+$ and $5/2^-$ (*). The maximum value of the likelihood

---

(*) The programme was unable to find a maximum for the J=7/2 hypotheses, which requires adjusting 31 parameters.

function, $\ln \mathcal{L}_{max}$, is also given in this table.

The value of these maxima cannot be used directly for goodness-of-fit tests. This would require hypotheses with equal numbers of adjustable parameters (which is not the case) or a priori knowledge that the likelihood function is normally distributed as a function of the Z_L^M (which we don't know). It is therefore necessary to make separate goodness-of-fit tests. This could be done by comparing the single variable experimental distributions with the curves resulting from the above fits. The projected distributions are shown in figure C.1, the corresponding χ^2/ND values given in table C.2. The expected distributions for the $\cos\Theta_3$, φ_3, $\cos\Theta_4$ and φ_4 projections are isotropic, independent of the J^P of B_1. We therefore cannot use these projections for a spin-parity discrimination. We have also performed a goodness-of-fit test on the multivariate data, using a so-called non-parametric comparison of two multi-dimensional point sets [Fr74]. This test gives the confidence levels also shown in table C.2. These numbers indicate that J=1/2 may be excluded as a possible J^P hypothesis. The better $\ln\mathcal{L}_{max}$ value for the $J^P=5/2^+$ hypothesis as compared to the J=3/2 hypotheses is not confirmed by the values of the confidence levels.

We conclude, that on the basis of the maximum likelihood fits, no discrimination is possible between J=3/2 and J=5/2.

Table C.1. Z_L^M values obtained from maximum likelihood fits to the three-step decay angular distribution of the decay $\Sigma(1660) \to \Lambda(1405) \to \Sigma^+ \to p$ for $\cos\theta^* > 0.7$.

	$J^P=1/2^+$	$J^P=1/2^-$	$J^P=3/2^+$	$J^P=3/2^-$	$J^P=5/2^+$	$J^P=5/2^-$
Z_1^0	.12 ± .15	-.13 ± .14	-.10 ± .08	.07 ± .09	.07 ± .07	-.07 ± .05
Z_2^0			-.59 ± .16	-.63 ± .16	-.70 ± .15	-.71 ± .15
Re Z_2^2			.38 ± .13	.37 ± .13	.41 ± .14	.40 ± .13
Im Z_2^2			-.20 ± .13	-.18 ± .13	-.27 ± .14	-.26 ± .13
Z_3^0			-.07 ± .21	.00 ± .22	.02 ± .19	-.02 ± .16
Re Z_3^2			-.01 ± .16	-.12 ± .15	.08 ± .13	-.04 ± .12
Im Z_3^2			.24 ± .16	-.26 ± .16	-.33 ± .11	.33 ± .10
Z_4^0					.54 ± .17	.33 ± .20
Re Z_4^2					.20 ± .13	.23 ± .13
Im Z_4^2					.29 ± .14	.36 ± .13
Re Z_4^4					-.12 ± .18	-.13 ± .18
Im Z_4^4					-.22 ± .18	-.16 ± .18
Z_5^0					.97 ± .21	.00 ± .27
Re Z_5^2					.02 ± .23	-.25 ± .17
Im Z_5^2					-.16 ± .19	-.26 ± .19
Re Z_5^4					-.14 ± .20	-.15 ± .20
Im Z_5^4					-.49 ± .16	.17 ± .19
$\ln\mathcal{L}_{max}$	-1176.5	-1176.5	-1163.1	-1163.1	-1151.7	-1156.9

Table C.2. Results of Goodness-of-Fit Tests.

		$J^P=1/2^+$	$J^P=1/2^-$	$J^P=3/2^+$	$J^P=3/2^-$	$J^P=5/2^+$	$J^P=5/2^-$
χ^2/ND for projected distributions(*)	$\cos\Theta_2$	22/10	22/10	5.1/10	4.9/10	8.8/10	6.7/10
	φ_2	11/11	11/11	5.9/11	5.9/11	6.0/11	6.0/11
Confidence level from multi-dimensional goodness-of-fit test		0.02	0.10	0.65	0.53	0.29	0.22

(*) The χ^2/ND values for the (in each case) isotropic projections $\cos\Theta_3$, φ_3, $\cos\Theta_4$ and φ_4 are 9.5/9, 13/11, 8.5/11 and 9.4/10 respectively.

Fig.C.1. Distribution of the decay angles in the three-step decay $\Sigma(1660) \rightarrow \Lambda(1405) \rightarrow \Sigma^+ \rightarrow p$ for $\cos\Theta^* > 0.7$. The curves result from the maximum likelihood fits for the hypotheses J=1/2, $J^P=3/2^-$ and $J^P=5/2^+$. The curves for $J^P=3/2^+$ and $J^P=5/2^-$ are very close to the curves for $J^P=3/2^-$ and $J^P=5/2^+$ respectively and are therefore not drawn. →

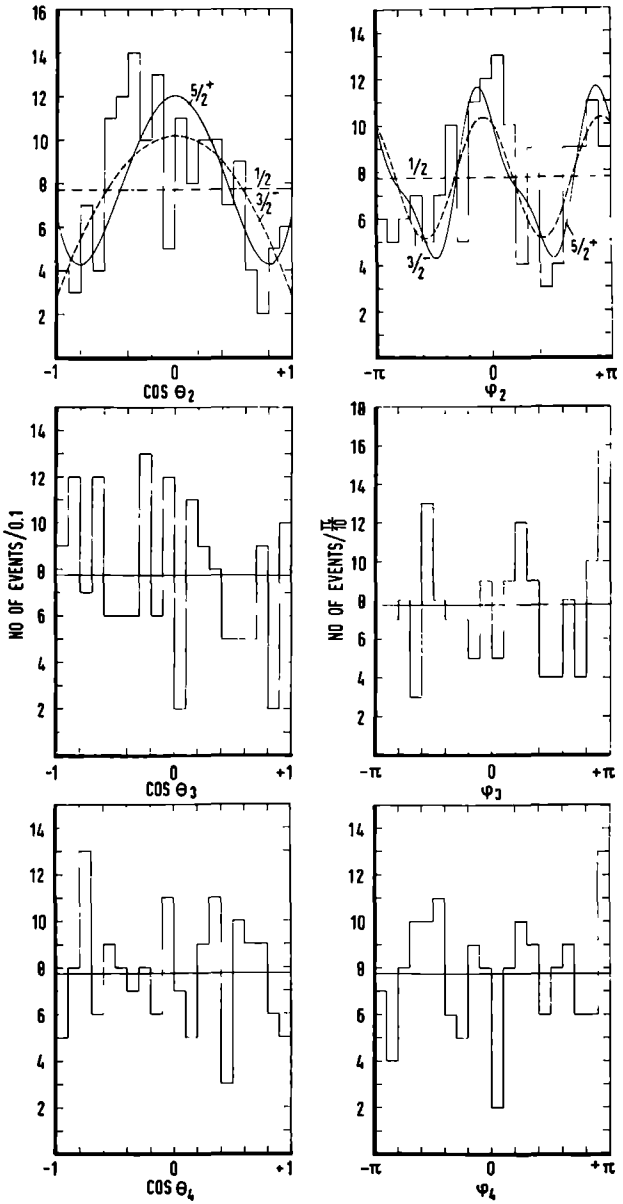
5/2+
1/2
3/2-
COS Θ2
1/2
3/2-
5/2+
φ2
NO OF EVENTS/0.1
COS Θ3
NO OF EVENTS/π/16
φ3
COS Θ4
φ4

REFERENCES

Ad55 R.K. Adair, Phys. Rev. 100(1955)1540.

Ag70 M. Aguilar-Benitez et al., Phys. Rev. Letters 25(1970)58.

Al62 G. Alexander et al., in 'Proceedings of the International Conference on High Energy Physics', Geneva 1962, (CERN Scientific Information Service, Geneva, 1962), p. 322.

Al63 L.W. Alvarez et al., Phys. Rev. Letters 10(1963)184.

Al67 W.W.M. Allison, D. Phil. thesis, Oxford, 1967.

Ap74 S.P. Apsell et al., Phys. Rev. 10D(1974)1419.

Ar68 R. Armenteros et al., Nuclear Physics B8(1968)195.

Ar69 R. Armenteros et al., Nuclear Physics B14(1969)91.

Ar69-2 R. Armenteros et al., Physics Letters 28B(1969)521.

Ba62 P.L. Bastien et al., in 'Proceedings of the International Conference on High Energy Physics', Geneva 1962, (CERN Scientific Information Service, Geneva, 1962), p. 373.

Ba63 P.L. Bastien and J.P. Berge, Phys. Rev. Letters 10(1963)188.

Ba75 P. Baillon and P.J. Litchfield, Nuclear Physics B94(1975)39.

Be72 J.P. Berge, private communication, 1972.

Bo70 R.J. de Boer et al., in 'Proceedings of the International Conference on Data Handling Systems in High-Energy Physics', Cambridge 1970, ed. by D.H. Lord and B.W. Powell, CERN 70-21, p. 709.

Br70 E.B. Brucker et al., in 'Hyperon Resonances-70', ed. by E.C. Fowler (Moore Publ. Co., Durham, N.C., 1970), p.155.

Br72 E. Bracci et al., High Energy Reactions Analysis Group, CERN/HERA 72-2, 1972.

Bu68 J. Button-Shafer, Phys. Rev. Letters 21(1968)1123.

Bu71 D. Budgen, Lettere al Nuovo Cimento 2(1971)85.

By63 N. Byers and S. Fenster, Phys. Rev. Letters 11(1963)52.

By67 N. Byers, 'On Determination of Spin, Decay Parameters and Density Matrix of Decaying States', CERN 67-20, 1967.

Ca61 R.H. Capps, Phys. Rev. 122(1961)929.

Cl73 A.G. Clark and D. Radojicic, 'Production of Two Resonances $\Sigma(1660)$ in the Reaction $K^-p \to \Sigma(1660)^+\pi^-$ at 3.13 and 3.3 GeV/c', paper submitted to the Second Aix-en-Provence Conference on Elementary Particles, 1973.

Cp1 See the CERN programme library for a description.
Long write-up no's :
X201 - THRESH/MDT
X601 - GRIND
Y100 - SLICE

Cr74 F.Crijns et al., in 'Proceedings of the Oxford Conference on Computer Scanning', ed. by P.G. Davey and B.M. Hawes, Oxford 1974, p. 43.

Da53 R.H. Dalitz, Phil. Mag. 44(1953)1068.

Da61 R.H. Dalitz and D.H. Miller, Phys. Rev. Letters 6(1961)562.

Do72 M.G. Doncel, L. Michel and P. Minnaert, Nuclear Physics B38(1972)477.

Eb67 P. Eberhard et al., Phys. Rev. 163(1967)1446.

Eb69 P. Eberhard et al., Phys. Rev. Letters 22(1969)200.

Eb72 P.H. Eberhard and W.O. Koellner, Comp. Phys. Comm. 3(1972)296.

En76 J.J. Engelen, private communication, 1976.

Es74 R.D. Estes, Ph.D. thesis, LBL-3827, 1974.

Fa57 U. Fano, Rev. Mod. Phys. 29(1957)74.

Fa72 D. Faiman and D.E. Plane, Nuclear Physics B50(1972)379.

Fe66 M. Ferro-Luzzi, in 'Proceedings of the XIIIth International Conference on High Energy Physics', Berkeley 1966, (University of California Press, Berkeley, Cal., 1967), p. 183.

Fe69 B.T. Feld, 'Models of Elementary Particles', (Blaisdell Publishing Company, Waltham, Mass., 1969), p. 93.

Fr74 J.H. Friedman, in 'Proceedings of the 1974 CERN School of Computing', CERN 74-23 (1974), p. 334.

Ga70 A. Barbaro-Galtieri, in 'Hyperon Resonances-70', ed. by E.C. Fowler (Moore Publ. Co., Durham, N.C., 1970), p.173.

Ga74 J.B. Gay, X42-note (internal report CERN), 1974.

Ga76 J.B. Gay et al., paper submitted to Physics Letters B, 1976.

Ga76-2 J.B. Gay, *private communication*, 1976.

Ge64 M. Gell-Mann, Physics Letters 8(1964)214.

Gr75 A.J. de Groot, Ph.D. thesis, Amsterdam, 1975.

He69 R.J. Hemingway and H. Whiteside, University of Maryland Technical Report no. 70-065, 1969.

He75 A.J.G. Hey, P.J. Litchfield and R.J. Cashmore, Nuclear Physics B95(1975)516.

Ho72 A.J. Van Horn, Ph.D. thesis, LBL-1370, 1972.

Ho75 A.J. Van Horn, Nuclear Physics B87(1975)145.

Hu69 D.O. Huwe, Phys. Rev. 181(1969)1824.

Ja59 M.Jacob and G.C. Wick, Annals of Physics 7(1959)404.

Ja65 J.D. Jackson, 'High Energy Physics - Les Houches 1965', ed. by C. de Witt and M. Jacob, (Gordon and Breach, New York, 1965), p. 360.

Ki71 J.K. Kim, Phys. Rev. Letters 27(1971)356.

Kr69 U.E. Kruse, J.S. Loos and E.L. Goldwasser, Phys. Rev. 177(1969)1951.

La72 W. Langbein and F. Wagner, Nuclear Physics B47(1972)477.

Le57 T.D. Lee et al., Phys. Rev. 107(1957)1367.

Le57-2 T.D. Lee and C.N. Yang, Phys. Rev. 108(1957)1645.

Le65 A. Leveque et al., Physics Letters 18(1965)69.

Li65 H.J. Lipkin and S. Meshkov, Phys. Rev. Letters 14(1965)670.

Lo66 G.W. London et al., Phys. Rev. 143(1966)1034.

Ls72 CERN-LSD group, in 'Proceedings of European Spiral Reader Symposium', Stockholm 1974, ed. by R. Budde G. Eksprong and S.O. Holmgren, CERN 72-16, p.21.

Ma71 G.C. Mason, Oxford Bubble Chamber Group Physics Notes no. 19, 1971.

Ma74 J. MacNaughton, Nucl. Instr. and Meth. 120(1974)47.

Ma76 G.C. Mason and C.G. Wohl, Nuclear Physics B103(1976)279.

Me72 W.J. Metzger, HEN97 (internal report Nijmegen), 1972.

Me75 W.J. Metzger, HEN138 (internal report Nijmegen), 1975.

NA71 Nijmegen-Amsterdam collaboration, 'Production of $\Sigma(1660)$ by K^-p at 4.2 GeV/c' , paper submitted to the Amsterdam International Conference on Elementary Particles, 1971.

Or58 J. Orear, UCRL-8417, 1958.

Os74 Output Scan Rules K^-p 4.2 GeV/c, HEN91 (internal report Nijmegen), 1974.

Pd76 Particle Data Group, 'Review of Particle Properties', Rev. Mod. Phys. 48(1976) number 2, part II.

Pi67 H. Pilkuhn, 'The Interactions of Hadrons', (North Holland Publishing Company, Amsterdam, 1967), p.26-28.

Po75 R.A. Ponte et al., Phys. Rev. 12D(1975)2597.

Pr74 J. Prevost et al., Nuclear Physics B69(1974)246.

Ro57 M.E. Rose, 'Elementary Theory of Angular Momentum', (John Wiley & Sons, New York, 1957).

Sa74 N.P. Samios, M. Goldberg and B.T. Meadows, Rev. Mod. Phys. 46(1974)49.

Si68 W.H. Sims et al., Phys. Rev. Letters 21(1968)1413.

St63 L. Stodolsky and J.J. Sakurai, Phys. Rev. Letters 11(1963)90.

St64 L. Stodolsky, Phys. Rev. 134B(1964)1099.

St74 Program STK, WRU-HEN91 (internal report Nijmegen), 1974.

Sw63 J.J. de Swart, Rev. Mod. Phys. 35(1963)916.

Ti74 H.G.J.M. Tiecke, Ph.D. thesis, Nijmegen, 1974.

To74 D.Z. Toet, Ph.D. thesis, Nijmegen, 1974.

Va72 R.T. Van de Walle, HEN99 (internal report Nijmegen), 1972.

Zw64 G. Zweig, CERN preprints TH401 and 412, 1964.

SUMMARY

In this thesis we describe an analysis of the production and decay of $\Sigma^+(1660)$ in K^-p interactions at 4.2 GeV/c incident momentum. The interactions were detected in the C.E.R.N. 2 metre hydrogen bubble chamber exposed to an electrostatically separated K^- beam. About 3 million pictures are being analysed by four European groups at Amsterdam, C.E.R.N., Nijmegen and Oxford. The results presented in this thesis are based on an analysis of approximately 1.5 million pictures.

The first chapter deals with the experimental details and contains a description of:

. the scanning, measurement and data reduction chain,
. the special case of the kinematic reconstruction of a charged particle decay, and
. the criteria used in the selection of events and the solution of ambiguous kinematical interpretations.

In chapter II we determine the cross sections for the channels used in our analysis of the $\Sigma^+(1660)$. The method used for the calculation of the cross sections is based on the counting of τ-decays. A description is given of the corrections applied to compensate for the losses characteristic of strange particle decay.

Chapter III is a short review of the history of the $\Sigma(1660)$. It describes some of the earlier analyses of $\Sigma(1660)$ with their (often) conflicting results in terms of production characteristics, branching ratios and spin-parity.

In chapter IV we examine the production of $\Sigma^+(1660)$ in the channels $K^-p \to \Sigma^+\pi^-\pi^+\pi^-$, $K^-p \to \Sigma^-\pi^+\pi^+\pi^-$, $K^-p \to \Sigma^0\pi^+\pi^-$, $K^-p \to \Lambda\pi^+\pi^-$, $K^-p \to p\bar{K}^0\pi^-$ and $K^-p \to \Lambda\pi^+\pi^0\pi^-$. Production of $\Sigma^+(1660)$ is observed in the $(\Sigma\pi\pi)^+$ effective mass distributions

of the first two channels. It is found that this decay mode consists almost entirely of $\Lambda(1405)\pi^+$. Fits to the effective mass distributions yield for the mass and width of the resonance:

. M_o = (1655 ± 3) MeV and Γ_o = (56 ± 7) MeV in the decay mode $\Sigma^+(1660) \rightarrow \Lambda(1405)\pi^+ \rightarrow \Sigma^+\pi^-\pi^+$;

. M_o = (1660 ± 4) MeV and Γ_o = (48 ± 7) MeV in the decay mode $\Sigma^+(1660) \rightarrow \Lambda(1405)\pi^+ \rightarrow \Sigma^-\pi^+\pi^+$.

The effective mass distributions $M(\Sigma^o\pi^+)$ from the channel $K^-p \rightarrow \Sigma^o\pi^+\pi^-$ and $M(\Sigma^+\pi^o)$ from the channel $K^-p \rightarrow \Sigma^+\pi^o\pi^-$ also show the production of $\Sigma^+(1660)$. The resonance parameters resulting from the fits to these effective mass distributions are:

. M_o = (1665 ± 3) MeV and Γ_o = (62 ± 9) MeV in the decay mode $\Sigma^+(1660) \rightarrow \Sigma^o\pi^+$;

. M_o = (1677 ± 7) MeV and Γ_o = (63 ± 17) MeV in the decay mode $\Sigma^+(1660) \rightarrow \Sigma^+\pi^o$.

For the remaining channels we can only determine upper limits for the production of $\Sigma^+(1660)$. An important result is that there is no production of $\Sigma^+(1660)$ in the channel $K^-p \rightarrow p\bar{K}^o\pi^-$.

A study of the production angular distributions shows a very significant difference between the distributions of $\Sigma^+(1660) \rightarrow \Lambda(1405)\pi^+$ and of $\Sigma^+(1660) \rightarrow (\Sigma\pi)^+$. This leads to the conclusion that (at least) two $\Sigma(1660)$ resonances are being produced. Using the number of resonance events in both the $\Sigma^+\pi^-\pi^+$ and $\Sigma^-\pi^+\pi^+$ mode, the cross section for the reaction $K^-p \rightarrow \Sigma^+(1660)\pi^-$ with $\Sigma^+(1660) \rightarrow \Lambda(1405)\pi^+$ is measured to be (23 ± 4) μb. The reaction cross section for the decay mode $\Sigma^+(1660) \rightarrow (\Sigma\pi)^+$ amounts to (33 ± 5) μb.

Chapter V describes the spin-parity analyses of the

$\Sigma(1660)$. In an analysis of the moments of the decay angle spherical harmonics we find a significantly non-zero L=2 moment, for both the $\Lambda(1405)\pi^+$ ($\rightarrow \Sigma^+\pi^-\pi^+$) and $\Sigma^o\pi^+$ decay modes, thus establishing that in both cases the spin is $J \geqslant 3/2$. An Adair analysis of the decay $\Sigma^+(1660) \rightarrow \Lambda(1405)\pi^+$ leads to a preference for J=3/2. We do not find any significantly non-zero odd-L moment in a Byers-Fenster analysis of the three-step decay chain $\Sigma(1660) \rightarrow \Lambda(1405) \rightarrow \Sigma^+ \rightarrow p$. A direct determination of the spin and the parity using these odd-L moments is thus impossible. However, if we assume all moments consistent with zero, to be identically zero, we find, using the rank condition for the spin density matrix, that the spin must be 3/2. Performing a Byers-Fenster analysis of the three-step decay chain $\Sigma(1660) \rightarrow \Sigma^o \rightarrow \Lambda \rightarrow p$ again does not yield any non-zero odd-L moment. The test using the rank condition shows that, when applied to the sample of events in the backward production angular region, the data are consistent with J=3/2. An analysis of the Dalitz plot for the decay $\Sigma^+(1660) \rightarrow \Sigma^-\pi^+\pi^+$ yields negative parity as the most probable hypothesis.

Finally, in chapter VI, we determine the branching ratios for $\Sigma(1660)$. They are, with the exception of the $\Lambda(1405)\pi$ rate, in agreement with those found in formation experiments. The $\Sigma(1660)$ which decays into $\Sigma\pi$ and possibly with J=3/2 thus seems to be the same object as the $J^P=3/2^-$ $\Sigma(1660)$ observed in formation experiments, while the $\Sigma(1660)$ which decays into $\Lambda(1405)\pi$ is a different resonance, but has also $J^P=3/2^-$. Furthermore, the branching ratios of $\Sigma(1660)$ produced in $\Sigma\pi$, agree with those predicted for the I=1 member of the $\alpha=0.625$, $J^P=3/2^-$ octet of the $[70,1^-]$ multiplet of $SU(6)_W$. The $\Sigma(1660)$ decaying into $\Lambda(1405)\pi$ can only be another $J^P=3/2^-$ member of the $[70,1^-]$ multiplet if one allows strong configuration mixing.

SAMENVATTING.

In dit proefschrift beschrijven we een analyse van de produktie en het verval van $\Sigma^+(1660)$ in K^-p interakties bij een inkomende impuls van 4.2 GeV/c. De interakties werden gedetekteerd in het C.E.R.N. 2 meter bellenvat dat bestraald werd door een elektrostatisch gesepareerde bundel K^- mesonen. Op dit moment worden ongeveer 3 miljoen bellenvatopnamen geanalyseerd in vier Europese groepen te Amsterdam, C.E.R.N., Nijmegen en Oxford. De resultaten in dit proefschrift zijn gebaseerd op een analyse van ongeveer 1½ miljoen opnamen.

Het eerste hoofdstuk handelt over experimentele details en geeft een beschrijving van:

. het scannen, het meten en de data reduktie keten,
. het speciale geval van de kinematische rekonstruktie van het verval van een geladen deeltje en
. de kriteria die zijn aangelegd bij het selekteren van verschijnselen en het oplossen van ambigue kinematische interpretaties.

In hoofdstuk II bepalen we de werkzame doorsnede voor de in onze analyse van de $\Sigma^+(1660)$ gebruikte kanalen. De gebruikte methode voor de berekening van de werkzame doorsneden is gebaseerd op het tellen van τ-vervallen. Er wordt een beschrijving gegeven van de korrekties toegepast ter kompensatie van de optredende verliezen, eigen aan het verval van vreemde deeltjes.

Hoofdstuk III bestaat uit een kort overzicht van de geschiedenis van de $\Sigma(1660)$. Het beschrijft enkele van de eerdere analyses van de $\Sigma(1660)$ met hun (dikwijls) tegenstrijdige resultaten omtrent de produktie kenmerken, vertakkingsverhoudingen en spin-pariteit.

In hoofdstuk IV onderzoeken we de produktie van $\Sigma^+(1660)$

in de kanalen $K^-p \to \Sigma^+\pi^-\pi^+\pi^-$, $K^-p \to \Sigma^-\pi^+\pi^+\pi^-$, $K^-p \to \Sigma^0\pi^+\pi^-$, $K^-p \to \Sigma^+\pi^0\pi^-$, $K^-p \to \Lambda\pi^+\pi^-$, $K^-p \to p\bar{K}^0\pi^-$ en $K^-p \to \Lambda\pi^+\pi^0\pi^-$. De produktie van $\Sigma^+(1660)$ is zichtbaar in de $(\Sigma\pi\pi)^+$ effektieve massa verdelingen van de eerste twee kanalen. Het blijkt dat deze vervalsmode vrijwel volledig bestaat uit $\Lambda(1405)\pi^+$. Aanpassingen aan de effektieve massa verdelingen geven als resultaat voor de massa en breedte van de resonantie:

. M_o = (1655 ± 3) MeV en Γ_o = (56 ± 7) MeV in de vervalsmode $\Sigma^+(1660) \to \Lambda(1405)\pi^+ \to \Sigma^+\pi^-\pi^+$;

. M_o = (1660 ± 4) MeV en Γ_o = (48 ± 7) MeV in de vervalsmode $\Sigma^+(1660) \to \Lambda(1405)\pi^+ \to \Sigma^-\pi^+\pi^+$.

Ook de effektieve massa verdelingen $M(\Sigma^0\pi^+)$ van het kanaal $K^-p \to \Sigma^0\pi^+\pi^-$ en $M(\Sigma^+\pi^0)$ van het kanaal $K^-p \to \Sigma^+\pi^0\pi^-$ laten de produktie van $\Sigma^+(1660)$ zien. De resultaten voor de resonantieparameters van de aanpassingen aan deze effektieve massa verdelingen zijn:

. M_o = (1665 ± 3) MeV en Γ_o = (62 ± 9) MeV in de vervalsmode $\Sigma^+(1660) \to \Sigma^0\pi^+$;

. M_o = (1677 ± 7) MeV en Γ_o = (63 ± 17) MeV in de vervalsmode $\Sigma^+(1660) \to \Sigma^+\pi^0$.

In de overige kanalen zijn we slechts in staat bovenlimieten voor de produktie van $\Sigma^+(1660)$ te bepalen. Een belangrijk resultaat is, dat er geen produktie van $\Sigma^+(1660)$ aanwezig is in het kanaal $K^-p \to p\bar{K}^0\pi^-$.

Een studie van de produktiehoek-verdelingen laat een groot verschil zien tussen de verdelingen voor $\Sigma^+(1660) \to \Lambda(1405)\pi^+$ en voor $\Sigma^+(1660) \to (\Sigma\pi)^+$. Dit leidt tot de konklusie dat er (minstens) twee $\Sigma(1660)$ resonanties worden geproduceerd. Gebruik makend van het aantal resonantie verschijnselen in zowel de $\Sigma^+\pi^-\pi^+$ als $\Sigma^-\pi^+\pi^+$ mode, vinden we voor de werkzame doorsnede

van de reaktie $K^- p \to \Sigma^+(1660)\pi^-$ met $\Sigma^+(1660) \to \Lambda(1405)\pi^+$ (23 ± 4)μb. De werkzame doorsnede van deze reaktie waarbij $\Sigma^+(1660) \to (\Sigma\pi)^+$ bedraagt (33 ± 5)μb.

Hoofdstuk V beschrijft de analyse van de spin-pariteit van de $\Sigma(1660)$. In een analyse van de momenten van de vervalshoek bolfuncties Y_L^M vinden we zowel voor de $\Lambda(1405)\pi^+$ ($\to \Sigma^+\pi^-\pi^+$) als voor de $\Sigma^o\pi^+$ vervalsmode een L=2 moment dat signifikant van nul verschilt, hetgeen betekent dat in beide gevallen de spin $J \geq 3/2$ is. Een Adair-analyse op het verval $\Sigma^+(1660) \to \Lambda(1405)\pi^+$ prefereert J=3/2. In een Byers-Fenster analyse op de vervalsketen $\Sigma(1660) \to \Lambda(1405) \to \Sigma^+ \to p$ worden geen signifikant van nul verschillende oneven-L momenten gevonden. Hierdoor is het niet mogelijk een direkte bepaling van de spin-pariteit te doen. Indien we echter aannemen dat alle momenten die in overeenstemming zijn met de waarde nul, inderdaad gelijk aan nul zijn, dan vinden we, door gebruik te maken van de rang voorwaarde voor de spin-dichtheidsmatrix, dat de spin gelijk moet zijn aan 3/2. In een zelfde analyse op de vervalsketen $\Sigma(1660) \to \Sigma^o \to \Lambda \to p$ worden eveneens geen van nul verschillende oneven-L momenten gevonden. De test met de rang voorwaarde toegepast op de verzameling van achterwaarts geproduceerde verschijnselen, laat zien dat de vervalshoek verdeling ook hier in overeenstemming is met de hypothese J=3/2. Een analyse van het Dalitz-diagram voor het verval $\Sigma^+(1660) \to \Sigma^-\pi^+\pi^+$ leidt tot de conclusie dat negatieve pariteit het meest waarschijnlijk is.

Tenslotte worden in hoofdstuk VI de vertakkingsverhoudingen voor $\Sigma(1660)$ bepaald. Met uitzondering van de $\Lambda(1405)\pi$ fraktie, zijn deze verhoudingen in overeenstemming met de resultaten van formatie-experimenten. De $\Sigma(1660)$ die in $\Sigma\pi$ vervalt en waarvoor mogelijk J=3/2 geldt, lijkt dus hetzelfde deeltje te zijn als

de $\Sigma(1660)$ met $J^P=3/2^-$ zoals waargenomen in formatie-experimenten. De $\Sigma(1660)$ die in $\Lambda(1405)\pi$ vervalt is daarentegen een andere resonantie, maar ook met $J^P=3/2^-$. De vertakkingsverhoudingen van $\Sigma(1660)$ zoals geproduceerd in $\Sigma\pi$ stemmen eveneens overeen met de voorspellingen voor het I=1 lid van het $\alpha=0.625$, $J^P=3/2^-$ octet uit het $[70,1^-]$ multiplet van $SU(6)_W$. De $\Sigma(1660)$ die naar $\Lambda(1405)\pi$ vervalt kan slechts dan een ander $J^P=3/2^-$ lid van het $[70,1^-]$ multiplet zijn, wanneer er een sterke opmenging tussen de verschillende $J^P=3/2^-$ Σ-toestanden bestaat.

CURRICULUM VITAE

Geboren op 8 maart 1945 te Meerssen.
Gedurende de periode 1957-1962 heb ik aan de Kath. Hogereburgerschool te Maastricht-Wijk mijn middelbare school opleiding genoten en het H.B.S.-B diploma behaald.
In 1962 begon ik vervolgens met mijn natuurkunde studie aan de Katholieke Universiteit te Nijmegen, waar in 1965 het kandidaatsexamen en in 1968 het doctoraal-examen in de experimentele natuurkunde met goed gevolg werden afgelegd.
Vanaf 1968 ben ik als wetenschappelijk medewerker in F.O.M.-dienst werkzaam aan de Katholieke Universiteit te Nijmegen op de afdeling experimentele hoge energie fysika onder leiding van Prof. dr. R.T. Van de Walle.

STELLINGEN

I

De door Apsell et al. gebruikte verdelingsfunktie voor het sequentiële verval $\Sigma(1660) \rightarrow \Lambda(1405) \rightarrow \Sigma \rightarrow N$ is onjuist.

S.P. Apsell et al., Phys. Rev. 10D(1974)1419.

II

De door Kocher en Wernhard gegeven fout op de α-parameter van het verval $\Omega^- \rightarrow \Lambda K^-$ is ongeveer een faktor 2 te klein. Hun gemeten waarde voor α is daarom slechts één standaardafwijking verschillend van nul.

D.J. Kocher en K.L. Wernhard, Physics Letters 51B(1974)193.

III

Het is meer aannemelijk de als P-golf geparametriseerde bijdrage tot het $(K^-\pi^+)$-systeem boven 1.2 GeV in $K^-p \rightarrow K^-\pi^+n$ bij 10 en 16 GeV/c, te interpreteren als een interferentie tussen S- en D-golven.

P. Lauscher et al., Nuclear Physics B86(1975)189.

IV

Het testen van de betrouwbaarheid van een meest aannemelijke aanpassing aan een multi-dimensionale verdelingsfunktie door middel van het vergelijken van de experimentele en voorspelde één-dimensionale geprojekteerde distributies en/of het vergelijken van de experimentele en voorspelde momenten van de multi-dimensionale verdeling, is in het algemeen niet voldoende.

V. Blobel et al., Nuclear Physics B97(1975)201.
G. Otter et al., Nuclear Physics B96(1975)365.

V

Een geautomatiseerd "single-pass" diagnostisch systeem van cel-herkenning voor het opsporen van baarmoederhalskanker is a priori voorbestemd om te mislukken.

M. Bibbo et al., Acta Cytologica 17(1973)340.

Het verdient aanbeveling om voor leidsters van peuterspeelzalen dezelfde rechtspositie-regeling te verwezenlijken als voor het overig onderwijzend personeel.

Nijmegen, 1 oktober 1976 J.J.M. Timmermans